

KfK 2669
Juli 1978

Applied Neutron Resonance Theory

F. H. Fröhner
Institut für Neutronenphysik und Reaktortechnik
Projekt Schneller Brüter

Kernforschungszentrum Karlsruhe

Als Manuskript vervielfältigt
Für diesen Bericht behalten wir uns alle Rechte vor

KERNFORSCHUNGSZENTRUM KARLSRUHE GMBH

KERNFORSCHUNGSZENTRUM KARLSRUHE

Institut für Neutronenphysik und Reaktortechnik
Projekt Schneller Brüter

KfK 2669

Applied Neutron Resonance Theory

F.H. Fröhner

Kernforschungszentrum Karlsruhe GmbH, Karlsruhe.

ABSTRACT

Utilisation of resonance theory in basic and applications-oriented neutron cross section work is reviewed. The technically important resonance formalisms, principal concepts and methods as well as representative computer programs for resonance parameter extraction from measured data, evaluation of resonance data, calculation of Doppler-broadened cross sections and estimation of level-statistical quantities from resonance parameters are described.

Angewandte Neutronenresonanztheorie

ZUSAMMENFASSUNG

Eine Übersicht über die Benutzung der Resonanztheorie bei grundlagen- und anwendungsorientierten Neutronenquerschnittsarbeiten wird gegeben. Die praktisch wichtigen Resonanzformalismen, grundlegenden Begriffe und Methoden sowie typische Rechenprogramme für Resonanzparameter-Analyse von Meßdaten, Generierung Doppler-verbreiteter Querschnitte und statistische Schätzung niveaustatistischer Größen aus Resonanzparametern wird beschrieben.

This review paper was prepared for the Winter Courses on Nuclear Physics and Reactors, Part I: Nuclear Theory for Applications, held at the International Centre for Theoretical Physics, Trieste, 16 January - 10 February 1978

TABLE OF CONTENT

1. Introduction
2. Parametrisation of resonance cross sections
 - 2.1. Preparation of resonance data for applications
 - Measurement
 - Reduction of raw data
 - Analysis of clean data
 - Data evaluation
 - Generation of group constants
 - International coordination
 - 2.2. Why parametrise?
 - 2.3. Practical resonance formalisms
 - 2.3.1. The Blatt-Biedenharn formalism
 - 2.3.2. The practically important R-matrix formulae
 - 2.3.3. Illustration: R-matrix formulation of single-particle interaction with a complex potential
 - 2.3.4. The principal approximations to the inverse level matrix
 - 2.3.5. Kapur-Peierls cross section formulae
 - 2.3.6. SLBW and MLBW " " "
 - 2.3.7. The Reich-Moore " " "
 - 2.3.8. The Adler-Adler " " "
 - 2.4. Theory of Doppler broadening
 - 2.4.1. Free-gas approximation
 - 2.4.2. Cubic crystal
 - 2.4.3. Voigt profiles vs. numerical broadening
 - 2.4.4. Temperature-dependent self-shielding, importance of level spins
 - 2.4.5. Westcott factors
 - 2.5. Observables
 - 2.5.1. Transmission
 - 2.5.2. Reaction yields
 - 2.5.3. Differential scattering yields
 - 2.5.4. Self-indication (n,x) data
 - 2.5.5. Semi-empirical determination of self-shielded group cross sections

Table of Content (cont.)

- 2.6. Experimental complications
 - 2.6.1. Backgrounds
 - 2.6.2. Resolution broadening
 - 2.6.3. Detector efficiency and flux
 - 2.6.4. Self-shielding and multiple scattering
- 2.7. Resonance parameter estimation
 - 2.7.1. The least-squares method
 - 2.7.2. Error propagation in least-squares fits
 - 2.7.3. Goodness of fit
 - 2.7.4. Area analysis
 - 2.7.5. Shape analysis
 - 2.7.6. Computer codes
- 2.8. Miscellaneous useful resonance-theoretical expressions
 - 2.8.1. Maxima and minima (windows) in the total cross section
 - 2.8.2. Distant levels
 - 2.8.3. Subthreshold ("negative") levels
- 3. Evaluation of resonance data
 - 3.1. Intercomparison of resonance parameter sets
 - 3.1.1. Different potential-scattering parameters
 - 3.1.2. Different boundary parameters B_c
 - 3.2. Conversion from Wigner-Eisenbud to Kapur-Peierls resonance parameters
 - 3.3. Applied resonance statistics
 - 3.3.1. The Porter-Thomas hypothesis
 - 3.3.2. Wigner's surmise and Hamiltonian ensemble theory
 - 3.3.3. Maximum-likelihood estimation of $\langle \Gamma^k \rangle$ and $\langle D \rangle$ from perfect samples
 - 3.3.4. Maximum-likelihood estimation of $\langle \Gamma^k \rangle$ and $\langle D \rangle$ in the case of missed levels
 - 3.3.5. Spin assignment for given resonance areas with Bayes' theorem
 - 3.3.6. Monte Carlo generation of level sequences
 - 3.3.7. Test statistics for purity of level sequences
- 4. Concluding remarks
- References

1. INTRODUCTION

This review on the practical applications of resonance theory originated from lecture notes distributed at a course organised by IAEA (Ref. 1).

The basic reaction formalism, in particular R-matrix theory, will be assumed to be known but we shall not hesitate to retrace the practically important parts of the theory. Although the basic principles of resonance theory are rather simple the general expressions can look quite formidable. A certain amount of repetition may help the reader to overcome this initial barrier and to realize that for practical work only few but thoroughly understood key formulae are needed.

We shall be concerned mainly with compound resonances, those prominent features of particle- and phonon-induced nuclear reactions which are due to excitation of relatively long-lived (quasi-stationary) states of the compound system. At low bombarding energies they appear fairly well separated, but as the energy increases their spacings decrease and their widths increase. Finally the overlap washes out all compound resonance structure and only broader structures like the single-particle or size resonances described by the optical model survive.

The more nucleons belong to the compound system the finer is the compound resonance structure. Typical level spacings observed in neutron reactions are of the order

- MeV for the lightest,
- keV for medium-mass and
- eV for the heaviest nuclei.

2. ANALYSIS OF RESONANCE DATA

The importance of resonance reactions for nuclear technology is obvious. Interpretation and prediction of reactor properties such as

- resonance absorption,
- resonance escape probability,
- resonance self-shielding
- temperature-dependent reactivity (Doppler coefficient)

require both a detailed understanding of resonance cross sections and comprehensive, machine-readable resonance data files.

2.1 The various steps in the preparation of resonance data for applications

The resonance data for reactor calculations and other applications (e.g. as cross section standards) are usually produced in several steps.

- (1) Measurement: Experimenters take data at pulsed accelerators or with the help of nuclear explosions. The time-of-flight technique is employed to cover broad energy ranges with high resolution and under exactly the same experimental conditions for all energies, isotopically pure or highly enriched samples to get reliable isotopic assignments and, in the most advanced experiments, polarized neutrons and targets to get reliable spin assignments for the observed resonances.

- (2) Reduction of raw data: Constant and time-dependent backgrounds are subtracted, sample impurities are corrected for, and, in the case of partial cross section (yield) data, flux and detector efficiency are factorised out.
- (3) Analysis of clean data: Resonance parameters ($E_0, \Gamma_n, \Gamma_\gamma, \Gamma_f, \dots, J\pi$) and potential-scattering parameters (R', \dots) are extracted. At the same time instrumental resolution and (except for transmission data) multiple scattering are accounted for.
- (4) Data evaluation: Resonance parameters from all available sources are collected by evaluators who try to understand and to reconcile the discrepancies. Gaps are filled with the help of level statistics, nuclear models and systematics. The complete sets of recommended cross section parameters ($E_0, \Gamma_n, \Gamma_\gamma, \Gamma_f, \dots, J\pi; R', \dots$) and the deduced level statistical parameters ($D_J, S_\ell, R_\ell^{\text{ex}}, \Gamma_{\gamma, \ell}, \Gamma_{f, J\pi}, \dots$) are put into a machine-readable (card, tape or disk) file.
- (5) Generation of group constants: Doppler-broadened point cross sections for various temperatures and all energetically possible reactions can now be calculated from the evaluated cross section parameters and averaged in a special way over relatively large energy intervals. The result is a set of group cross sections and self-shielding factors suitable as input for reactor codes.

International coordination

All these steps require time and years may pass before resonance data needed for technological applications become available in the required form of machine-readable evaluated data files. The great effort to speed up this process and to coordinate the work on an international scale is described for instance in Ref. 2. It may suffice here to mention that regional and international nuclear data committees (INDC, NEANDC, ...) collect and screen formal requests for data which are periodically published by IAEA/NDS in WRENDA, the World Request List for Nuclear Data. Measured data are collected by data centres, neutron data in particular by the four-centre network consisting of

- NNDC (National Nuclear Data Centre)
at Brookhaven, servicing the US and Canada,
- CCDN (Centre de Compilation de Données Neutroniques,
NEA Data Bank)
at Saclay, France, servicing the non-American OECD
countries,
- CJD (Centr po Jadernym Dannym)
at Obninsk, servicing the Soviet Union, and
- NDS (Nuclear Data Section, IAEA)
in Vienna, servicing all other countries.

Regular data exchange ensures that the data base is essentially the same at all four centres. Evaluated data are also collected, the most important evaluated files being

- ENDF, the US Evaluated Nuclear Data File,
- UKNDL, the UK Nuclear Data Library,
- KEDAK, the German file Kerndaten Karlsruhe,
- SOKRATOR, the USSR file.

Moreover, the Four Centres produce periodically such widely used handbooks as the Computer Index of Neutron Data (CINDA) (Ref. 3) or the "barn book" BNL 325 (Ref. 4) which contains resonance parameters and cross section plots.

Associated computer programs, for instance resonance analysis programs or codes generating cross sections from resonance parameters, are collected and distributed to requestors by the

- US Code Center at ANL, USA;
- CPL, the Computer Program Library, NEA Data Bank at Saclay (formerly at Ispra)
- RSIC, the Radiation Shielding Information Center at Oak Ridge, USA.

Information as to where other types of data and programs are available can be obtained from NDS/IAEA, Vienna.

2.2 Why parametrise?

Practically all resonance cross section data that go into reactor calculations (in group constant form or directly, e.g. in Monte Carlo calculations) are generated from resonance parameters. It might be asked why one cannot use the best measured high-resolution cross sections directly and thus eliminate the need for resonance parameter extraction. There are several reasons:

- (1) Resonance parameters along with consequent utilisation of resonance theory enable us to represent the often staggering detail of cross section structure by relatively few numbers.

Example: The 400 presently known resonances of the compound system $^{238}\text{U}+n$ are specified by 1600 parameters (E_0 , Γ_n , Γ_γ , $J\pi$ for each level) whereas a reasonably accurate point-wise representation of the capture and the scattering cross section requires about $2 \cdot 10^4$ data points, i.e. $4 \cdot 10^4$ numbers. If one considers also angular distributions and different temperatures one gets easily several 10^6 cross section points that would be needed to describe the behaviour of ^{238}U in a fast reactor.

- (2) Temperature broadening of resonances is often more easily calculated in terms of resonance parameters than from point data.
- (3) Resonance parameters and an inherently unitary cross section formalism such as R-matrix theory guarantee consistency with physical limits such as the unitarity limits for the total cross section in each reaction channel ($0 < \sigma_c < 4\pi\lambda_c^2 g_c$ where g_c is the spin factor, see below) or Wick's limit for scattering in the forward direction ($d\sigma_{cc}(0)/d\Omega_c \geq \sigma_c^2 / (4\pi\lambda_c)^2$).

Another consistency is more subtle but practically at least equally important, especially for the calculation of self-shielded group cross sections. Theory tells us that there is a very rigid relationship between the line shape in one reaction channel and the line shape corresponding

to the same compound level in other channels. This relationship is guaranteed if cross sections are generated from a coherent set of resonance parameters, but not with measured data.

- (4) At least equally important is the fact that even the best measured resonance data are affected by resolution and Doppler broadening and (except transmission data) by multiple scattering. The most reliable way to correct for these effects is full-scale resonance parameter analysis of the data.
- (5) Extrapolation into the region of non-measured or unresolved resonances by level-statistical (Hauser-Feshbach) cross section calculations require statistical parameters such as average level spacings and strength functions. These in turn must be estimated from resonance parameters.

2.3 Practical resonance formalisms

In applications-oriented neutron resonance work and especially in evaluated neutron data files the following formalisms are used almost exclusively.

- BB (Blatt-Biedenharn formalism),
- SLBW (single-level Breit-Wigner formulae),
- MLBW (multi- " " " "),
- RM (" " Reich-Moore "),
- AA (" " Adler-Adler "),

The first one is quite general. It shows how cross sections can be expressed in terms of the unitary, symmetric collision matrix with special emphasis on angular distributions and the influence of particle spins. It can be combined with any of the other four which provide different approximations to the collision matrix.

In the following sections the notation of the comprehensive review written by Lane and Thomas (Ref. 5) will be used.

2.3.1 The Blatt-Biedenharn formalism

We remember that in reaction theory one employs the concept of reaction channels which are fully specified by

- α , the partition into reaction partners, e.g. $^{235}\text{U}+n$ or $^{236}\text{U}+\gamma$,
- J , the total angular momentum in units of \hbar ,
- ℓ , the orbital " " " " \hbar ,
- s , the channel spin " " " " \hbar ,

with $\vec{J} = \vec{\ell} + \vec{s}$, i.e. $|\ell - s| \leq J \leq \ell + s$, (1)

$\vec{s} = \vec{I} + \vec{i}$, i.e. $|I - i| \leq s \leq I + i$, (2)

where I and i are the spins of the (two) collision partners. Total energy, total angular momentum and parity are conserved quantities in nuclear reactions, therefore the Hamilton operator can be taken as real, symmetric and invariant under rotations and spatial reflections.

We further remember that for spinless, neutral particles one can solve the Schrödinger equation for the boundary condition "ingoing plane wave + outgoing spherical wave" with the result that the differential cross section for elastic scattering is given by

$$d\sigma_{\alpha\alpha} = \pi\lambda_\alpha^2 \left| \sum_{\ell=0}^{\infty} (2\ell+1)(1-U_\ell) P_\ell(\cos\theta) \right|^2 \frac{d\Omega}{4\pi} \quad (3)$$

where P_ℓ is the ℓ -th order Legendre polynomial (angular-momentum eigenfunction). The sum ℓ terms with $\ell=0,1,2,3,\dots$ are said to belong to the s-, p-, d-, f-,... wave, a nomenclature taken over from atomic spectroscopy. The collision function U_ℓ describes the modification of the ℓ -th outgoing partial wave relative to the case without interaction, its absolute value giving the reduction in amplitude, its argument the phase shift. With $P_\ell P_{\ell'} = \sum_L (\ell\ell'00, L0)^2 P_L$, where $(\ell\ell'00, L0)$ is a Clebsch-Gordan coefficient (vanishing unless $|\ell-\ell'| \leq L \leq \ell+\ell'$ and $(-)^{\ell+\ell'+L} = (-)^L$), one can write this as a simple expansion in Legendre polynomials,

$$d\sigma_{\alpha\alpha} = \lambda_\alpha^2 \sum_{L=0}^{\infty} B_L P_L(\cos\theta) d\Omega, \quad \text{with} \quad (4)$$

$$B_L = \frac{1}{4} \sum_{\ell, \ell'} (2\ell+1)(2\ell'+1)(\ell\ell'00, L0)^2 (1-U_\ell^*)(1-U_{\ell'}), \quad (5)$$

Blatt and Biedenharn (Ref. 6) worked out the generalisation for particles with spins and for partition-changing (rearrangement) collisions. For zero Coulomb interaction they obtained

$$d\sigma_{\alpha\alpha'} = \frac{\lambda_\alpha^2}{(2i+1)(2I+1)} \sum_{s, s'} \sum_{L=0}^{\infty} B_L(\alpha s, \alpha' s') P_L(\cos\theta) d\Omega \quad (6)$$

$$B_L(\alpha s, \alpha' s') = \frac{(-)^{s-s'}}{4} \sum_{J_1, J_2} \sum_{\ell_1, \ell_2} \sum_{\ell'_1, \ell'_2} \bar{Z}(\ell_1, J_1, \ell_2, J_2, s, L) \bar{Z}(\ell'_1, J_1, \ell'_2, J_2, s', L) \cdot (\delta_{\alpha\alpha'} \delta_{\ell_1 \ell'_1} \delta_{s s'} - U_{\alpha \ell_1 s, \alpha' \ell'_1 s'}^{J_1})^* (\delta_{\alpha\alpha'} \delta_{\ell_2 \ell'_2} \delta_{s s'} - U_{\alpha \ell_2 s, \alpha' \ell'_2 s'}^{J_2}), \quad (7)$$

$$\bar{Z}(\ell_1, J_1, \ell_2, J_2, s, L) = \sqrt{(2\ell_1+1)(2\ell_2+1)(2J_1+1)(2J_2+1)} \cdot (\ell_1 \ell_2 00, L0) W(\ell_1, J_1, \ell_2, J_2, s, L), \quad (8)$$

where $W(\ell_1, J_1, \ell_2, J_2, s, L)$ is a Racah coefficient (see e.g. Ref. 7). Our phase convention for the \bar{Z} is that of Ref. 5, a slightly different convention is used in the \bar{Z} -coefficient tabulation Ref. 8. The \bar{Z} coefficients vanish unless the triangle conditions for the vector sums

$$\vec{\ell}_1 + \vec{\ell}_2 = \vec{L} = \vec{\ell}'_1 + \vec{\ell}'_2, \quad (9)$$

$$\vec{\ell}_i + \vec{s} = \vec{J}_i = \vec{\ell}'_i + \vec{s}' \quad (i = 1, 2) \quad (10)$$

are fulfilled. Parity conservation in nuclear reactions demands that $(-)^{\ell_i} \Pi_\alpha = \Pi_i = (-)^{\ell_i} \Pi_{\alpha'}$, where $\Pi_\alpha, \Pi_{\alpha'}$ are the eigen-parities of the in- and outgoing particles (positive for neutrons, protons and alpha-particles) and Π_i is the parity of the compound system with total angular momentum J_i ($i = 1, 2$).

If there is Coulomb interaction between the collision partners additional terms must be included (see Ref. 5).

Let us now integrate Eq. 6 over all angles. Because all terms with $L > 0$ vanish due to the orthogonality of the P_L and because of

$$\bar{Z}(\ell_1 J_1 \ell_2 J_2, s_0) = (-)^{J_1 + s} \sqrt{2J_1 + 1} \delta_{J_1 J_2} \delta_{\ell_1 \ell_2} \quad (11)$$

(cf. Ref. 7) one finds

$$\sigma_{\alpha\alpha'} = \pi \lambda_\alpha^2 \sum_J \sum_{\ell, \ell'} \sum_{s, s'} \mathcal{E}_J \left| \delta_{\alpha\alpha'} \delta_{\ell\ell'} \delta_{ss'} - U_{\alpha\ell s, \alpha'\ell's'}^J \right|^2 \quad (12)$$

where

$$\mathcal{E}_J = \frac{2J+1}{(2i+1)(2I+1)} \quad (13)$$

is the so-called spin factor.

We shall not go into the details of angular distributions but point out that they show interference between different partial waves, e.g. s- and p-wave interference, whereas angle-integrated cross sections do not. The latter are simple sums over terms with given ℓ and s without mixed terms. Nevertheless, a certain connexion exists between different partial waves provided they can excite the same compound states. As mentioned already the compound system and its quasi-stationary states are characterised, apart from energy, by the total angular momentum J and the parity Π . Table 1 shows, for given target spin I and positive target parity, the possible combinations of ℓ, s and J if the incident particles have spin $i = 1/2$. (If the target parity is negative all signs in the table must be reversed.)

We see that certain $J\Pi$ values can be formed through more than one channel if $\ell > 0$ and $I > 0$. If $I\Pi = 1/2+$, for instance, resonances with $J\Pi = 1-$ can be excited by the two p-waves ($\ell=1$) with $s=0$ and $s=1$, and the $2+$ levels can be excited by the two d-waves ($\ell=2$) with $s=0$ and $s=1$. The SLBW neutron widths (see below) of $1-$ and $2+$ levels are therefore sums of two partial widths, for $s=0$ and $s=1$. For $I\Pi = 1+$ the $1/2+$ levels can even be excited by two partial waves with different ℓ (s-wave with $s=1/2$, d-wave with $s=3/2$), while the $3/2+$ levels are accessible to three partial waves, the s-wave with $s=3/2$ and the two d-waves with $s=1/2$ and $s=3/2$, etc.

This means that the same resonances (with the same total widths) may show up in channels with different ℓ and s if the spin and parity selection rules allow this. In this context it should be understood that the term s- or p-wave resonance actually means that the resonance can be excited by the s- or p-wave but possibly also by the next higher partial wave with the same parity. As an

example the $3/2+$ s-wave resonance peaks of a target nucleus with $\Pi_0=1+$ contain also a d-wave component. The fact that certain d-, f- etc. resonance sequences are masked by s-, p- etc. sequences, respectively, must be kept in mind if the J-dependence of level densities is discussed and compared to resonance data. Finally we note that the sum of all spin factors for a given ℓ is always equal to $2\ell+1$ as shown in the table.

Table 1: Possible combinations of target spin I, orbital angular momentum ℓ and channel spin s resulting in total spin and parity $J\Pi$ and spin factor g for positive target parity Π_0 and incident particles with spin $1/2$:

Π_0	ℓ	s	$J\Pi$	g	$\sum g$	spectroscopic symbol
0+	0	1/2	1/2+	1	1	s
	1	1/2	1/2-, 3/2-	1, 2	3	p
	2	1/2	3/2+, 5/2+	2, 3	5	d
		etc.				
1/2+	0	0	0+	1/4	}1	s
		1	1+	3/4		
	1	0	1-	3/4	}3	p
		1	0- 1- 2-	1/4, 3/4, 5/4		
	2	0	2+	5/4	}5	d
		1	1+ 2+ 3+	3/4, 5/4, 7/4		
		etc.				
1+	0	1/2	1/2+	1/3	}1	s
		3/2	3/2+	2/3		
	1	1/2	1/2-, 3/2-	1/3, 2/3	}3	p
		3/2	1/2-, 3/2-, 5/2-	1/3, 2/3, 3/3		
	2	1/2	3/2+, 5/2+	2/3, 3/3	}5	d
		3/2	1/2+, 3/2+, 5/2+, 7/2+	1/3, 2/3, 3/3, 4/3		
		etc.				

2.3.2 The practically important R-matrix formulae

The angle-integrated cross section $\sigma_{\alpha\alpha'}$, Eq. 12, is a sum over partial cross sections $\sigma_{cc'}$, summed over all those entrance channels $c = \{\alpha J \ell s\}$ and exit channels $c' = \{\alpha' J \ell' s'\}$ which lead from partition α to partition α' . In slightly simplified notation we can write

$$\sigma_{cc'} = \pi \lambda_c^2 g_c |\delta_{cc'} - U_{cc'}|^2. \quad (14)$$

The collision matrix U is **symmetric** (because the Hamiltonian is invariant under time reversal) and **unitary** (because the total probability for transitions into exit channels is equal to unity).

Due to the unitarity of U one gets for the total cross section

$$\sigma_c = \sum_{c'} \sigma_{cc'} = 2\pi \lambda_c^2 g_c (1 - \text{Re } U_{cc}) \quad , \quad (15)$$

while the symmetry of U yields the reciprocity relation for the cross section $\sigma_{c'c}$ describing the inverse reaction,

$$\frac{\sigma_{c'c}}{g_{c'} \lambda_{c'}^2} = \frac{\sigma_{cc'}}{g_c \lambda_c^2}. \quad (16)$$

These equations are quite general. The wave length $2\pi\lambda_c$ is that corresponding to the total kinetic energy in the centre-of-mass system, $\lambda_c = \lambda_{\alpha} = \pi / (\mu_c v_{\text{rel}})$, where μ_c is the reduced mass and v_{rel} the relative speed. It should be noted that σ_c being a linear function of U is easier to calculate and to average etc. than $\sigma_{cc'}$.

Next we invoke R-matrix theory. It teaches us that one can express the collision matrix either in terms of the channel matrix (resonance parameter matrix) R ,

$$\begin{aligned} U_{cc'} &= e^{-i(\phi_c + \phi_{c'})} P_c^{1/2} \{ [1 - R(L-B)]^{-1} [1 - R(L^* - B)] \}_{cc'} P_{c'}^{-1/2} \\ &= e^{-i(\phi_c + \phi_{c'})} \{ \delta_{cc'} + 2i P_c^{1/2} [(1 - RL^0)^{-1} R]_{cc'} P_{c'}^{1/2} \}, \quad (17) \end{aligned}$$

$$R_{cc'} = \sum_{\lambda} \frac{\gamma_{\lambda c} \gamma_{\lambda c'}}{E_{\lambda} - E} \quad , \quad (18)$$

$$L_{cc'}^0 \equiv (L-B)_{cc'} = L_c^0 \delta_{cc'} = (L_c - B_c) \delta_{cc'} \equiv (S_c + iP_c - B_c) \delta_{cc'} \quad (19)$$

or, alternatively, in terms of the level matrix A ,

$$U_{cc'} = e^{-i(\phi_c + \phi_{c'})} (\delta_{cc'} + i \sum_{\lambda, \mu} \Gamma_{\lambda c}^{1/2} A_{\lambda \mu} \Gamma_{\mu c'}^{1/2}) \quad , \quad (20)$$

$$\Gamma_{\lambda c}^{1/2} = \gamma_{\lambda c} \sqrt{2P_c} \quad , \quad (21)$$

$$(A^{-1})_{\lambda \mu} = (E_{\lambda} - E) \delta_{\lambda \mu} - \sum_c \gamma_{\lambda c} L_c^0 \gamma_{\mu c} \quad . \quad (22)$$

Here ϕ_c is the potential-scattering phase, S_c and P_c are level shift factor and centrifugal-barrier penetrability, B_c is the arbitrary boundary constant at the channel radius, E_{λ} an energy eigenvalue (resonance energy), $\gamma_{\lambda c}$ a reduced width amplitude and $\Gamma_{\lambda c}$ the corresponding partial width. Roman subscripts refer to reaction channels, Greek subscripts to compound levels. We mention here that in applied work all energies, resonance widths etc. are given in the laboratory system, i. e. in the reference frame in which the target nucleus is at rest.

It is useful to remember that ϕ_c and L_c depend only on the values of the precisely known in- or outgoing radial wave functions I_c and O_c at the channel radius a_c ,

$$\phi_c = \arg O_c(a_c) = \arctan \frac{\text{Im } O_c(a_c)}{\text{Re } O_c(a_c)}, \quad (23)$$

$$L_c = a_c \frac{O'_c(a_c)}{O_c(a_c)} = a_c \left(\frac{\partial}{\partial r_c} \ln O_c \right)_{r_c=a_c} \quad (24)$$

For neutral particles one has, with $k_c \equiv 1/\lambda_c$,

$$O_c = I_c^* = ik_c r_c h_\ell^{(1)}(k_c r_c) (\approx i^{-\ell} e^{ik_c r_c} \text{ for } k_c r_c \gg \sqrt{\ell(\ell+1)}), \quad (25)$$

where $h_\ell^{(1)}$ is a spherical Hankel function of the first kind. With the recursion relations for spherical cylinder functions (cf. e.g. Ref. 5) one gets Table 2.

Table 2: Channel wave functions and related quantities for neutral particles
($\rho \equiv k_c r_c$, $\alpha \equiv k_c a_c$)

ℓ	O_c	ϕ_c	S_c	P_c
0	$e^{i\rho}$	α	0	α
1	$e^{i\rho} \left(\frac{1}{\rho} - i \right)$	$\alpha - \arctan \alpha$	$\frac{1}{\alpha^2 + 1}$	$\frac{\alpha^3}{\alpha^2 + 1}$
2	$e^{i\rho} \left(\frac{3}{\rho^2} - \frac{3i}{\rho} - 1 \right)$	$\alpha - \arctan \frac{3\alpha}{3 - \alpha^2}$	$\frac{3(\alpha^2 + 6)}{\alpha^4 + 3\alpha^2 + 9}$	$\frac{\alpha^5}{\alpha^4 + 3\alpha^2 + 9}$
	etc.			

Note that $S_c = 0$ for $\ell = 0$, so that one can choose $B_c = S_c = 0$ which simplifies all s-wave formulae. S_c and P_c for photon and fission channels are usually taken as constant.

The basic resonance parameters E_λ , $\gamma_{\lambda c}$ depend on the very complicated nuclear interaction and can therefore normally not be calculated. In most technological applications they are just fit parameters of the theory. Depending on the choice of B_c they can be real and constant or complex and energy-dependent.

The Wigner-Eisenbud version of R-matrix theory (Ref. 9) is obtained if the boundary quantities B_c are chosen as real constants. Then the resonance parameters E_λ and $\gamma_{\lambda c}$ are also real and constant, and the energy dependence of U is exclusively due to ϕ_c and L_c^O , i.e. it is explicitly specified. This renders the Wigner-Eisenbud version the most suitable formalism for most purposes. A major problem, however, is the required inversion of either a channel matrix ($1 - RL^O$ in Eq. 17) or a level matrix (A^{-1} in Eq. 22). In practice it is overcome by various approximations to the level matrix A^{-1} as we shall see below.

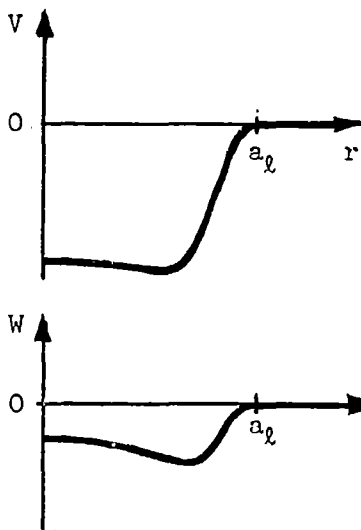
The Kapur-Peierls version of R-matrix theory (Ref. 10) is obtained with the choice $B = L$, i.e. $L^0 = 0$. This removes the matrix inversion problem completely ($1 - RL^0 = 1$) but leads to complex $E_\lambda, \gamma_{\lambda C}$ which implicitly depend on energy in a rather obscure way. Nevertheless formulae of the Kapur-Peierls type are convenient in narrow energy ranges, for instance for Doppler broadening.

The R-matrix equations reviewed so far are practically all that is needed in applied work from the whole apparatus of resonance theory. They should be thoroughly understood, however, and experience shows that this is not easy for the beginner. He might therefore wish to look at a simple illustration which shows the essential steps in the development of R-matrix theory and exhibits the meaning of the various quantities without the complexities of spin algebra and matrix notation. The more experienced reader can immediately go to Sect. 2.3.4.

2.3.3 Illustration: R-matrix formulation of single-particle interaction with a complex potential

(1) Schrödinger equation and boundary conditions:

Consider the interaction of a spinless, neutral particle with a spherical complex potential $V+iW$. From the Schrödinger equation



$$\left(\frac{-\hbar^2}{2m} \nabla^2 + V + iW\right)\psi = E\psi \quad (26)$$

one finds with the usual partial-wave expansion in Legendre polynomials,

$\psi = \sum_{\ell} u_{\ell}(r)P_{\ell}(\cos\theta)/r$, the radial wave equation

$$u_{\ell}'' + \left[k^2 - \frac{2m}{\hbar^2}(V+iW) - \frac{\ell(\ell+1)}{r^2}\right]u_{\ell} = 0. \quad (27)$$

($E = \hbar^2 k^2 / (2m)$). The boundary conditions

$$u_{\ell}(0) = 0, \quad u_{\ell}(r) = I_{\ell} - U_{\ell} O_{\ell} \quad \text{for } r \geq a_{\ell} \quad (28)(29)$$

follow from the requirements that probabilities, i.e. $|\psi|^2$, remain finite and that outside the range of the potential (which is assumed to vanish for radial separations $r \geq a_{\ell}$) one has incoming and outgoing spherical waves I_{ℓ}, O_{ℓ} , where the outgoing wave O_{ℓ} is modified, relative to

Fig. 1

the case without interaction, by a complex factor U_{ℓ} , the collision function. The channel wave functions I_{ℓ}, O_{ℓ} are given by Eq. 25. Note that in our example a channel is completely specified by the orbital (or, since $\ell = J$, the total) angular momentum.

(2) Orthogonal base in the internal region ($r \leq a_{\ell}$)

Next we introduce, for each ℓ , a base of real, orthogonal functions $u_{\lambda\ell}$ by demanding

$$u_{\lambda\ell}'' + \left[k_{\lambda}^2 - \frac{2m}{\hbar^2}V - \frac{\ell(\ell+1)}{r^2}\right] u_{\lambda\ell} = 0, \quad (r \leq a_{\ell}) \quad (30)$$

$$u_{\lambda\ell}(0) = 0, \quad a_{\ell} u'_{\lambda\ell}(a_{\ell}) = B_{\ell} u_{\lambda\ell}(a_{\ell}), \quad (31) (32)$$

where B_ℓ , the boundary parameter, is seen to be essentially the logarithmic derivative of the internal eigenfunctions $u_{\lambda\ell}$ at the channel radius a_ℓ . Compare the similar definition of L_ℓ in terms of external wave functions, Eq. 24. Since we omitted the imaginary part of the potential in the differential equation (30) everything becomes real, including the eigenfunctions, if we choose B_ℓ real. (Similarly the self-adjoint Hamiltonian in the general theory leads to real eigenfunctions for real B_c .) The orthogonality of the eigenfunctions is checked as follows. The wave equation (30) yields

$$\int_0^{a_\ell} dr (u''_{\lambda\ell} u_{\mu\ell} - u_{\lambda\ell} u''_{\mu\ell}) = (k_\mu^2 - k_\lambda^2) \int_0^{a_\ell} dr u_{\lambda\ell} u_{\mu\ell}$$

$$= u'_{\lambda\ell}(a_\ell) u_{\mu\ell}(a_\ell) - u_{\lambda\ell}(a_\ell) u'_{\mu\ell}(a_\ell). \quad (33)$$

The integration by parts leading to the last line corresponds to the application of Green's theorem in the general R-matrix case. The whole expression vanishes because of the boundary condition (32). This proves the orthogonality, i.e.

$$\int_0^{a_\ell} dr u_{\lambda\ell} u_{\mu\ell} = a_\ell \delta_{\lambda\mu}, \quad (34)$$

where the normalisation constant a_ℓ ensures the correct dimensions.

(3) Surface equation

We can now expand the true wave function inside the interaction sphere as follows

$$u_\ell = \sum_\lambda c_{\lambda\ell} u_{\lambda\ell} \quad (r \leq a_\ell) \quad (35)$$

with
$$c_{\lambda\ell} = \frac{1}{a_\ell} \int_0^{a_\ell} dr u_{\lambda\ell} u_\ell. \quad (36)$$

Specific information about the last integral, i.e. about the expansion coefficients $c_{\lambda\ell}$, must come from the wave equations and boundary conditions. We employ the same procedure that we just used to study the quite similar orthogonality integral. From the wave equations (27), (30) we get

$$\int_0^{a_\ell} dr (u''_\ell u_{\lambda\ell} - u_\ell u''_{\lambda\ell}) = (k_\lambda^2 - k_\ell^2 + i \frac{2m}{\hbar^2} \bar{W}_\lambda) \int_0^{a_\ell} dr u_\ell u_{\lambda\ell} \quad (37)$$

where
$$\bar{W}_\lambda \equiv \frac{\int_0^a dr u_\ell u_{\lambda\ell} W}{\int_0^a dr u_\ell u_{\lambda\ell}} \quad (38)$$

is a volume average over the absorptive potential. Integrating by parts ("Green's theorem") and using the boundary conditions (Eqs. 28, 31, 32) one finds

$$[a_\ell u'_\ell(a_\ell) - B_\ell u_\ell(a_\ell)] u_{\lambda\ell}(a_\ell) = \frac{2m}{\hbar^2} (E_\lambda - E - i \bar{W}_\lambda) a_\ell^2 c_\ell \quad (39)$$

where $E_\lambda = \hbar^2 k_\lambda^2 / (2m)$. Inserting c_ℓ from this equation in the expansion (35) one obtains

$$u_\ell = R_\ell (a_\ell u'_\ell - B_\ell u_\ell) \quad \text{for } r = a_\ell, \quad (40)$$

where
$$R_\ell \equiv \sum_\lambda \frac{\gamma_{\lambda\ell}^2}{E_\lambda - E - i \Gamma_{\lambda a} / 2} \quad (41)$$

with
$$\gamma_{\lambda\ell} \equiv \sqrt{\frac{\hbar^2}{2ma_\ell^2}} u_{\lambda\ell}(a_\ell), \quad \Gamma_{\lambda a} \equiv -2\bar{W}_\lambda. \quad (42)(43)$$

The "surface equation" (40) is the analogue of the matrix equation $V=R(D-BV)$ of the general theory which connects the "value" and "derivative quantities" V and D at the surface by means of the R matrix. Eq. (42) shows that the reduced width amplitudes $\gamma_{\lambda\ell}$ are essentially the values of the eigenfunctions at the channel radius.

(4) R-function expression for the collision function

Our ultimate goal is an expression of the collision function U_ℓ (from which the cross sections can be calculated) free of the unknown quantities u'_ℓ and u_ℓ . In general this requires matching of the external and internal wave functions at $r=a_\ell$. With the surface equation this is surprisingly easy. We simply replace the internal quantities in Eq. 40 by the channel quantities I_ℓ and O_ℓ with the help of the matching conditions,

$$r=a_\ell: \quad u_\ell = I_\ell - U_\ell O_\ell, \quad (44)$$

$$a_\ell u'_\ell = a_\ell (I'_\ell - U_\ell O'_\ell) = L_\ell^* I_\ell - U_\ell L_\ell O_\ell, \quad (45)$$

and solve for U_ℓ . The final result,

$$U_\ell = \frac{I_\ell}{O_\ell} \frac{1-R_\ell(L_\ell^*-B_\ell)}{1-R_\ell(L_\ell-B_\ell)} = e^{-2i\phi_\ell} \left(1 + \frac{2iR_\ell P_\ell}{1-R_\ell L_\ell^*} \right), \quad (46)$$

with R_ℓ given by Eq. 41, is the analogue of the general Eqs. 17, 18.

In contrast to the Wigner-Eisenbud R -matrix, Eq. 18, our R -function, Eq. 41, is complex. It looks, in fact, exactly like the reduced R -matrix of the Reich-Moore approximation (see below) where $\Gamma_{\lambda a}$ is the radiation width and originates from elimination of all photon channels λ^a by means of the Teichmann-Wigner prescription (Ref. 11) if the width amplitudes $\gamma_{\lambda c}$ of the eliminated channels are relatively small and have random signs. The absorptive potential W is thus equivalent to reactions leading from the entrance channel to other eliminated channels.

A more rigorous connexion with the theory of compound resonances is established as follows. One averages the collision matrix element U_{cc} over an energy interval that is so wide that it contains many compound levels but small enough that weak energy dependences (of λ , ϕ_ℓ , L_ℓ and of level statistics) can be neglected. With a Lorentzian weight function centered at E and having the width I (FWHM) one finds, because U_{cc} has no poles above the real axis,

$$\bar{U}_{cc}(E) = U_\ell(E) \text{ with } R_\ell(E) = R_{cc}(E+iI). \quad (47)(48)$$

Thus \bar{U}_{cc} is given by the optical-model expression (46), with R_ℓ replaced by R_{cc} evaluated at the complex energy $E+iI$. This means that the average total cross section can be calculated from the optical model. If in R_{cc} the summation over levels is replaced by an integration, and I is treated as a small quantity, one gets

$$R_{cc}(E+iI) \equiv R_c^\infty + i\pi s_c \quad (49)$$

with
$$s_c = \frac{\sqrt{\gamma_c^2}}{D_c} \quad (\text{pole strength function}), \quad (50)$$

$$R_c^\infty(E) = \oint_{-\infty}^{\infty} dE' \frac{s_c(E')}{E' - E} \quad (\text{distant-level parameter}), \quad (51)$$

where D_c is the average level spacing and \oint denotes Cauchy's principal value. At low energies ($E \rightarrow 0$) the effective potential-scattering radius that follows from Eqs. 33 and 36 is

$$R'_c = a_c (1 - R_c^\infty). \quad (53)$$

The strength function $S_{\ell J}$ normally used in applied work is related to s_c by

$$S_{\ell J} = 2k_c a_c s_c \sqrt{1eV/E}. \quad (54)$$

The important fact for us is that level-statistical quantities such as $\sqrt{\gamma_c^2}/D_c$ can be used to adjust the parameters of the optical potential.

(5) Square-well optical potential

For a little numerical exercise let us specialise to a three-dimensional complex square-well potential as in Fig. 2, with the same well radius a for the real and the imaginary part. The natural choice for the channel radii is $a_\ell = a$ for all ℓ .

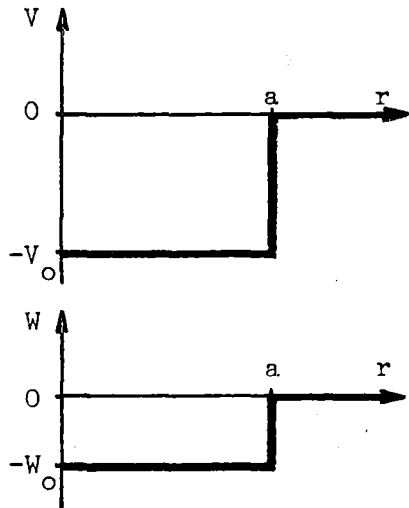


Fig. 2

The eigenfunctions for $r < a$ can now be expressed in terms of the spherical Bessel functions j_ℓ :

$$u_{\lambda \ell}(r) = K_\lambda r j_\ell(K_\lambda r) \quad \text{with} \quad K_\lambda^2 = \frac{2m}{\hbar^2} (E_\lambda - V_0). \quad (55)$$

$$(u_{\lambda 0}(r) = \sin K_\lambda r, u_{\lambda 1}(r) = \sin K_\lambda r / (K_\lambda r) - \cos K_\lambda r, \text{ etc.})$$

For the eigenvalues K_λ or E_λ one has, from Eq. 32,

$$\text{for } \ell=0 \quad B_0 \sin K_\lambda a = K_\lambda a \cos K_\lambda a \quad (56)$$

$$\text{for } \ell \geq 1 \quad B_\ell K_\lambda a j_\ell(K_\lambda a) = (K_\lambda a)^2 j_{\ell-1}(K_\lambda a) - \ell K_\lambda a j_\ell(K_\lambda a) \quad (57)$$

The last equation follows from the recursion relations for spherical Bessel functions. With $B_\ell = -\ell$, the choice suggested by Eqs. 42 and 43, one finds

$$\begin{aligned} \text{for } \ell=0 & \quad \cos K_\lambda a = 0, \text{ i.e. } E_\lambda = \left(\frac{2\lambda+1}{2}\pi\right)^2 \frac{\hbar^2}{2ma^2} - V_0, \quad \gamma_{\lambda 0}^2 = \frac{\hbar^2}{2ma^2}; \quad (58) \\ \text{for } \ell=1 & \quad \sin K_\lambda a = 0, \text{ i.e. } E_\lambda = (\lambda\pi)^2 \frac{\hbar^2}{2ma^2} - V_0, \quad \gamma_{\lambda 1}^2 = \frac{\hbar^2}{2ma^2}; \\ \text{for } \ell=2 & \quad \tan K_\lambda a = K_\lambda a \quad \text{etc.} \end{aligned}$$

As could be expected from an optical, i.e. wave-mechanical, model the eigenvalues correspond to certain simple ratios between the internal wave length $\Lambda = 2\pi/K$ and the diameter of the potential:

$$2a = \Lambda/2, 3\Lambda/2, 5\Lambda/2, \dots \quad \text{for } \ell=0,$$

$$2a = \Lambda, 2\Lambda, 3\Lambda, \dots \quad \text{for } \ell=1.$$

The $\gamma_{\lambda 0}^2$ and $\gamma_{\lambda 1}^2$ for the square well are the same for all λ and depend only on the range (a) of the real potential. Furthermore, Eqs. 43 and 38 show that $\Gamma_{\lambda a}/2 = W_0$ for all λ and ℓ .

Inserting numbers that are compatible with average neutron cross sections,

$$a = 1.4 \text{ fm} \cdot A^{1/3}, \quad V_0 = 50 \text{ MeV}, \quad W_0 = 3 \text{ MeV}$$

one gets for a heavy nucleus with $A = 238$ the resonance parameters of Table 3.

The scattering widths given in Table 3 are defined as usual by

$$\Gamma_{\lambda \ell}(E) = 2P_\ell(E)\gamma_{\lambda \ell}^2 = \Gamma_{\lambda \ell}(|E_\lambda|)P_\ell(E)/P_\ell(|E_\lambda|), \quad (59)$$

the absolute values ensuring the validity of this definition for subthreshold ("negative") single particle states ($E_\lambda < 0$) as well as for continuum states with $E_\lambda > 0$. The levels are rather broad, with total widths $\Gamma_{\lambda a} + \Gamma_{\lambda \ell}$ of about 10 MeV and spacings of about 30 MeV near threshold ($E=0$).

One can also compare with the neutron strength functions and effective radii observed in the region of resolved resonances ($E < 1 \text{ MeV}$) as a function of A (or a). For $E=0$ our model yields

$$R_\ell^\infty + i\pi s_\ell = \sum_\lambda \frac{\gamma_{\lambda \ell}^2 E_\lambda}{E_\lambda^2 + \Gamma_{\lambda a}^2/4} + i \sum_\lambda \frac{\gamma_{\lambda \ell}^2 \Gamma_{\lambda a}/2}{E_\lambda^2 + \Gamma_{\lambda a}^2/4}. \quad (60)$$

The maxima ("size resonances") of s_ℓ are seen to occur where $E_\lambda(a)=0$, i.e. at

$$\begin{aligned} a &= \frac{2\lambda+1}{2} \pi \frac{\hbar}{\sqrt{2mV_0}} \quad \text{for } \ell=0, \\ a &= \lambda\pi \frac{\hbar}{\sqrt{2mV_0}} \quad \text{for } \ell=1, \quad \text{etc.} \end{aligned} \quad (61)$$

With $a = 1.4 \text{ fm} A^{1/3}$, $V_0 = 50 \text{ MeV}$ one finds the size resonance positions that are listed in Table 4 together with the observed positions.

Table 3: Resonance parameters for a three-dimensional complex square-well potential with $a = 1.4 \text{ fm } A^{1/3}$, $A = 238$, $V+iW = \begin{cases} -(50+3i)\text{MeV} & \text{for } r \leq a, \\ 0 & \text{for } r > a. \end{cases}$

ℓ	spectroscopic symbol	E_λ (MeV)	$\gamma_{\lambda\ell}^2$ (MeV)	$2P_\ell(E_\lambda)$	$\Gamma_{\lambda\ell}(E_\lambda)$ (MeV)	$\Gamma_{\lambda a}$ (MeV)
0	1s	-49.32	0.275	26.77	7.37	6
	2s	-43.89	"	25.26	6.95	"
	3s	-33.02	"	21.91	6.03	"
	4s	-16.73	"	15.59	4.29	"
	5s	5.00	"	8.52	2.34	"
	6s	32.17	"	21.62	5.95	"
	etc.	"				
1	1p	-47.28	0.275	13.03	3.59	6
	2p	-39.14	"	11.84	3.26	"
	3p	-25.55	"	9.53	2.62	"
	4p	-6.54	"	4.68	1.29	"
	5p	17.91	"	7.94	2.19	"
	6p	47.78	"	13.10	3.61	"
	etc.					

Table 4: Size resonance peak positions

ℓ	spectroscopic symbol	nucleon number at peak	
		calculated ^{a)}	observed
0	3s	47	~55
	4s	129	~150
1	2p	24	~25
	3p	81	~90
	4p	193	~210

a) Eqs. 61 with $a = 1.4 \text{ fm } A^{1/3}$, $V = -50 \text{ MeV}$ for $r < a$.

This should suffice to show the use of level-statistical data in the adjustment of optical-model parameters. Let us now return to the discussion of the various resonance approximations.

2.3.4 The principal approximations to the inverse level matrix

A convenient starting point for the various practically important approximations is the inverse level matrix:

Wigner-Eisenbud representation (exact)

with B_c real and constant,

$$(A^{-1})_{\lambda\mu} = (E_\lambda - E)\delta_{\lambda\mu} - \sum_c \gamma_{\lambda c} L_c^O \gamma_{\mu c} \quad (20)$$

Kapur-Peierls representation (exact)

with $B_c = L_c$, i.e. $L_c^O = 0$,

$$(A^{-1})_{\lambda\mu} = (\mathcal{E}_\lambda - E)\delta_{\lambda\mu} \quad (62)$$

(eigenvalues \mathcal{E}_λ complex, E-dependent).

SLBW approximation

Only one level is retained,

$$(A^{-1})_{\lambda\mu} \rightarrow A^{-1} = E_0 - E - \sum_c L_c^O \gamma_{\lambda c}^2 \equiv E_0 + \Delta - E - i\Gamma/2 \quad (63)$$

(Δ : level shift, $\Gamma = \sum_c \Gamma_c$: total width, both E-dependent, real).

MLBW approximation

All off-diagonal elements are neglected,

$$(A^{-1})_{\lambda\mu} = (E_\lambda - E - \sum_c L_c^O \gamma_{\lambda c}^2)\delta_{\lambda\mu} \equiv (E_\lambda + \Delta_\lambda - E - i\Gamma_\lambda/2)\delta_{\lambda\mu} \quad (64)$$

(Δ_λ : level shift, $\Gamma_\lambda = \sum_c \Gamma_{\lambda c}$: total width, both E-dependent, real).

Reich-Moore approximation

Off-diagonal contributions from photon channels ($c \in \gamma$) are neglected,

$$(A^{-1})_{\lambda\mu} = (E_\lambda + \Delta_{\lambda\gamma} - E - i\Gamma_{\lambda\gamma}/2)\delta_{\lambda\mu} - \sum_{c \notin \gamma} \gamma_{\lambda c} L_c^O \gamma_{\mu c} \quad (65)$$

($\Delta_{\lambda\gamma}$: level shift caused by photon channels, $\Gamma_{\lambda\gamma} = \sum_{c \in \gamma} \Gamma_{\lambda c}$: radiation width).

Adler-Adler approximation

The energy dependence of L_c^O is neglected:

$$(A^{-1})_{\lambda\mu} = (E_\lambda - E)\delta_{\lambda\mu} - \sum_c \gamma_{\lambda c} \sqrt{L_c^O(E_\lambda)L_c^O(E_\mu)} \gamma_{\mu c} \quad (66)$$

It should be remembered that for $l=0$ everywhere, for $l \geq 1$ locally at a given energy, Δ_λ and $\Delta_{\lambda\lambda'}$ can be made to vanish in all these expressions, and that the P_c contain (at least) a factor \sqrt{E} for elastic channels (cf. Table 1) but are practically constant for fission and capture channels.

2.3.5 Kapur-Peierls cross section formulae

The Kapur-Peierls collision matrix is

$$U_{cc'} = e^{-i(\phi_c + \phi_{c'})} \left(\delta_{cc'} + i \sum_{\lambda} \frac{G_{\lambda c}^{1/2} G_{\lambda c'}^{1/2}}{\mathcal{E}_{\lambda} - E} \right) \quad (67)$$

where we write \mathcal{E}_{λ} , $G_{\lambda c} = 2P_c g_{\lambda c}^2$ to distinguish the complex eigenvalues and partial widths from their real Wigner-Eisenbud counterparts E_{λ} , $\Gamma_{\lambda c} = 2P_c \gamma_{\lambda c}^2$. The corresponding cross section expressions are, in a notation that is convenient for the discussion of Doppler broadening,

$$\begin{aligned} \sigma_c &= 4\pi\lambda_c^2 g_c \left[\sin^2 \phi_c + \sum_{\lambda} \frac{|G_{\lambda c}|}{\Gamma_{\lambda}} (\psi_{\lambda} \cos 2\phi_{\lambda} + \chi_{\lambda} \sin 2\phi_{\lambda}) \right] \\ &= 4\pi\lambda_c^2 g_c \left[\sin^2 \phi_c + \sum_{\lambda} \frac{\text{Re } G_{\lambda c}}{\Gamma_{\lambda}} (\psi_{\lambda} \cos 2\phi_c + \chi_{\lambda} \sin 2\phi_c) \right. \\ &\quad \left. + \sum_{\lambda} \frac{\text{Im } G_{\lambda c}}{\Gamma_{\lambda}} (\psi_{\lambda} \sin 2\phi_c - \chi_{\lambda} \cos 2\phi_c) \right], \quad (68) \end{aligned}$$

$$\begin{aligned} \sigma_{cc} &= 4\pi\lambda_c^2 g_c \left[\sum_{\lambda} \frac{|G_{\lambda c}|^2}{\Gamma_{\lambda}^2} (\psi_{\lambda} \text{Re } C_{\lambda cc} + \chi_{\lambda} \text{Im } C_{\lambda cc}) \right. \\ &\quad \left. + \sum_{\lambda} \left(-\frac{\text{Re } G_{\lambda c}}{\Gamma_{\lambda}} \psi_{\lambda} + \frac{\text{Im } G_{\lambda c}}{\Gamma_{\lambda}} \chi_{\lambda} \right) \right] + \sigma_c, \quad (69) \end{aligned}$$

$$\sigma_{cc'} = 4\pi\lambda_c^2 g_c \sum_{\lambda} \frac{|G_{\lambda c} G_{\lambda c'}|}{\Gamma_{\lambda}^2} (\psi_{\lambda} \text{Re } C_{\lambda cc'} + \chi_{\lambda} \text{Im } C_{\lambda cc'}), \quad (70)$$

with

$$\phi_{\lambda} = \phi_c - \arg g_{\lambda c} = \phi_c - \frac{1}{2} \arctan \frac{\text{Re } G_{\lambda c}}{\text{Im } G_{\lambda c}}, \quad (71)$$

$$C_{\lambda cc'} = 1 + \sum_{\mu \neq \lambda} \frac{g_{\mu c}}{g_{\lambda c}} \frac{g_{\mu c'}}{g_{\lambda c'}} \frac{i\Gamma_{\lambda}}{\mathcal{E}_{\lambda}^* - \mathcal{E}_{\mu}}, \quad (72)$$

$$\mathcal{E}_{\lambda} \equiv E_{\lambda} - i\Gamma_{\lambda}/2, \quad G_{\lambda c} = 2P_c g_{\lambda c}^2, \quad (73)(74)$$

and
$$\psi_\lambda = \frac{\Gamma_\lambda^2/4}{(E-E_\lambda)^2 + \Gamma_\lambda^2/4} \equiv \frac{1}{1+x_\lambda^2}, \quad (75)$$

$$x_\lambda = \frac{(E-E_\lambda)\Gamma_\lambda/2}{(E-E_\lambda)^2 + \Gamma_\lambda^2/4} = \frac{x_\lambda}{1+x_\lambda^2}. \quad (76)$$

zero-temperature
Voigt profiles

In the derivation of Eqs. 69 and 70 we used the partial-fraction decomposition

$$\frac{1}{\epsilon_\lambda - E} \frac{1}{\epsilon_\mu^* - E} = \frac{1}{\epsilon_\mu^* - \epsilon_\lambda} \left(\frac{1}{\epsilon_\lambda - E} - \frac{1}{\epsilon_\mu^* - E} \right). \quad (77)$$

It is thus seen that apart from the potential-scattering term $4\pi\kappa_c^2 g_c \sin^2 \phi_c$ all cross sections can be expressed by the symmetric (Lorentzian) and asymmetric Breit-Wigner line shape functions ψ_λ and x_λ with coefficients that contain a factor P_c (which in turn contains a factor $E^{-1/2}$) and are otherwise weakly energy-dependent. The line shape functions themselves are also slightly distorted because E_λ and Γ_λ are weakly energy-dependent. Note that $\Gamma_\lambda \neq \sum_c |\Gamma_{\lambda c}|$ in contrast to the Wigner-Eisenbud relationship $\Gamma_\lambda = \sum_c \Gamma_{\lambda c}$.

2.3.6 SLBW and MLBW cross section formulae

Rather than writing down the well-known SLBW formulae we go immediately to the MLBW case. The collision matrix obtained with Eq. 64 is

$$U_{cc'} = e^{-i(\phi_c + \phi_{c'})} \left(\delta_{cc'} + i \sum_\lambda \frac{\Gamma_{\lambda c}^{1/2} \Gamma_{\lambda c'}^{1/2}}{E_\lambda + \Delta_\lambda - E - i\Gamma_\lambda/2} \right). \quad (78)$$

Comparison with the Kapur-Peierls collision matrix (67) shows that we can take over the Kapur-Peierls cross section formulae with the change $E_\lambda \rightarrow E_\lambda + \Delta_\lambda$, $\Gamma_\lambda \rightarrow \sum_c \Gamma_{\lambda c}$, $\epsilon_{\lambda c} \rightarrow \gamma_{\lambda c}$. The result is

$$\sigma_c = 4\pi\kappa_c^2 g_c \left[\sin^2 \phi_c + \sum_\lambda \frac{\Gamma_{\lambda c}}{\Gamma_\lambda} (\psi_\lambda \cos 2\phi_c + x_\lambda \sin 2\phi_c) \right] \quad (79)$$

$$\sigma_{cc} = 4\pi\kappa_c^2 g_c \sum_\lambda \left[\frac{\Gamma_{\lambda c}^2}{\Gamma_\lambda^2} (\psi_\lambda \operatorname{Re} C_{\lambda cc} + x_\lambda \operatorname{Im} C_{\lambda cc}) - \frac{\Gamma_{\lambda c}}{\Gamma_\lambda} \psi_\lambda \right] + \sigma_c \quad (80)$$

$$\sigma_{cc'} = 4\pi\kappa_c^2 g_c \sum_\lambda \frac{\Gamma_{\lambda c} \Gamma_{\lambda c'}}{\Gamma_\lambda^2} (\psi_\lambda \operatorname{Re} C_{\lambda cc'} + x_\lambda \operatorname{Im} C_{\lambda cc'}), \quad (81)$$

with
$$C_{\lambda cc'} = 1 + \sum_{\mu \neq \lambda} \frac{\gamma_{\mu c}}{\gamma_{\lambda c}} \frac{i\Gamma_\lambda}{E_\lambda + \Delta_\lambda - E_\mu - \Delta_\mu + i(\Gamma_\lambda + \Gamma_\mu)/2} \frac{\gamma_{\mu c'}}{\gamma_{\lambda c'}} \quad (82)$$

The SLBW formulae are obtained by specialisation to a single level, with $C_{\lambda cc} = 1$. (The sum in Eq. 82 describes level-level interference.)

In contrast to the Kapur-Peierls and the SLBW collision matrices the MLBW collision matrix is not unitary. Therefore non-physical cross sections ($\sigma_c < 0$ or $\sigma_c > 4\pi\kappa_c^2 g_c$)

can occur, but for mild level overlap the MLBW approximation is quite good. In any case it is better than the very popular but often very bad approximation, sometimes termed "many-level Breit-Wigner approximation", that results from omission of the level-level interference sum in Eq. 82 and amounts to simply adding SLBW resonance terms (plus the potential-scattering term in σ_c and σ_{cc}).

The MLBW definition used in the US file ENDF (Ref. 12) is such that Eq. 80 is used for σ_{cc} but level-level interference is neglected by putting $C_{\lambda cc'} = 1$ for σ_{cc} . This is often justified because level-level interference is usually quite weak for capture (if not for fission or inelastic-scattering) cross sections. The total cross section must then be computed as the sum of all partial cross sections rather than from Eq. 79.

The MLBW approximation corresponds to the first term of the expansion

$$A = (D-N)^{-1} = D^{-1} + D^{-1}ND^{-1} + D^{-1}ND^{-1}ND^{-1} + \dots \quad (83)$$

of the level matrix in powers of the nondiagonal part $-N$ of its inverse,

$$N_{\lambda\mu} = (1-\delta_{\lambda\mu}) \sum_c \gamma_{\lambda c} L_c^O \gamma_{\mu c} \quad (84)$$

$$D_{\lambda\mu} = (E_\lambda + \Delta_\lambda - E - i\Gamma_\lambda/2) \delta_{\lambda\mu} \quad (85)$$

Retaining also the second term (Ref. 13) one gets an improved collision matrix,

$$U_{cc'} = e^{-i(\phi_c + \phi_{c'})} \left(\delta_{cc'} + i \sum_\lambda \frac{\Gamma_{\lambda c}^{1/2} W_{\lambda cc'} \Gamma_{\lambda c'}^{1/2}}{E_\lambda + \Delta_\lambda - E - i\Gamma_\lambda/2} \right) \quad (86)$$

with

$$W_{\lambda cc'} = 1 + \sum_{\mu \neq \lambda} \left(\frac{\gamma_{\mu c}}{\gamma_{\lambda c}} + \frac{\gamma_{\mu c'}}{\gamma_{\lambda c'}} \right) \frac{\sum_{c''} \gamma_{\lambda c''} L_{c''}^O \gamma_{\mu c''}}{E_\mu + \Delta_\mu - E - \Delta_\lambda - i(\Gamma_\mu - \Gamma_\lambda)/2} \quad (87)$$

Again one can take over the Kapur-Peierls cross section expressions with $E_\lambda \rightarrow E_\lambda + \Delta_\lambda$, $\Gamma_\lambda \rightarrow \sum_c \Gamma_{\lambda c}$, $G_{\lambda c} \rightarrow \Gamma_{\lambda c} W_{\lambda cc}$, $G_{\lambda c} G_{\lambda c'} \rightarrow \Gamma_{\lambda c} W_{\lambda cc'} \Gamma_{\lambda c'}$. The partial widths are now complex but the complex poles of the improved collision matrix, Eq. 85, are still the same as those of the MLBW collision matrix, Eq. 78. This is no longer true if higher-order terms of the von Neumann series Eq. 83 are retained as in Ref. 14.

2.3.7 The Reich-Moore cross section formulae

The inverse level matrix in Reich-Moore approximation, Eq. 65, is exactly what one would derive from a "reduced" R-matrix for particle channels only, with E_λ replaced by $E_\lambda + \Delta_\lambda - i\Gamma_{\lambda\gamma}/2$. In fact, exactly such a reduced R-matrix results if one eliminates the photon channels by means of the Teichmann-Wigner channel elimination method which is the usual way to derive the Reich-Moore formulae (Ref. 15). One can thus calculate all cross sections except that for radiative capture from Eqs. 14, 15 and 17 where R is to be taken as the reduced R-matrix

$$R_{cc'} = \sum_\lambda \frac{\gamma_{\lambda c} \gamma_{\lambda c'}}{\epsilon_{\lambda\gamma} - E} \quad (c, c' \neq \gamma) \quad (87)$$

with

$$\epsilon_{\lambda\gamma} = E_\lambda + \Delta_\lambda - i\Gamma_{\lambda\gamma}/2. \quad (88)$$

The capture cross section can be either calculated as difference,

$$\sigma_{c\gamma} = \sigma_c - \sum_{c' \neq \gamma} \sigma_{cc'} \quad , \quad (89)$$

or, according to Harris (Ref. 16) as

$$\sigma_{c\gamma} = \pi \lambda_c^2 g_c \sum_{\lambda} \Gamma_{\lambda\gamma} \left| \frac{\sum_{c' \neq \gamma} [(1-RL^0)^{-1}]_{cc'} \Gamma_{\lambda c'}^{1/2}}{\epsilon_{\lambda\gamma} - E} \right|^2 \quad . \quad (90)$$

The calculation is quite fast since double sums over levels as in MLBW approximation (cf. Eq. 81) are not needed. The inversion of the reduced matrix $1-RL^0$ is unproblematic since it is usually of rank 1, 2 or 3.

In the most frequent case the only open particle channel is the elastic channel and all matrices reduce to scalar functions. With the definitions

$$\rho_{cc} \equiv \frac{-iR_{cc} P_c}{1-R_{cc} L_c^0} = \frac{-i \sum_{\lambda} \frac{\Gamma_{\lambda c}/2}{\epsilon_{\lambda\gamma} - E}}{1 - \frac{L_c^0}{P_c} \sum_{\lambda} \frac{\Gamma_{\lambda c}/2}{\epsilon_{\lambda\gamma} - E}} \quad (91)$$

$$x \equiv \frac{\text{Im } \rho_{cc}}{\text{Re } \rho_{cc}} \quad , \quad y^2 \equiv \frac{|\rho_{cc}|^2}{\text{Re } \rho_{cc}} \quad (92) \quad (93)$$

one gets then expressions which have the formal (and in single-level situations the factual) SLBW form, viz.

$$\sigma_c = 4\pi \lambda_c^2 g_c (\sin^2 \phi_c + y^2 \frac{\cos 2\phi_c + x \sin 2\phi_c}{1+x^2}) \quad , \quad (94)$$

$$\sigma_{c\gamma} = 4\pi \lambda_c^2 g_c y^2 (1-y^2) \frac{1}{1+x^2} \quad . \quad (95)$$

For pure elastic scattering, $y^2=1$, one gets, of course, the exact single-channel R-function with

$$x^{-1} = \sum_{\lambda} x_{\lambda}^{-1} = \sum_{\lambda} \frac{\Gamma_{\lambda}/2}{E-E_{\lambda}} \quad . \quad (96)$$

The Reich-Moore formalism is thus exact in the limit of one level or one channel and otherwise very accurate. It is fast. Its (nonreduced) collision matrix is unitary (as long as the number of levels does not exceed the number of photon channels which can always be assumed without loss of generality) so that non-physical cross sections are not produced.

2.3.8 The Adler-Adler cross section formulae

The approximation Eq. 66 to the inverse level matrix means essentially that the energy dependence of level shifts (if any) and total widths is ignored. This works very well for fissile nuclei in restricted energy ranges where

$\Gamma_{\lambda} \approx \Gamma_{\lambda\gamma} + \Gamma_{\lambda f} \approx \text{const}$, but not for light or medium-mass nuclei for which $\Gamma_{\lambda}^{\lambda} \approx \Gamma_{\lambda n} = 2P_0^{\lambda}(E)\gamma_{\lambda}^2$ with $P_0(E)$ given in Table 1. Diagonalising the inverse level matrix Eq. 66 by orthogonal transformation one finds a collision matrix of the Kapur-Peierls form, Eq. 67. Its poles ϵ_{λ} and reduced width amplitudes $g_{\lambda c}$

are energy-independent as in the S-matrix formalism developed by Siegert, Humblet and Rosenfeld (Refs. 18, 19), but unitarity is not automatically guaranteed.

The Adler-Adler cross section formulae (Refs. 17, 20, 21) are usually written not for specific channels (c, c') but for specific reaction types (total, n, f, γ , ...) and restricted to $\ell=0$:

$$\sigma \equiv \sum_{c \in n} \sigma_c = \sigma_p + \frac{1}{\sqrt{E}} \sum_{\lambda} \frac{1}{v_{\lambda}} (G_{\lambda}^{(T)} \psi_{\lambda} - H_{\lambda}^{(T)} \chi_{\lambda}) , \quad (97)$$

$$\sigma_x \equiv \sum_{c \in n} \sum_{c' \in x} \sigma_{cc'} = \frac{1}{\sqrt{E}} \sum_{\lambda} \frac{1}{v_{\lambda}} (G_{\lambda}^{(x)} \psi_{\lambda} - H_{\lambda}^{(x)} \chi_{\lambda}) , \quad (x=\gamma, f, n) , \quad (98)$$

where σ_p is the potential-scattering cross section, the $G_{\lambda}^{(x)}/(\sqrt{E}v_{\lambda})$, $H_{\lambda}^{(x)}/(\sqrt{E}v_{\lambda})$ are sums over all coefficients of ψ_{λ} , χ_{λ} in Eqs. 68-70, respectively, with $v_{\lambda} \equiv \Gamma_{\lambda}/2$ and \sqrt{E} stemming from $P_c(E)$. The λ -sums extend over all contributing levels irrespective of $J\pi$, the spin factors g_c being absorbed in the coefficients $G_{\lambda}^{(x)}$, $H_{\lambda}^{(x)}$. In principle one could even define Adler-Adler parameters for isotopic mixtures by similarly absorbing the relative abundances also in the $G_{\lambda}^{(x)}$, $H_{\lambda}^{(x)}$.

Inversion of the usually quite high-dimensional matrix A^{-1} is possible by brute force on modern computers (Refs. 17, 20, 21) but the orthogonal transformation involved is so complicated that simple conversion formulae giving the \mathcal{E}_{λ} , $g_{\lambda c}$ (or $G_{\lambda}^{(x)}$, $H_{\lambda}^{(x)}$) in terms of the E_{λ} , $\gamma_{\lambda c}$ are not available except for the case of a single level (see Sect. 3.2 below). As a consequence the statistical laws for Adler-Adler or, generally, Kapur-Peierls parameters could not be derived from the known statistics of the Wigner-Eisenbud parameters. An improvement of the conversion with respect to energy-dependent partial widths was recently discussed by Segev (Ref. 22).

Further discussion of the advantages and weaknesses of the various approximate resonance formalisms will be deferred until Doppler broadening has been treated.

2.4. Theory of Doppler broadening

In most practical applications of resonance cross sections these are needed in Doppler-broadened form. It is sometimes argued that for light nuclei Doppler broadening can be neglected. This, however, is true only for the broad s-wave levels but certainly not for the very narrow p-, d- ... wave levels of these nuclei which in the case of structural materials contribute significantly to resonance absorption and Doppler coefficient in fast reactors.

2.4.1 Free-gas approximation

Doppler broadening is caused by thermal motion of the target nuclei. Consider a parallel beam of monoenergetic particles with lab velocity v colliding with target nuclei whose velocities \vec{u} are distributed in such a way that $p(\vec{u})d^3u$ is the fraction with velocities in a small three-dimensional region d^3u around \vec{u} . If ρ_1 and ρ_2 are the densities of beam and target particles, respectively, the number of reactions occurring per unit time and unit volume is

$$\rho_1 \rho_2 \int d^3u p(\vec{u}) |\vec{v} - \vec{u}| \sigma(|\vec{v} - \vec{u}|) \equiv \rho_1 \rho_2 v \bar{\sigma}(v) \quad (99)$$

where $\bar{\sigma}(v)$ is the effective or Doppler-broadened cross section for incident particles with speed v . Obviously a $1/v$ cross section is not affected by Doppler broadening. Let us now assume that the target nuclei have the same velocity

distribution as the atoms of an ideal gas, i.e. the Maxwell-Boltzmann distribution,

$$p(\vec{u})d^3u = \frac{1}{\pi^{3/2}} \exp\left(-\frac{u^2}{u_T^2}\right) \frac{d^3u}{u_T^3}, \quad \frac{M}{2}u_T^2 \equiv kT, \quad (100)$$

where M is the nuclear mass and kT the gas temperature in energy units. Integrating over all possible relative velocities $\vec{w} = \vec{v} - \vec{u}$ and using polar coordinates, $d^3u = d^3w = w^2 dw d(\cos \Theta) d\phi$, with the polar axis parallel to the beam, one finds the exact free-gas expression for the Doppler-broadened cross section,

$$\bar{\sigma}(v) = \frac{1}{v\pi} \int_0^\infty \frac{dw}{u_T} \frac{w^2}{v^2} \left(e^{-\frac{(v-w)^2}{u_T^2}} - e^{-\frac{(v+w)^2}{u_T^2}} \right) \sigma(w) \quad (101)$$

In terms of lab energies, $E = mv^2/2$, this is

$$\bar{\sigma}(E) = \frac{1}{\Delta\sqrt{\pi}} \int_0^\infty dE' \left(e^{-\frac{4(E-\sqrt{EE'})^2}{\Delta^2}} - e^{-\frac{4(E+\sqrt{EE'})^2}{\Delta^2}} \right) \sqrt{\frac{E'}{E}} \sigma(E') \quad (102)$$

where
$$\Delta = \sqrt{\frac{4kTE}{M/m}} = 2 \frac{u_T}{v} E \quad (103)$$

is called the Doppler width. For $E \gg \Delta$, i.e. $v \gg 2u_T$, which is the case above a few eV, one can simplify by retaining only the first two terms of the expansion

$$\sqrt{EE'} = E + \frac{E'-E}{2} + \dots, \quad (104)$$

by neglecting the second exponential and by replacing \int_0^∞ by $\int_{-\infty}^\infty$ in the first integral. The result is

$$\sqrt{E} \bar{\sigma}(E) = \frac{1}{\Delta\sqrt{\pi}} \int_{-\infty}^\infty dE' e^{-\frac{(E'-E)^2}{\Delta^2}} \sqrt{E'} \sigma(E'). \quad (105)$$

2.4.2 Cubic crystal

Lamb (Ref. 23) obtained the same expression for radiative capture by the bound atoms of a Debye crystal if $\Gamma + \Delta > 4 kT_D$, where T_D is the Debye temperature. The only difference is that one must use an effective ("Lamb-corrected") temperature

$$T_L = T \left(\frac{T}{T_D} \right)^3 \frac{3}{2} \int_0^{\frac{T_D}{T}} dx x^3 \coth \frac{x}{2} = T \left(1 + \frac{1}{20} \frac{T_D^2}{T^2} - + \dots \right) \quad (106)$$

that is usually only a few percent higher than the actual crystal temperature T . Using the theory of quasi-free scattering one can extend these results to scattering and to cubic crystals in general (Ref. 24). It is common practice to compute Doppler-broadened cross sections with Eq. 105. For very low energies it may be better to use Eq. 102, i.e. the exact free-gas kernel. In any case the Doppler width, Eq. 104, must be calculated with the Lamb-corrected temperature, Eq. 106, for which a curve is given in Ref. 23 (see also Ref. 56, p.26).

2.4.3 Voigt profiles vs. numerical broadening

Let us now consider Doppler broadening of resonances. We saw that all resonance cross sections in SLBW, MLBW and Adler-Adler approximation can be written as sums of terms of the form $c/(1+x^2)$ or $cx/(1+x^2)$ where the coefficients c contain a factor $E^{-1/2}$ and otherwise depend only weakly on energy. As a consequence one needs the convolutions of $1/(1+x^2)$ and $x/(1+x^2)$ with a Gaussian, the so-called Voigt profiles (Ref. 25),

$$\psi(x, \beta) = \frac{1}{\beta\sqrt{\pi}} \int_{-\infty}^{\infty} dx' e^{-(x-x')^2/\beta^2} \frac{1}{1+x'^2} \quad (107)$$

$$\chi(x, \beta) = \frac{1}{\beta\sqrt{\pi}} \int_{-\infty}^{\infty} dx' e^{-(x-x')^2/\beta^2} \frac{x'}{1+x'^2} \quad (108)$$

with
$$x = \frac{E-E_0}{\Gamma/2}, \quad \beta = \frac{\Delta}{\Gamma/2} \quad (109)(110)$$

The quantity β is called the Doppler parameter, Δ, Γ and possibly a level shift (here absorbed in E_0) are to be calculated at the energy for which the broadened cross section is needed. These functions, which occur also in the theory of atomic spectra, are well known (Refs. 25, 26). Fast algorithms are available for computer calculations (Ref. 27). This explains the popularity of SLBW and MLBW formulae even in cases of strongly interfering levels where they are quite inadequate.

The Kapur-Peierls, MLBW and Adler-Adler cross section expressions (Eqs. 68-70, 79-81, 97-98) remain valid also for Doppler-broadened cross sections if the zero-temperature Voigt profiles $\psi_\lambda, \chi_\lambda$ are replaced by the broadened profiles, Eqs. 107-108.

An interesting property of both the exact and the approximate free-gas formulae (Eqs. 102 and 105) is that if one knows the effective cross section for a temperature T_1 one can get that for a higher temperature T_2 by simply broadening with a Doppler width calculated for the difference $T_2 - T_1$, without going back to the unbroadened cross section (Ref. 28). Likewise one can combine Doppler and resolution broadening (see below) of a cross section if the resolution function has the same form as the Doppler kernel, e.g. Gaussian. One simply replaces Δ by $\sqrt{\Delta^2 + W^2}$ where W is the resolution width defined analogously to Δ (Ref. 28).

Cross sections of the Reich-Moore type must be numerically broadened. Once enough unbroadened cross section points for linear interpolation with a given accuracy are calculated the problem is reduced to piece-wise convolution of a straight line and a Gaussian which results in error functions and exponentials, again well known and rapidly calculated functions (cf. also Ref. 27). With modern computers these methods can be quite fast, and the Reich-Moore formalism is so attractive, that the recent decision to strike it from the ENDF conventions appears ill-considered.

Assessing merits and drawbacks of the various approximate resonance formulae one should realise that the fastest way to calculate unbroadened cross sections on a computer is not by way of explicit cross section expressions such as Eqs. 68-70, 79-81, 97-98. It is much faster to compute the required collision matrix elements and then to use Eqs. 14 and 15. Use of the explicit cross section expressions is necessary only if resonance broadening is to be calculated by means of the Voigt profiles. In other words, the Voigt profiles require considerable preparatory computations that are not needed for numerical broadening. The convenience of MLBW or Adler-Adler parameters for Doppler broadening should therefore not be overestimated - in multi-level situations it is at least partially offset by the need to utilize the explicit cross section expressions with their time-consuming double sums. Furthermore, the approximations involved lead to cross sections that differ from the exact R-matrix cross sections. The difference is sometimes added as a "smooth" cross section which is considered as unaffected by Doppler broadening (e.g. in the ENDF system). This entails additional preparatory work and, since the "smooth" component is not really smooth near strongly interfering resonances (cf. Ref. 20b) still does not remove all discrepancies for Doppler-broadened cross sections.

In the case of Adler-Adler parameters additional problems exist: If they are derived from Wigner-Eisenbud (e.g. Reich-Moore) parameters one must invert large level matrices, if they are directly determined in a fit procedure one has the consistency problems connected with the unitarity of the collision matrix: There are about twice as many real parameters as in the Wigner-Eisenbud case, but a closer look shows that the number of really independent parameters is the same, the remaining ones being fixed by conditions imposed by unitarity. These conditions, however, are complicated and not easily utilised.

In conclusion it is perhaps fair to say that the real, constant R-matrix parameters of the Wigner-Eisenbud or Reich-Moore type should be considered as basic, whereas the complex Kapur-Peierls or Adler-Adler parameters should be considered as an auxiliary representation for Doppler broadening.

2.4.4 Temperature-dependent self-shielding, importance of level spins

In reactor calculations cross sections are usually not required in the form of "microscopic" data with the whole detailed resonance structure. Instead one employs group cross sections. These are defined as flux-weighted averages over certain energy (or rather lethargy) intervals, the group intervals. In the widely used narrow-resonance approximation, which is based on the assumption that the Doppler-broadened resonances are narrow compared to the average energy loss of a scattered neutron, $(\Delta^2 + \Gamma^2)^{1/2} \ll 2AE/(A+1)^2$, the flux over a resonance is proportional to the inverse total cross section. The group cross section of a given nuclide (or element) for the (n,x) reaction can then be written as

$$\bar{\sigma}_x = \frac{\left\langle \frac{\sigma_x}{\sigma+d} \right\rangle}{\left\langle \frac{1}{\sigma+d} \right\rangle}, \quad (111)$$

where σ_x and $\sigma = \sum_x \sigma_x$ are the (n,x) and total Doppler-broadened cross sections of the nuclide (or element), d is the so-called dilution cross section describing the admixture of other elements, and

$$\langle \dots \rangle \equiv \int_{\Delta E} dE N(E) \dots \quad (112)$$

is an integral over the group interval ΔE with the smooth collision function $N(E)$ as weight function. The dilution cross section d is usually taken as constant in ΔE . The self-shielding factors f_x are defined by the factorisation (T denotes the temperature)

$$\bar{\sigma}_x(d,T) \equiv \bar{\sigma}_x(\infty,T) \cdot f_x(d,T), \quad \text{with} \quad (113)$$

$$\bar{\sigma}_x(\infty,T) = \langle \sigma_x \rangle. \quad (114)$$

The group cross section for infinite dilution is just the (collision-function-weighted) average cross section in the usual sense. It is independent of d and, apart from edge effects at the interval boundaries, also of T. Thus f_x contains all d and almost all T dependence. With the usual definition of the covariance,

$$\text{cov}(x,y) = \langle (x - \langle x \rangle)(y - \langle y \rangle) \rangle, \quad (115)$$

one can write

$$f_x(d,t) = 1 + \text{cov}\left(\frac{\sigma_x}{\langle \sigma_x \rangle}, \frac{1/(\sigma+d)}{\langle 1/(\sigma+d) \rangle}\right). \quad (116)$$

Now peaks in σ_x coincide usually with dips in $1/(\sigma+d)$ and vice versa. The covariance is then negative and

$$0 < f_x < 1. \quad (117)$$

Growing dilution or growing temperature both tend to reduce the covariance so that normally

$$\frac{\partial f_x}{\partial d} > 0, \quad \frac{\partial f_x}{\partial T} > 0. \quad (118)(119)$$

Exceptional behaviour may be caused by

- edge effects at the group boundaries, or
- inadequacy of the narrow-resonance approximation near very broad resonances, or
- pronounced resonance-potential interference dips ("windows") in the total cross section. These have no counterparts in the fission or capture cross section and can therefore over-compensate the influence of the peaks on the covariance.

We get more insight with explicit cross section expressions. Neglecting edge effects, level-level interference and resonance-potential interference we write

$$\sigma = \sum_{\lambda} (\sigma_o \psi)_{\lambda} + \sigma_p, \quad (120)$$

$$\sigma_x = \sum_{\lambda} (\sigma_o \psi \frac{\Gamma_x}{\Gamma})_{\lambda}, \quad (121)$$

where $\sigma_o = 4\pi\lambda(E_o)^2 g \Gamma_n / \Gamma$ is the peak total cross section (unbroadened), ψ the symmetric Voigt profile and σ_p the potential scattering cross section. If the resonances are very narrow and well separated one can treat their contributions to σ_x independently which results in

$$\bar{\sigma}_x(d,T) \approx \frac{1}{\Delta E} \sum_{\lambda} N(E_{\lambda}) A_{\lambda x} f(\beta_{\lambda}, \kappa_{\lambda}), \quad (122)$$

$$\bar{\sigma}_x(\infty, T) \approx \frac{1}{\Delta E} \sum_{\lambda} N(E_{\lambda}) A_{\lambda x}, \quad (123)$$

with
$$A_{\lambda x} = \int dE (\sigma_o \psi \frac{\Gamma_x}{\Gamma})_{\lambda} = 2\pi^2 \lambda (E_{\lambda})^2 (g \frac{\Gamma_n \Gamma_x}{\Gamma})_{\lambda} \text{ (peak area),} \quad (124)$$

$$f(\beta, \kappa) = \frac{2}{\pi} \kappa \int_0^{\infty} dx \frac{\psi(x, \beta)}{\psi(x, \beta) + \kappa} = \frac{2}{\pi} \kappa J(\beta, \kappa), \quad (125)$$

$$\beta_{\lambda} = \frac{\Delta(E_{\lambda})}{\Gamma_{\lambda}/2}, \quad \kappa_{\lambda} = \frac{d + \sigma_p}{\sigma_{o\lambda}}. \quad (126)(127)$$

The universal function $f(\beta, \kappa)$ can be interpreted as the self-shielding factor of an isolated, symmetric, narrow resonance which depends on the Doppler parameter β and the dilution parameter κ . It obeys the inequalities 117-119 as can be seen from Fig. 3. With Eqs. 122 and 123 one gets

$$f_x(d,T) \approx \frac{\sum_{\lambda} N(E_{\lambda}) A_{\lambda x} f(\beta_{\lambda}, \kappa_{\lambda})}{\sum_{\lambda} N(E_{\lambda}) A_{\lambda x}}. \quad (128)$$

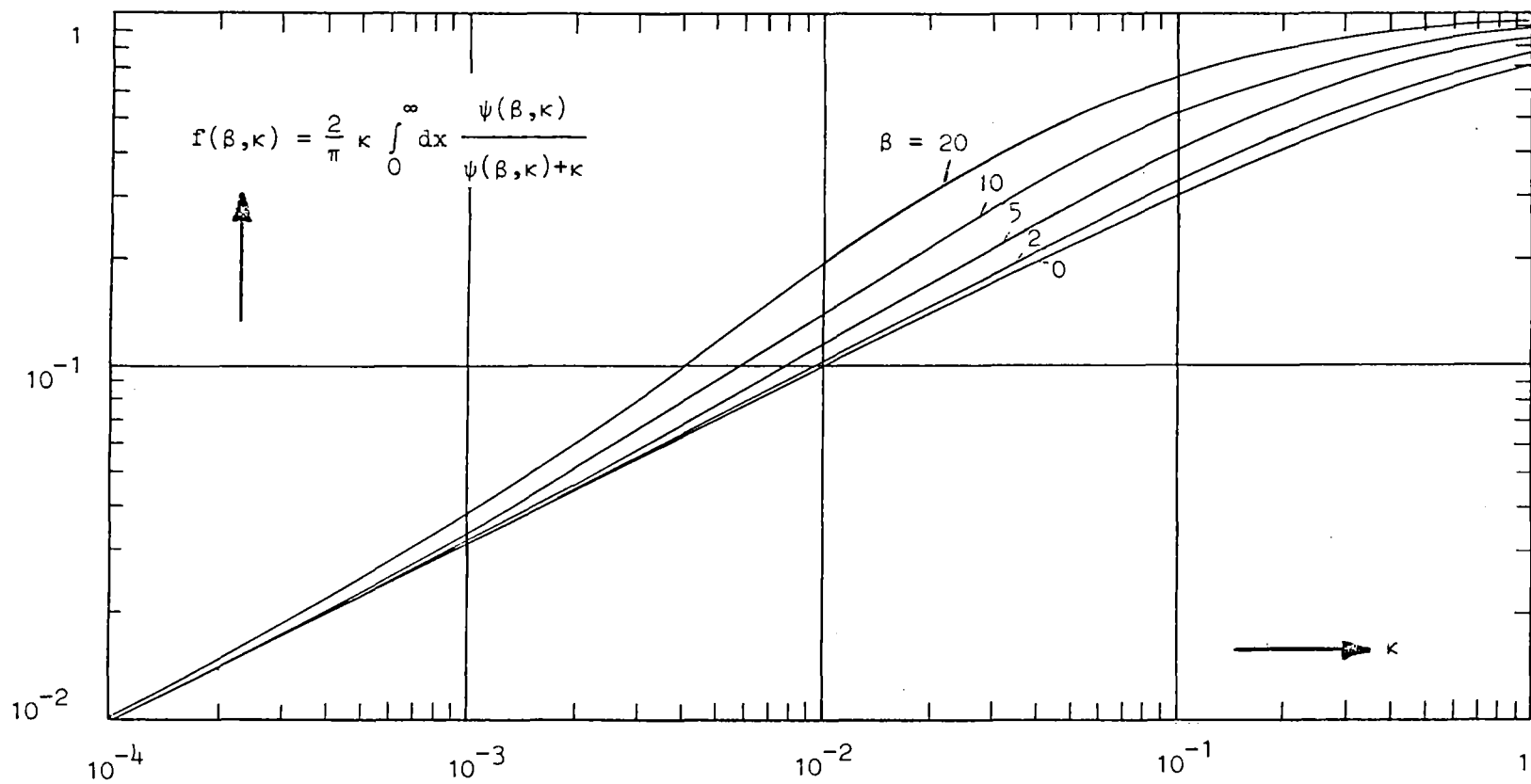


Fig. 3 - Dependence of the narrow-resonance self-shielding factor $f(\beta, \kappa)$ on temperature ($\beta = 2\Delta/\Gamma$) and dilution ($\kappa = (d+\sigma_p)/\sigma_0$).

Thus f_x is a weighted average of the individual narrow-resonance self-shielding factors, the weights being proportional to the areas of the (n,x) cross section peaks $A_{\lambda x}$ and to the local collision densities $N(E_\lambda)$. Eqs. 120-128 were derived for a single isotope. They are also valid for isotopic mixtures if $\sigma_{o\lambda}$ and $A_{\lambda x}$ are taken as containing the isotopic abundance as a factor.

An important remark concerns the **level** spins. The SLBW peak area is proportional to $g\Gamma_n\Gamma_x/\Gamma$. For narrow resonances this quantity is, apart from E_o , usually the only information one has. For broad resonances one knows frequently also $g\Gamma_n$ and, mostly for s-wave levels, even g . Now knowledge of E_o and $g\Gamma_n\Gamma_x/\Gamma$ enables one to calculate $\bar{\sigma}_x(\infty, T)$, cf. Eq. 123, but not $\bar{\sigma}_x(d, T)$ or $f_x(d, T)$. The reason is that in order to calculate $f(\beta, \kappa)$ one must know Γ and this requires knowledge of g , $g\Gamma_n$ and $g\Gamma_n\Gamma_x/\Gamma$. In other words, the peak area alone does not tell whether the peak is broad or narrow, and even the quantity $g\Gamma_n$ does not help much. For a given peak area it is mainly the spin that determines the width and thus the contribution to the self-shielded cross section and especially to its temperature variation: The narrower a resonance, the stronger its response to temperature changes.

An illustration is provided by the so-called structural materials (iron, nickel and other steel components). Their capture cross sections are dominated by very narrow p-, d-...wave levels for which capture peak areas are measured but not Γ or g (excepting very recent data on ^{56}Fe , Ref. 31). In order to calculate realistic self-shielded group constants one must resort to Monte Carlo sampling of spin and neutron widths based on level statistics (Ref. 32). In a fast reactor the increase of neutron capture with temperature (due to increasing f , see Fig. 3 and Eq. 122) expressed by the so-called Doppler coefficient, is the only inherent, automatically functioning safety feature. Hence the practical importance of good data on g (besides $g\Gamma_n$ and $g\Gamma_n\Gamma_x/\Gamma$) is obvious. Experimental spin determination for p, d, ...wave levels is at present a widely open field.

2.4.5 Westcott factors

The energy distribution of the neutrons in a thermal reactor is well described by the Maxwell-Boltzmann energy distribution obtained from Eq. 100 by integration over all angles,

$$p(E)dE = \frac{2}{\sqrt{\pi}} \exp\left(-\frac{E}{kT}\right) \sqrt{\frac{E}{kT}} \frac{dE}{kT}, \quad (129)$$

and a $1/E$ tail. The (n,x) reaction rate induced by this spectrum can be written as

$$\int_0^\infty dE p(E) \sqrt{E} \bar{\sigma}_x(E) \equiv \sqrt{kT} \bar{\sigma}_x(kT) g_W \quad (130)$$

where $\bar{\sigma}_x(E)$ is the Doppler-broadened (n,x) cross section for temperature T and $\sqrt{kT} \bar{\sigma}_x(kT)$ is the result one would get for a $1/v$ cross section. The factor g_W defined by Eq. 130, the so-called Westcott factor, is thus seen to correct the reaction rate for deviations from $1/v$ behaviour of the Doppler-broadened cross section. Westcott factors are convenient for reaction rate calculations in thermal fluxes since usually the (Doppler-broadened) thermal cross sections $\bar{\sigma}_x(kT)$ are well known, and since low-energy reaction cross sections show $1/v$ behaviour more or less modified by nearby positive or negative levels. Westcott factors are normally tabulated for room temperature, $kT = 0.0253$ eV.

2.5 Observables

Cross section measurements, as a rule, do not yield cross sections directly but more or less complicated functions or functionals of the cross sections.

2.5.1 Transmission

The simplest measurement is that of the total cross section σ . One measures that fraction of beam particles of a given energy which traverses without interaction a sample of given thickness n (atoms/b). This fraction, the transmission, for a very small thickness of material Δn is $1 - \sigma \Delta n$. For finite thickness it is

$$T = \lim_{n/\Delta n \rightarrow \infty} (1 - \sigma \Delta n)^{n/\Delta n} = e^{-n\sigma}. \quad (131)$$

The cross section is thus essentially the logarithm of the observable.

2.5.2 Reaction yield

The (n,x) reaction yield Y_x ($x=f, \gamma, \dots$), i.e. the fraction of beam particles that undergoes an (n,x) reaction in the sample, is composed of contributions from multiple-collision events with zero, one, two etc. preceding scattering collisions,

$$Y_x = Y_{x0} + Y_{x1} + Y_{x2} + \dots \quad (132)$$

where

$$Y_{x0} = \frac{1-T}{\sigma} \sigma_x,$$

$$Y_{x1} = \frac{1-T}{\sigma} \sigma_n \left\langle \frac{1-T_1}{\sigma_1} \sigma_{x1} \right\rangle_1, \quad (133)$$

$$Y_{x2} = \frac{1-T}{\sigma} \sigma_n \left\langle \frac{1-T_1}{\sigma_1} \sigma_{n1} \left\langle \frac{1-T_2}{\sigma_2} \sigma_{x2} \right\rangle_2 \right\rangle_1$$

etc.

The numerical subscript indicates the number of preceding collisions so that $1-T_1$, for instance, is the probability that after the first collision the scattered neutron interacts again in the sample. The brackets $\langle \rangle_1$, $\langle \rangle_2$ etc. denote averages over all first, second etc. scattering collisions, which means over all possible spatial coordinates and scattering angles. Note that in each elastic scattering collision the energy of a beam particle changes from E to E' according to

$$E' = E \frac{A^2 + 2A\mu_c + 1}{(A+1)^2} \quad (134)$$

if the target particle is at rest initially. Here μ_c is the cosine of the c.m.s. scattering angle and A the mass ratio (target to beam particle). In the resonance region this means that the cross sections to be used before and after the collision can differ dramatically. The multiple-collision yields Y_{x1} , Y_{x2} etc. are therefore very complicated functionals of σ_x , σ_n and σ . If inelastic scattering is energetically possible σ_n is to be taken as the sum of the elastic and inelastic scattering cross sections, and $\langle \rangle_1$ etc. include averaging over all possible scattering modes. The thin-sample approximation,

$$Y_x \approx n\sigma_x \quad \text{for} \quad n\sigma \ll 1, \quad (135)$$

is often accurate enough for fission yields ($x=f$) where the sample must be so thin that the fission fragments can get out. In capture data analysis, however, one must usually include multiple-collision terms and the self-shielding factors $(1-T)/(n\sigma)$ because samples are thicker and the ratios σ_x/σ are much greater than in fission data analysis.

2.5.3 Differential scattering yield

Sample thickness effects, i.e. self-shielding and multiple scattering, are also quite important in scattering measurements. In analogy to Eqs. 132-133 one has

$$dY_n = dY_{n1} + dY_{n2} + dY_{n3} + \dots \quad (136)$$

where

$$dY_{n1} = \frac{1-T}{\sigma} \frac{d\sigma_n}{d\Omega} \left\langle T_1 \right\rangle_1 d\Omega$$

$$dY_{n2} = \frac{1-T}{\sigma} \sigma_n \left\langle \frac{1-T_1}{\sigma_1} \frac{d\sigma_{n1}}{d\Omega_1} \left\langle T_2 \right\rangle_2 \right\rangle_1 d\Omega \quad (137)$$

$$dY_{n3} = \frac{1-T}{\sigma} \sigma_n \left\langle \frac{1-T_1}{\sigma_1} \sigma_{n1} \left\langle \frac{1-T_2}{\sigma_2} \frac{d\sigma_{n2}}{d\Omega_2} \left\langle T_3 \right\rangle_3 \right\rangle_2 \right\rangle_1 d\Omega$$

etc.

Here $d\Omega$ is a solid-angle element covered by the detector.

2.5.4 Self-indication (n,x) data

From our discussion of (n,x) yields it is clear that (except for very thin samples) extraction of the (n,x) cross section σ_x from (n,x) yields requires also the total cross section σ . Quite generally one can state that the availability of good total cross section data is a prerequisite for good partial cross section data analysis. Another data type which is valuable especially for area analysis (see below) is obtained with the self-indication method. One uses two samples of the same material, a filter sample (thickness n_1) and a detector sample (thickness n_2). The probability for a beam particle to undergo an (n,x) reaction in the second sample is

$$S_x(n_1, n_2) = T(n_1) Y_x(n_2). \quad (138)$$

The result is essentially a measurement of the filter-sample transmission with a detector system (detector sample plus detector) that has enhanced efficiency across the transmission dips (at the resonance energies).

2.5.5 Semi-empirical determination of self-shielded group cross sections

An interesting application of the self-indication method is the semi-empirical determination of self-shielded group cross sections (Ref. 33). Observed data are always resolution-broadened. Indicating this broadening by average brackets we can write self-indication data taken with a thin detector sample

$$\frac{1}{n_2} \left\langle T(n_1) Y_x(n_2) \right\rangle = \left\langle e^{-n_1 \sigma} \sigma_x \right\rangle \quad \text{for } n_2 \sigma \ll 1. \quad (139)$$

Suppose this quantity and also the average transmission was measured with a sufficient number of different filter samples to permit numerical evaluation of the integrals

$$\int_0^{\infty} dn \langle e^{-n\sigma} \rangle = \left\langle \frac{1}{\sigma} \right\rangle \quad (140)$$

$$\int_0^{\infty} dn e^{-nd} \langle e^{-n\sigma} \rangle = \left\langle \frac{1}{\sigma+d} \right\rangle \quad (141)$$

$$\int_0^{\infty} dn e^{-nd} \langle e^{-n\sigma} \sigma_x \rangle = \left\langle \frac{\sigma_x}{\sigma+d} \right\rangle \quad (142)$$

where e^{-nd} with arbitrary d is applied artificially. Comparison with the definition of group cross sections, Eq. 111, shows that this method yields group cross sections for zero dilution as well as for arbitrary dilution cross section d , for the temperature of the samples and for a group interval that corresponds to the resolution width (which can be arbitrarily enlarged by additional numerical broadening, of course).

Various types of observables are shown in Figs. 10-12, 15-19.

2.6 Experimental complications

We shall now briefly review the main causes for corrections and uncertainties in nuclear resonance data measurements.

2.6.1 Backgrounds

In time-of-flight measurements there are always two types of background: constant and time-dependent. Constant background may be due to radioactivity of the sample and its environs, time-dependent backgrounds are produced by the accelerator pulses and the sample. An example is the background caused by resonance-scattered neutrons in neutron resonance capture measurements (Refs. 34,35) that reflects the resonance structure of the scattering cross section and is thus violently energy-dependent. This influence of the sample on backgrounds makes "sample-out" background determinations often quite doubtful. Therefore one uses "notch filters", special samples placed in front of the sample under study. The ideal notch filter has a few widely spaced resonances and is so thick that at their peaks all beam particles are removed. Counts observed at these notch energies are then pure background. This allows background measurements at a few points during the actual run. Of course no "true" data can be measured across the notches, so one uses a few complementary notch filters.

2.6.2 Resolution broadening

It was already mentioned that observed data are always resolution-broadened. Strictly speaking the observables are

$$\bar{T}(E) = \int dE' r(E',E)T(E'), \quad \bar{Y}_x(E) = \int dE' r(E',E)Y_x(E'), \quad \dots \quad (143)(144)$$

where $dE'r(E',E)$ is the probability that an event observed at energy E (or the corresponding flight time) was actually due to a beam particle with an energy E' in dE' . The main causes are:

- finite accelerator pulse width (t_b) ,
- finite time channel width (t_c) ,
- electronic drifts, jitter (t_d) ,
- uncertain starting point (e.g. in moderator slab or booster) and end point (e.g. in sample or ${}^6\text{Li}$ glass detector) of flight path (δL) ,
- finite angular resolution in scattering experiments $(\delta\theta)$.

The resolution function $r(E', E)$ is normally not well known. Frequently a Gaussian is assumed in data fitting work,

$$r(E', E) = \frac{1}{W\sqrt{\pi}} e^{-(E'-E)^2/W^2} \quad (145)$$

with, for instance (cf. Refs. 36-38)

$$W = 2E \left[2 \left(\frac{\delta L}{L} \right)^2 + \frac{E}{3mL^2} (t_b^2 + t_c^2 + t_d^2) \right]^{1/2} = E \sqrt{c_1 + c_2 E} \quad (146)$$

Often slight variation of c_1, c_2 improves the fit but sometimes it is necessary to use other, asymmetric resolution functions, e.g. χ^2 functions (Ref. 38) or Gaussians with tails (Ref. 39).

2.6.3 Detector efficiency and flux

In partial cross section measurements the raw data are count rates,

$$c = \phi Y_x \epsilon \quad (\approx \phi n \sigma_x \epsilon \text{ for } n\sigma \ll 1). \quad (147)$$

Absolute determination of the flux ϕ and the detector efficiency ϵ is difficult and is therefore almost always avoided. One usually measures relative to a reference sample (subscript r),

$$\frac{c}{c_r} = \frac{Y_x \epsilon}{Y_r \epsilon_r} \quad (\approx \frac{n \sigma_x \epsilon}{n_r \sigma_r \epsilon_r} \text{ for } n\sigma \ll 1, n_r \sigma_r \ll 1), \quad (148)$$

for which Y_r is known with good accuracy. This eliminates the need to know the flux but still one may have problems with n/n_r and ϵ/ϵ_r as the thin-sample expression shows. Frequently used reference cross sections are listed in Table 5 together with the accuracies achieved at present.

Table 5: Reference cross sections and accuracies
(1 standard deviation, indicative only)

Reaction	Accuracy	Energies	Detector systems
${}^1\text{H}(n,p)$	$\pm 1 \%$	$< 10 \text{ MeV}$	plastic and liquid scintillators, counter telescopes
${}^6\text{Li}(n,t)$	$\pm 2 \%$	$< 100 \text{ keV}$	glass scintillators, semiconductor detectors
${}^{10}\text{B}(n,\alpha\gamma)$	$\pm 2 \%$	$< 100 \text{ keV}$	slab samples viewed by γ -detectors
${}^{12}\text{C}(n,n)$	$\pm 2 \%$	$< 5 \text{ MeV}$	graphite samples
${}^{197}\text{Au}(n,\gamma)$	$\pm 4 \%$	$< 3.5 \text{ MeV}$	metal foils viewed by γ -detectors
${}^{235}\text{U}(n,f)$	$\pm 3 \%$	$< 8 \text{ MeV}$	fission chambers

If the energy dependence of ϵ/ϵ_x is known one can determine the absolute value, i.e. the calibration, by normalising to an accurately known cross section value, for instance the thermal cross section. If no suitable known value exists one can often use the saturated-resonance (black-sample) technique: One uses a special sample which is so thick that at a well known resonance the transmission is practically zero (cf. Fig. 11 below). Quite generally one has

$$(1-T) \frac{\sigma_x}{\sigma} < Y_x < 1-T. \quad (149)$$

With $c = \phi Y_x \epsilon$ this gives at the resonance peak, $E = E_0$, where the sample is black,

$$c < \epsilon \phi < c \frac{\sigma(E_0)}{\sigma_x(E_0)}. \quad (150)$$

If $\sigma \approx \sigma_x$ (i.e. $\Gamma \approx \Gamma_x$) one gets, without further calculation, a quite accurate value for $\epsilon \phi$. The 4.9 eV resonance of $^{197}\text{Au} + n$, for example, was frequently used for black-sample normalisation of capture data. With the resonance parameters in the "barn book" (Ref. 4) one calculates in SLBW approximation $\sigma(E_0)/\sigma_x(E_0) \approx 1.12$, i.e. a $\pm 6\%$ uncertainty of $\epsilon \phi$ which is easily reduced further by a multiple-scattering calculation which obviously need not be very accurate. Serious problems are created if the detector efficiency varies from isotope to isotope or, even worse, from resonance to resonance. This is a persistent source of difficulties, for example, with capture measurements. Here the detector response depends on the gamma spectrum (binding energy, transition strength to low-lying levels etc.) and thus fluctuates from level to level in an unpredictable way, especially for relatively light nuclei. A reliable estimation of ϵ/ϵ_x is then impossible without supplementary data on the gamma spectra of individual resonances (Ref. 40).

2.6.4 Self-shielding and multiple scattering

All partial cross section data are more or less affected by self-shielding and multiple scattering. The corresponding corrections are practically most important for neutron capture and scattering data. Fission cross section measurements based on the observation of fission fragments, on the other hand, require such thin samples that self-shielding and multiple scattering are much less important than self-absorption of fission fragments in the sample. The effect of self-shielding is described by the beam-attenuation factors $(1-T)/(n\sigma)$ in Eqs. 133 and 137 whereas multiple scattering leads to the higher-order terms in the collision expansions Eqs. 132 and 136. As these equations show the two effects are inter-related and cannot be treated separately. Both together are referred to as sample-thickness effects.

As mentioned above the multiple-collision yields are complicated functionals of the cross sections. This means that they depend not simply on the cross sections for the primary energy but on all cross sections for the whole range of energies that a neutron can attain successively during a multiple-collision event (cf. Eq. 134). The average brackets $\langle \dots \rangle_k$ in Eqs. 133 and 137 denote averages for the k-th collision over

- the distribution of scattering angles θ ,

$$p(\mu) d\mu = \frac{4\pi}{\sigma_{nk}} \frac{d\sigma_{nk}}{d\Omega} \frac{d\mu}{2}, \quad -1 < \mu \equiv \cos \theta \leq 1, \quad (151)$$

- the distribution of azimuths ϕ (uniform for zero polarisation)

$$p(\phi) d\phi = \frac{d\phi}{2\pi}, \quad 0 < \phi \leq 2\pi \quad (152)$$

- the distribution of the number s of mean free paths to the next collision,

$$p(s)ds = \frac{e^{-s}}{1-e^{-s_k}}, \quad 0 < s \leq s_k \equiv n_k \sigma_k \quad (153)$$

where n_k is the material thickness (nuclei/b) that a neutron would have to traverse after the k -th collision in order to reach the sample surface and to escape. Since n_k and σ_k depend on the particulars (spatial coordinates, angles, corresponding energy losses) of all preceding collisions one sees that the multiple-collision yields are given by multi-dimensional integrals of rapidly increasing dimensionality. Already the second-collision yield for the simplest sample geometry, viz. infinite slab, looks fairly complicated:

$$Y_{x1} = (1-e^{-n\sigma}) \frac{4\pi}{\sigma} \int_{-1}^1 \frac{d\mu}{2} \frac{d\sigma}{d\Omega} \left(1 - \frac{1-e^{-t-t'}}{t-t'} \frac{t}{1-e^{-t}}\right) \quad (154)$$

with $t \equiv \mu \frac{n\sigma}{|\mu|}$, $t' \equiv \frac{n\sigma_1}{|\mu|}$, (155)(156)

The simplest way to calculate such complicated integrals on a computer is to sample the multi-dimensional integrands at random and then to average, which is tantamount to simulation of multiple-collision events with the Monte Carlo technique. For each subsequent collision of such an event one must sample the distributions (151)-(153) and, if inelastic scattering is energetically allowed, also the relative probabilities for elastic or inelastic scattering.

Practical sampling methods employ a random-number generator. This is a function subroutine that is usually part of the computer software just as exponentials, sines, cosines etc. Each time it is called it returns a floating-point number picked at random (i.e. from a uniform distribution) in the interval 0...1. Two principal methods exist to sample a distribution $p(x)dx$ with the help of a random-number generator:

- (1) Call the random-number generator once. Equate the random number ρ to the integral distribution,

$$\rho = P(x) = \int_0^x p(x')dx', \quad (157)$$

and solve for x . The frequency distribution of the x values thus obtained is just $p(x)dx$. This method is convenient if x can be expressed in closed form (examples: Eqs. 152, 153, counter-example: Gaussian distribution).

- (2) Rejection method (v. Neumann): Rescale, if necessary, so that $0 < x' < 1$, $0 < p(x') < 1$. If the range of the distribution is infinite one can substitute e.g. $x=x'/(1-x')$ (if $0 \leq x < \infty$) or $x'=(1+\tanh x)/2$ (if $-\infty < x < \infty$) etc. Get two numbers ρ_1, ρ_2 from the random-number generator. Accept $x'=\rho_1$ if $\rho_2 \leq p(\rho_1)$, reject otherwise and begin again. This works always, even for very complicated or tabulated $p(x)$.

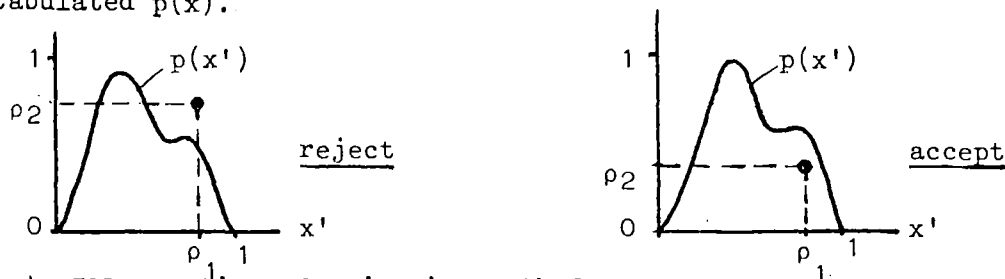


Fig. 4: Illustration of rejection method

Usually it is most convenient to sample the c.m.s. scattering angles and then to convert to the lab system (cf. Ref. 38). At low energies, for example, (s-wave) scattering is isotropic in the c.m.s. system so that $p(\mu_c)d\mu_c = d\mu_c/2$ with $\mu_c = \cos \theta_c$ (the subscript c indicates c.m.s. quantities). From μ_c one gets the energy of the scattered neutron (Eq. 134) and thus the new cross sections. The latter must be available in tabulated form for convenient interpolation. The new total cross section and the distance to the sample surface determine the total interaction probability $(1-T_k$ in Eqs. 133, 137). A flow diagram for multiple-collision capture yield calculation is shown in Fig. 5.

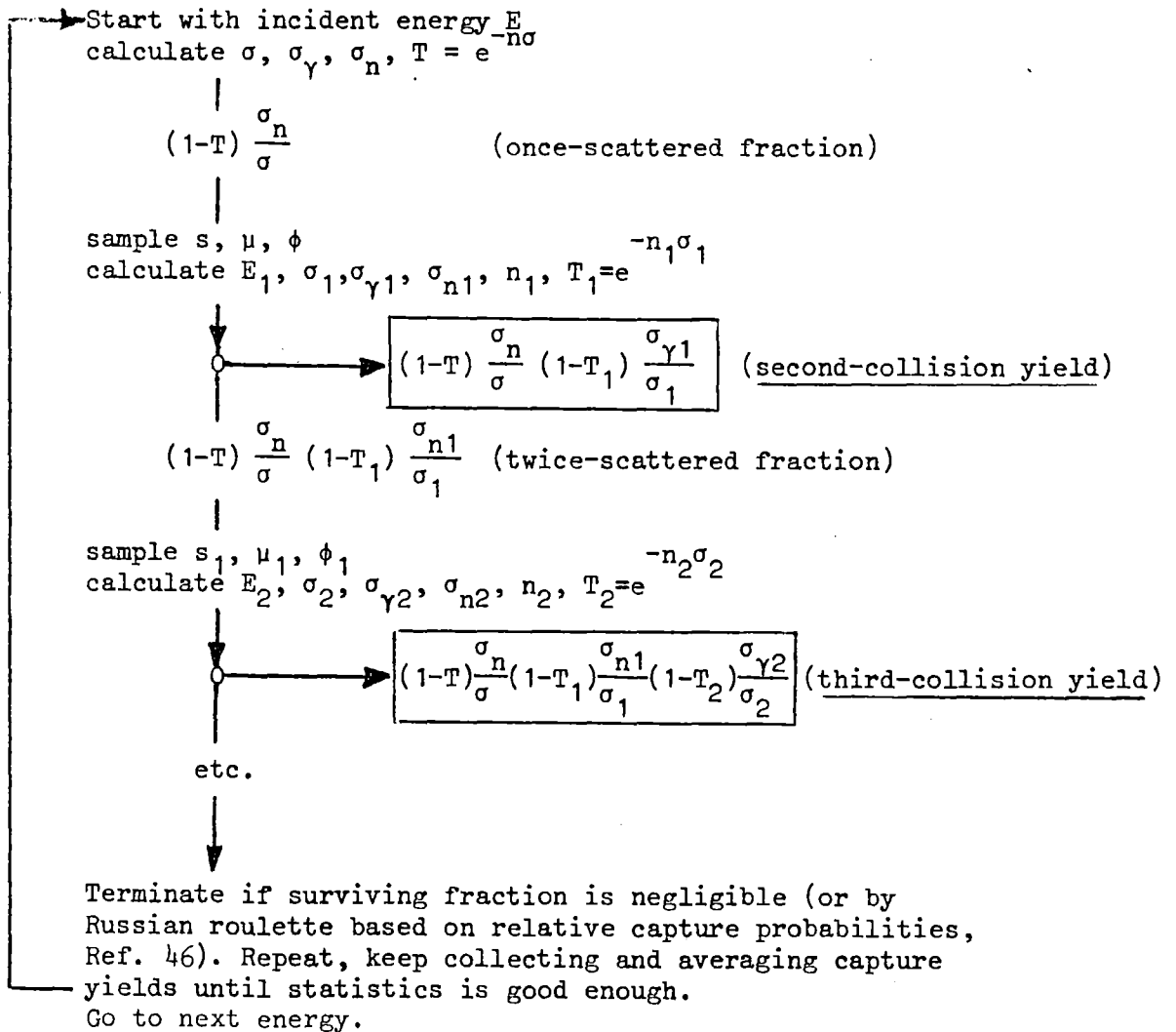


Fig. 5: Flow diagram for multiple-collision capture yield calculation by Monte Carlo simulation

2.7 Resonance parameter estimation

The ideal resonance parameter analysis is based on data measured with isotopically pure samples and proceeds as follows.

(1) From transmission data one determines essentially

$$\begin{aligned} E_0, \Gamma_n, \Gamma, g & \text{ for } \ell = 0, \\ E_0, g\Gamma_n & \text{ for } \ell \geq 1. \end{aligned}$$

(2) The transmission results permit calculation of sample-thickness corrections for yield data from which one gets essentially

$$\begin{aligned} E_0, \Gamma_x & \text{ if } \Gamma_n, g \text{ are known,} \\ E_0, g\Gamma_x & \text{ if } g\Gamma_n \text{ is known.} \end{aligned}$$

(3) If transmission results are not available (p-, d-, ... levels are not easily observed in transmission experiments) one gets only

$$E_0, g\Gamma_n \Gamma_x / \Gamma \quad \text{if } g\Gamma_n \text{ is not known.}$$

The determination of $J\ell$ (and thus g) is usually based on transmission or scattering data. Apart from complications for fissile nuclei or strong level overlap one can usually use the interference between resonant and potential scattering to determine ℓ or at least to distinguish between $\ell=0$ and $\ell \geq 1$, whereas the resonance peak height (see Eq. 195 below) and level-level interference allow determination of J .

The best way to extract resonance parameters from transmission, yield, self-indication etc. data is by least-squares analysis. Because of its practical importance and for convenient reference we briefly review the least-squares formalism with explicit account of statistical and systematic errors.

2.7.1 The least-squares method

Let us consider

$$\begin{aligned} \text{observables } y_i & \quad (i = 1, 2, \dots, I), \\ \text{parameters } x_\mu & \quad (\mu = 1, 2, \dots, M < I), \end{aligned}$$

and a mathematical model

$$y_i = y_i(x_1, x_2, \dots, x_M) \equiv y_i(\vec{x}) \quad (158)$$

that allows us to calculate the observables (e.g. resolution-broadened transmissions, yields etc.) from the (resonance) parameters. Let us further assume that all y_i were measured with the results $\eta_i \pm \sigma_i$ (σ_i : standard deviation), which actually means that the true value y_i lies in dy_i with the probability

$$p(y_i) dy_i = \exp\left[-\frac{1}{2} \left(\frac{y_i - \eta_i}{\sigma_i}\right)^2\right] \frac{dy_i}{\sigma_i \sqrt{2\pi}} \quad (159)$$

if we assume a Gaussian distribution of the errors as is usual in error estimation. What is the parameter vector x which best explains the observed data η_i ? It is not very difficult to see (Ref. 41) that it is determined by the requirement that the

joint probability $\prod_i p(y_i) dy_i$ for all the measurements be maximal, or

$$\frac{\partial \chi^2}{\partial x_\mu} = \frac{\partial}{\partial x_\mu} \sum_i \left(\frac{y_i - \eta_i}{\sigma_i} \right)^2 = 0, \quad \mu = 1, 2, \dots, M. \quad (160)$$

This is the least-squares principle. The M Eqs. 160 for the M unknown parameters x_μ can be solved immediately if the relationship between y_i and \vec{x} is linear. In our case it is definitely not linear so we must iterate. Let \vec{x}' be an approximation to \vec{x} so that

$$y_i(\vec{x}) = y_i(\vec{x}') + \sum_\mu y_{i,\mu}(\vec{x}') (x_\mu - x'_\mu) + \dots \quad (161)$$

with

$$y_{i,\mu} \equiv \frac{\partial y_i}{\partial x_\mu}. \quad (162)$$

Truncating the Taylor series (161) after the linear term and introducing the notation

$$(B^{-1})_{\mu\nu} \equiv \sum_{i=1}^I \frac{y_{i,\mu}(\vec{x}')}{\sigma_i} \frac{y_{i,\nu}(\vec{x}')}{\sigma_i} = (B^{-1})_{\nu\mu} \quad (163)$$

$$c_\mu \equiv \sum_{i=1}^I \frac{y_{i,\mu}(\vec{x}')}{\sigma_i} \frac{\eta_i - y_i(\vec{x}')}{\sigma_i} \quad (164)$$

we get the linear system of "normal equations"

$$\sum_{\nu=1}^M (B^{-1})_{\mu\nu} (x_\nu - x'_\nu) = c_\mu \quad \text{or} \quad B^{-1}(\vec{x} - \vec{x}') = c \quad (165)$$

Its solution,

$$x_\mu = x'_\mu + \sum_{\nu=1}^M B_{\mu\nu} c_\nu \quad \text{or} \quad \vec{x} = \vec{x}' + Bc \quad (166)$$

can be improved by iteration until χ^2 remains constant. It is seen that in each step the $M \times M$ matrix B^{-1} must be inverted and values for all observables and their derivatives must be computed.

2.7.2 Error propagation in least-squares fits

What uncertainty in the adjusted parameters x_μ follows from the data uncertainties σ_i ? If we denote the unknown errors of the η_i by $\delta\eta_i$ we have, in linear approximation,

$$\delta x_\mu = \sum_i \frac{\partial x_\mu}{\partial \eta_i} \delta \eta_i = \sum_i \sum_\nu B_{\mu\nu} \frac{y_{\nu,i}}{\sigma_i} \delta \eta_i \quad (167)$$

(cf. Eq. 166). The uncertainty to be quoted for x_μ is the square root of $\text{var}(x_\mu) = \langle \delta x_\mu^2 \rangle$ where the average brackets indicate the expectation value. Generalising slightly we calculate

$$\langle \delta x_\mu \delta x_\nu \rangle = \sum_{i,j} \sum_{\kappa,\lambda} B_{\mu\kappa} \frac{y_{\kappa,i}}{\sigma_i} \langle \delta \eta_i \delta \eta_j \rangle \frac{y_{j,\lambda}}{\sigma_j} B_{\lambda\nu}. \quad (168)$$

If the data uncertainties $\delta\eta_i$ are mutually independent,

$$\langle \delta \eta_i \delta \eta_j \rangle = \text{var}(\eta_i) \delta_{ij} = \sigma_i^2 \delta_{ij}, \quad (169)$$

one gets simply

$$\langle \delta x_\mu \delta x_\nu \rangle = (B B^{-1} B)_{\mu\nu} = B_{\mu\nu}. \quad (170)$$

In most cases, however, $\sigma_i^2 = \text{var}(x_\mu)$ is a sum of squared statistical and systematic uncertainties. The statistical errors are usually uncorrelated but the systematic errors are not. One has then instead of Eqs. 169, 170

$$\langle \delta\eta_i \delta\eta_j \rangle = \sigma_i^2 \delta_{ij} + \tau_{ij} (1 - \delta_{ij}), \quad (171)$$

$$\langle \delta x_\mu \delta x_\nu \rangle = B_{\mu\nu} + \sum_{i,j \neq i} \sum_{\kappa, \lambda} B_{\mu\kappa} \frac{y_{j,\kappa}}{\sigma_i^2} \tau_{ij} \frac{y_{j,\lambda}}{\sigma_j^2} B_{\lambda\nu} \quad (172)$$

where τ_{ij} describes the correlation. Let us take, for example, the η_i as time-of-flight count rates all affected by the same error δb in background subtraction. Then $\tau_{ij} = (\delta b)^2$ and $\sigma_i^2 = (\sqrt{\eta_i})^2 + (\delta b)^2$, $\sqrt{\eta_i}$ being the statistical error. If there is also a common normalisation error δc one has $\tau_{ij} = (\delta b)^2 + \eta_i \eta_j (\delta c/c)^2$, $\sigma_i^2 = (\sqrt{\eta_i})^2 + (\delta b)^2 + \eta_i^2 (\delta c/c)^2$ etc. This illustrates how important it is that experimenters state clearly and in as much detail as possible the statistical and systematic error components. One might add that it is similarly important that those who extract cross section parameters from experimental data should state not just the parameters x_μ and the variances $\langle \delta x_\mu^2 \rangle$ or the corresponding standard deviations but also at least the more important elements of the covariance matrix $\langle \delta x_\mu \delta x_\nu \rangle$. The uncertainty of a function f of the parameters x_μ , for instance a calculated cross section or transmission value, is given by the square root of the variance

$$\langle \delta f^2 \rangle = \left\langle \left(\sum_{\mu} \frac{\partial f}{\partial x_\mu} \delta x_\mu \right)^2 \right\rangle = \sum_{\mu, \nu} \frac{\partial f}{\partial x_\mu} \langle \delta x_\mu \delta x_\nu \rangle \frac{\partial f}{\partial x_\nu}, \quad (173)$$

so that a good error estimation or sensitivity study is not possible without the covariance matrix or at least its more important elements.

2.7.3 Goodness of fit

The minimal χ^2 obtained provides a means to check the consistency of mathematical model (Eq. 158) and data and the goodness of fit. The probability that a measurement of I observables y_i results in a χ^2 -value within $d\chi^2$ is derived as follows: The range $\chi^2 \dots \chi^2 + d\chi^2$ corresponds to a "spherical" shell in the I -dimensional space of the y_i/σ_i . Replacing the volume element $\Pi_i (dy_i/\sigma_i)$ in Eq. 159 by the volume of this infinitesimal shell and normalising properly one finds the probability

$$p(\chi^2) d\chi^2 = \Gamma\left(\frac{I}{2}\right)^{-1} \left(\frac{\chi^2}{2}\right)^{I/2-1} \exp\left(-\frac{\chi^2}{2}\right) \frac{d\chi^2}{2}. \quad (174)$$

In practice one does not know the true χ^2 (relative to the true y_i) but only that relative to the most likely estimate. This can be taken into account if I is replaced by $I-M$, the effective degree of freedom (M : number of estimated parameters), so that

$$p(\chi^2) d\chi^2 = \Gamma\left(\frac{I-M}{2}\right)^{-1} \left(\frac{\chi^2}{2}\right)^{(I-M)/2-1} \exp\left(-\frac{\chi^2}{2}\right) \frac{d\chi^2}{2} \quad (177)$$

with the expectation values

$$\langle \chi^2 \rangle = I-M, \quad \text{var } \chi^2 = 2(I-M). \quad (178)(179)$$

Thus χ^2 can be expected to be about equal to the effective degree of freedom: $\chi^2 \approx (I-M) \pm \sqrt{2(I-M)}$. If it is much larger the fit must be considered as bad because either

- the mathematical model is inadequate, or
- the data are faulty, or
- the data errors were underestimated.

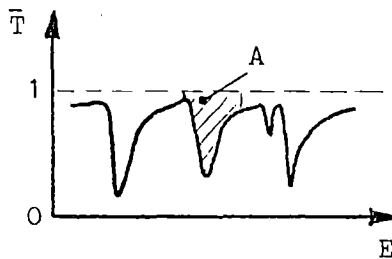
Frequently the last explanation is the correct one: systematic errors are often underestimated or not recognised at all. One should then rescale all errors as follows,

$$\sigma_i \rightarrow \sigma_i \sqrt{\frac{\chi^2}{I-M}}, \quad \delta x_\mu \rightarrow \delta x_\mu \sqrt{\frac{\chi^2}{I-M}}. \quad (180)(181)$$

Inadequacy of the mathematical model can mean that an unrecognised resonance is present or a resonance spin is wrong.

2.7.4 Area analysis

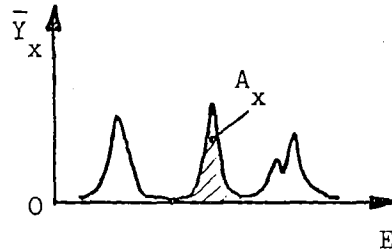
The simplest method to extract resonance parameters from measured data is area analysis. The fitted quantities (y_i in the least-squares formulae of the preceding sections) are taken to be the areas of transmission dips



$$A = \int dE (1 - e^{-n\bar{\sigma}}) \approx \frac{\Gamma}{2} \int_{-\infty}^{\infty} dx (1 - e^{-n\sigma_0 \psi(x, \beta)}), \quad (182)$$

(n,x) peaks,

$$A_x \approx \int dE (1 - e^{-n\bar{\sigma}}) \frac{\bar{\sigma}_x}{\bar{\sigma}} \approx A \frac{\Gamma_x}{\Gamma}, \quad (183)$$



or ratios of such areas, e.g. the (n,x) self-indication ratio

$$R \approx \frac{\int dE e^{-n'\bar{\sigma}} (1 - e^{-n\bar{\sigma}}) \frac{\bar{\sigma}_x}{\bar{\sigma}}}{\int dE (1 - e^{-n\bar{\sigma}}) \frac{\bar{\sigma}_x}{\bar{\sigma}}} \approx \frac{A(n+n') - A(n')}{A(n)} \quad (184)$$

Fig. 6

where the bars denote Doppler broadening, ψ is the Voigt profile, Eq. 75, and

$$\sigma_0 = (4\pi\lambda^2 \frac{\Gamma_n}{g\Gamma})_{E=E_0}, \quad x = \frac{E-E_0}{\Gamma/2}. \quad (185)(186)$$

Ideally all these quantities are measured with the same set-up in the same flux. A capture measurement, for example, is easily extended to yield transmission and self-indication data, too, by insertion of a filter sample in front of the capture sample. One can then measure in alternating cycles filter transmission (capture sample out), self-indication data (both samples in) and capture yield (filter sample out). In order to optimise the sample thicknesses and choice of observables one considers (Refs. 42, 43) the SLBW thin- and thick-sample expressions that follow from the properties of the Voigt profiles if potential and multiple scattering is neglected (or subtracted out),

$$A = \pi n \sigma_0 \Gamma / 2, \quad A_x = \pi n \sigma_0 \Gamma_x / 2 \quad (n\bar{\sigma} \ll 1), \quad (187)(188)$$

$$A = \Gamma \sqrt{\pi n \sigma_0}, \quad A_x = \Gamma_x \sqrt{\pi n \sigma_0} \quad (n\bar{\sigma} \gg 1). \quad (189)(190)$$

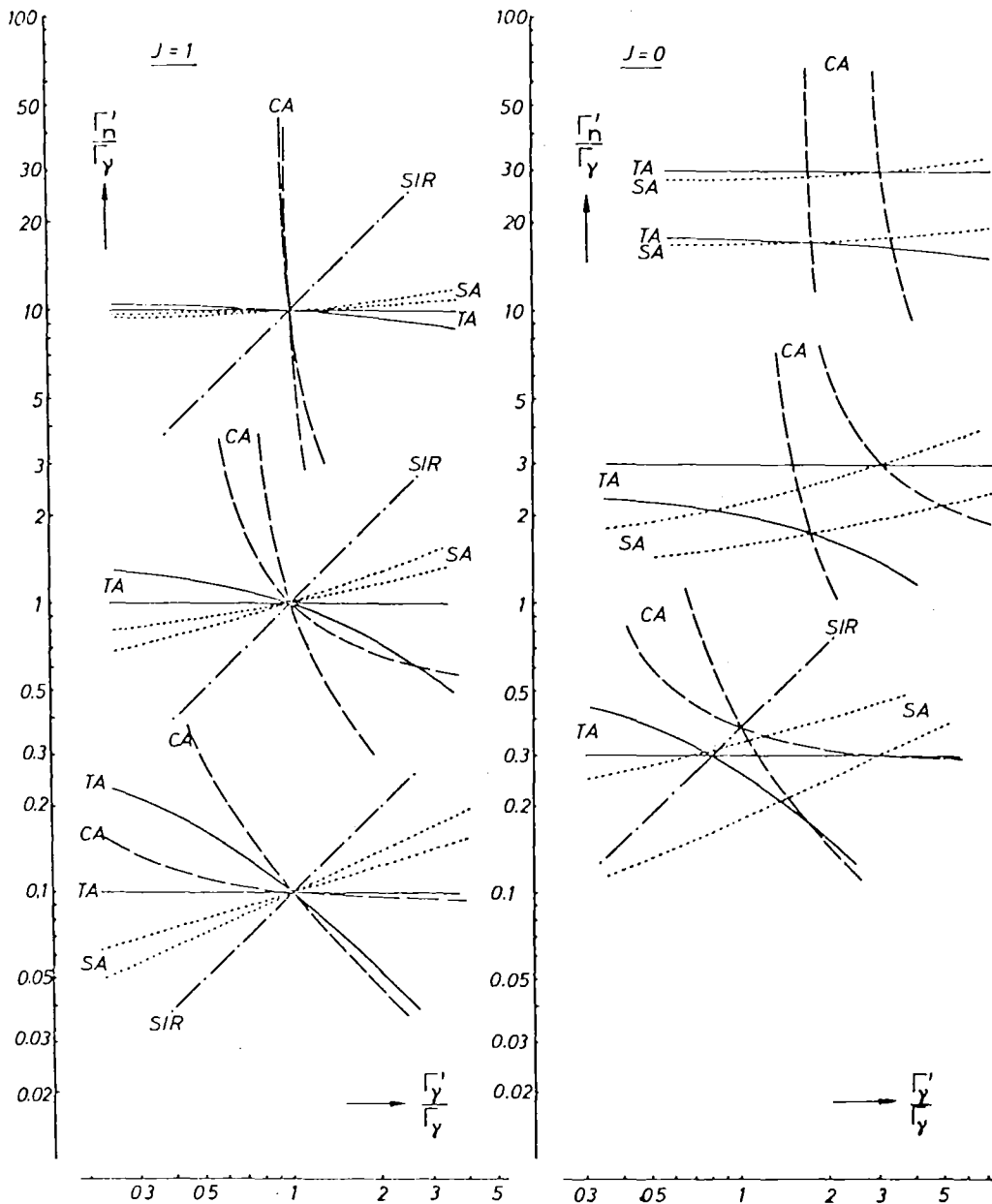


Fig. 7 - Idealised area analysis curves derived under the assumption that the samples are either very thin or very thick for transmission areas (TA), capture areas (CA) and scattering areas (SA), and that self-indication ratios (SIR) were measured with a thick filter and a thin detector sample, or vice versa. Abscissae and ordinates are calculated values Γ'_y and Γ'_n in units of the true radiation width Γ_y , on a log-log scale. Three cases are shown: strong, intermediate and weak scattering ($\Gamma_n:\Gamma_y = 10, 1, 0.1$, respectively). The curves on the left were derived with the correct spin factor - they are independent of J . The curves on the right demonstrate what happens if the spin factor is taken three times too small - this corresponds to an incorrect compound spin $J = 0$ and a correct spin $J = 1$. A realistic example is shown in Fig. 9 (Ref. 43).

Similarly one gets for thick filter and thin detector sample

$$R_x = \frac{1}{\sqrt{\pi n' \sigma_0}} \quad (n' \bar{\sigma} \gg 1, n \bar{\sigma} \ll 1). \quad (191)$$

Equating these theoretical expressions to the measured quantities one sees that, for given level energy E_0 and spin factor g , each one defines an equation between the partial widths of the form $\eta_i = y_i(\Gamma_n, \Gamma_\gamma, \Gamma_f, \dots)$. The most important case for non-fissile nuclei, $\Gamma = \Gamma_n + \Gamma_\gamma$ is represented by 2-dimensional plots (Ref. 43) in Fig. 7. Each equation defines a curve, for the correct g and zero experimental errors all curves intersect in one point. In practice the intersection is not perfect but usually much better than that for an incorrect spin, so that the correct spin is readily recognised. One wants the curves to intersect at angles approaching 90° so that the parameter pair is well defined. For which choice of observables this is achieved depends on the ratio Γ_n/Γ_γ , see Table 6. Very weak resonances are difficult to see in transmission data, even with thick samples.

Table 6: Best Combinations of Observables for Area Analysis if $\Gamma = \Gamma_n + \Gamma_\gamma$

Resonance Type	Best Combinations	Uncertainties (%)	
		$\delta\Gamma_n/\Gamma_n$	$\delta\Gamma_\gamma/\Gamma_\gamma$
$\Gamma_n > \Gamma_\gamma$, strong scattering	(A_γ, A) , (R_γ, A)	~ 2	10 - 20
$\Gamma_n \sim \Gamma_\gamma$, intermediate "	(R_γ, A) , (R_γ, A_γ)	~ 5	5 - 10
$\Gamma_n < \Gamma_\gamma$, weak "	(R_γ, A) , (R_γ, A_γ)	5 - 10	10 - 20
$\Gamma_n \ll \Gamma_\gamma$, very weak "	(R_γ, A_γ)	5 - 10	$\gtrsim 20$

The uncertainties $\delta\Gamma_\gamma$ for strong resonances are mainly due to those of multiple-collision calculations while those for weak levels are mostly caused by backgrounds and statistics.

The principal advantage of area analysis is the insensitivity of areas to resolution broadening, at least as far as the resonance dips or peaks are well separated.

2.7.5 Shape analysis

If adjacent resonances (doublets, triplets etc.) are incompletely resolved instrumentally and the resolution function is well known shape analysis is superior to area analysis. The same is true if very many levels must be analysed. In general shape analysis is more convenient and utilises all the information contained in the data.

The y_i in our least-squares formulae are now the individual data points. There is nothing in the formalism that restricts one to a single resonance or a single set of data points. In a single computer run one can adjust all resonance parameters within a given energy range by simultaneously fitting all relevant transmission, capture, fission ... data points irrespective of experiment, sample thickness, instrumental resolution etc. The only condition is that for all η_i the corresponding theoretical values y_i and their derivatives $y_{i,u}$ with respect to the adjusted parameters can be calculated. Of course this is normally beyond hand calculation and one relies heavily on computer codes which in turn have their own limitations as to data types, number of data points, number of cross section parameters that can be handled etc. As mentioned already it is best to analyse all transmission data before one starts fitting yield data.

2.7.6 Computer codes

The initially employed graph methods for area analysis of neutron resonances (Refs. 37, 44) are no longer needed since least-squares computer codes have been developed. A widely used area analysis code was written by Atta and Harvey (Ref. 45) for transmission data analysis. The TACASI code (Ref. 46) for combined transmission area, capture area and self-indication ratio analysis contains the necessary Monte Carlo subroutines for simulation of multiple-collision events. Both these codes employ the "many-level" Breit-Wigner formalism (simple sums over SLBW resonance terms), Doppler broadening by means of Voigt profiles and resolution broadening with a Gaussian. The Atta-Harvey code, however, uses the approximation $\phi_c \ll 1$ which may cause difficulties with s-wave levels at keV energies. An area analysis code for scattering data is under development at CBNM Geel (Ref. 47). As an example TACASI handles simultaneously

- ≤ 20 observed transmission areas, capture areas and/or self-indication ratios,
- ≤ 7 resonances, i.e. one main resonance with adjusted Γ_n and Γ_γ , plus up to 6 subresonances with fixed parameters for the calculation of resonance overlap and sample impurity corrections.

TACASI versions that also handle a single observed quantity and adjust one parameter, e.g. Γ_γ , were developed at KfK (Ref. 48) and CBNM Geel (Ref. 49).

The next generation of codes was developed for shape analysis. Some shape analysis codes require data reduced to cross section form, the more convenient ones handle transmission and yield data directly. The following codes fit Doppler- and resolution-broadened cross sections:

- the Reich-Moore code for σ_T and σ_f developed by Derrien, described in Ref. 50;
- the very flexible Reich-Moore program ACSAP (Ref. 51) for $\sigma_T, \sigma_n, \sigma_\gamma, \sigma_f$;
- the Adler-Adler program CODILLI (Ref. 52) for σ_T and σ_f , restricted to heavy nuclei.

Examples for automatic shape analysis codes for transmission data are

- the Atta-Harvey many-level Breit-Wigner shape code, Ref. 45, restricted to nonfissile nuclei and cases with $\phi_c \ll 1$ (below few keV for s-wave levels);
- The MLBW code SIOB ("seven in one blow", i.e. 7 transmission runs fitted simultaneously) suited for heavy non-fissile nuclei (Ref. 53);
- the elaborate and ponderous one-channel Reich-Moore code REFIT (Ref. 54) that fits up to 20 transmission runs simultaneously by adjustment of up to 100 cross section parameters; suited for heavy as well as for light nuclei;
- the FANAL code (Ref. 36) that was written for light and medium-mass nuclei below 400 keV. It employs two-channel Reich-Moore formulae without Doppler broadening for (1 elastic, 1 inelastic) s-wave channels, SLBW formulae for p-, d-... wave channels, fits 5 runs simultaneously by adjustment of up to 50 parameters and is very fast due to the hybrid cross section representation.

All these codes include Doppler-broadening (numerical for Reich-Moore cross sections, exception: s-wave levels in FANAL) and resolution broadening.

Automatic shape analysis programs for yield data are not so numerous yet. The multiple-collision yield, usually calculated by Monte Carlo simulation, presents difficulties in the least-squares formalism because its derivatives are not normally available. One operational shape code is

- FANAC (Ref. 38). It is written for light and medium-mass nuclei below 400 keV, employs the same hybrid cross section formalism as FANAL (see above) but contains, in addition, Monte Carlo subroutines for multiple-collision simulation. It fits up to 5 experimental runs by adjustment of up to 20 resonance parameters.
- The REFIT program (see above) is being extended to include capture shape analysis, too.

Illustrations for some of these codes are given in Figs. 9-19.

2.8 Miscellaneous useful resonance-theoretical expressions

2.8.1 Maxima and minima (windows) in the total cross section

Setting the cross section derivative with respect to energy equal to zero one finds expressions for the energies where the extrema of the cross section occur. Neglecting slow energy dependences (of λ_c , L_c , ϕ_c) one gets in SLBW approximation for the maximum

$$E_+ = E_0 + \frac{\Gamma}{2} \tan \phi_c, \quad \sigma_c(E_+) = 4\pi\lambda_c^2 g_c, \quad (192)(193)$$

and for the minimum ("window") caused by interference between potential and resonant scattering

$$E_- = E_0 - \frac{\Gamma}{2} \cot \phi_c, \quad \sigma_c(E_-) = 4\pi\lambda_c^2 g_c \left(1 - \frac{\Gamma_n}{\Gamma}\right), \quad (194)(195)$$

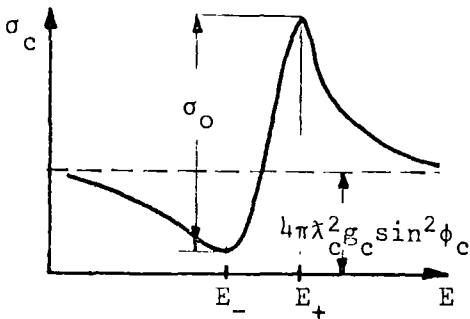


Fig. 8

whence

$$E_0 = E_+ \cos^2 \phi_c + E_- \sin^2 \phi_c, \quad (196)$$

$$\Gamma = (E_+ - E_-) \sin 2\phi_c, \quad (197)$$

$$\sigma_0 = 4\pi\lambda_c^2 g_c \frac{\Gamma_n}{\Gamma} = \sigma_c(E_+) - \sigma_c(E_-). \quad (198)$$

For light and medium-weight nuclei, for which Doppler and resolution broadening are often negligible, these relationships are quite useful to determine g_c , i.e. J (Eq. 193), as well as first guesses for E_0 , Γ and Γ_n (Eqs. 196-198) directly from the observed extrema. Note that the nominal resonance energy, E_0 , is different from the energy at the peak, E_+ . The interference dip is the deeper the less absorption one has. For pure elastic scattering ($\Gamma = \Gamma_n$) one gets $\sigma_c(E_-) = 0$. In the minima the observed total cross section may therefore be dominated by other channels (partial waves), other levels and impurities. Other relationships that can provide starting values for least-squares analysis are the SLBW area expressions

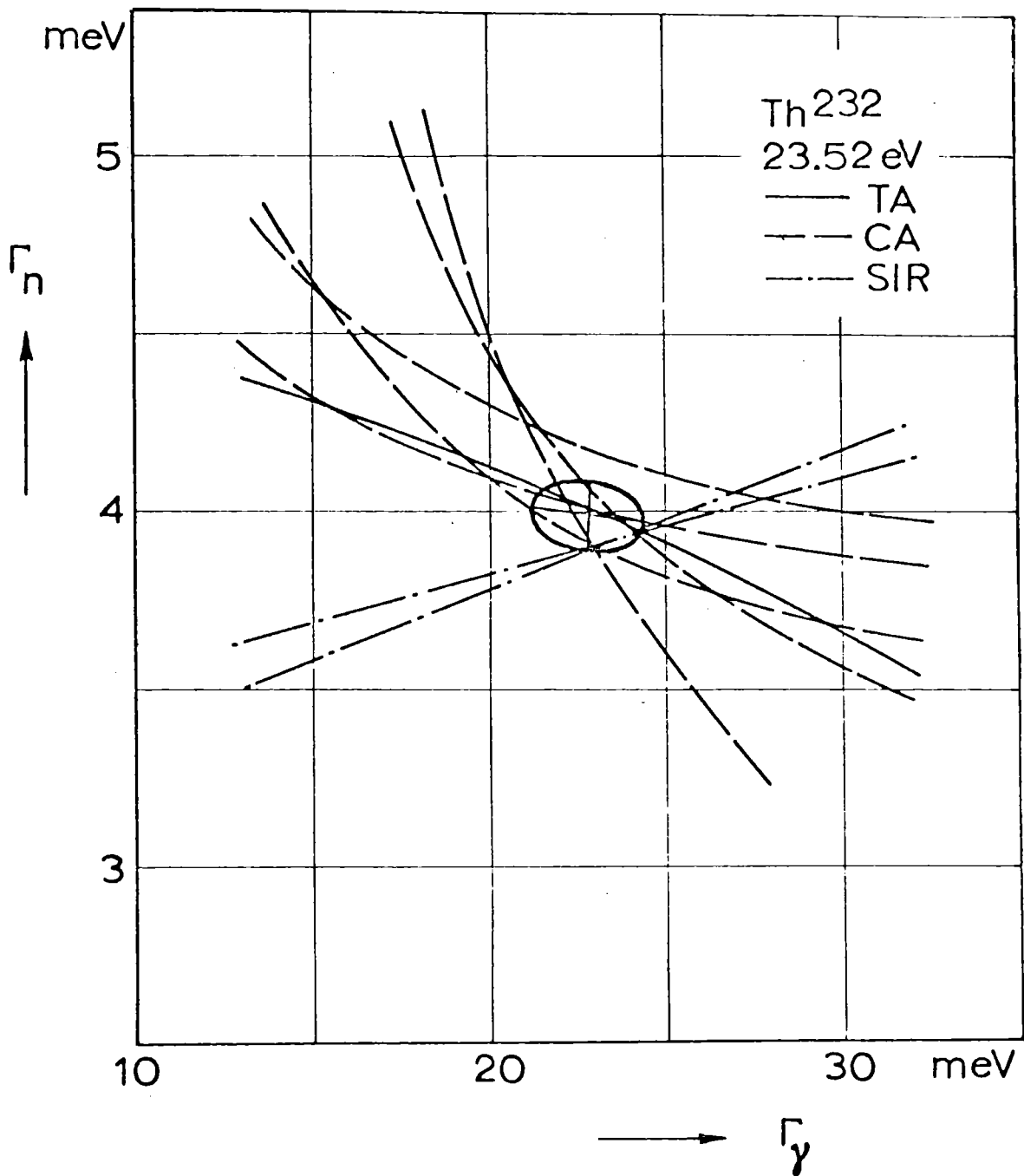


Fig. 9 - Area analysis curves from transmission areas, capture areas and self-indication ratios (TA, CA, SIR) measured for a resonance of $^{232}\text{Th}+n$ with different sample thicknesses. The error ellipse illustrates the final result of a simultaneous fit with the TACASI code, viz. Γ_γ , Γ_n , the uncertainties and the correlation (see Ref. 46).

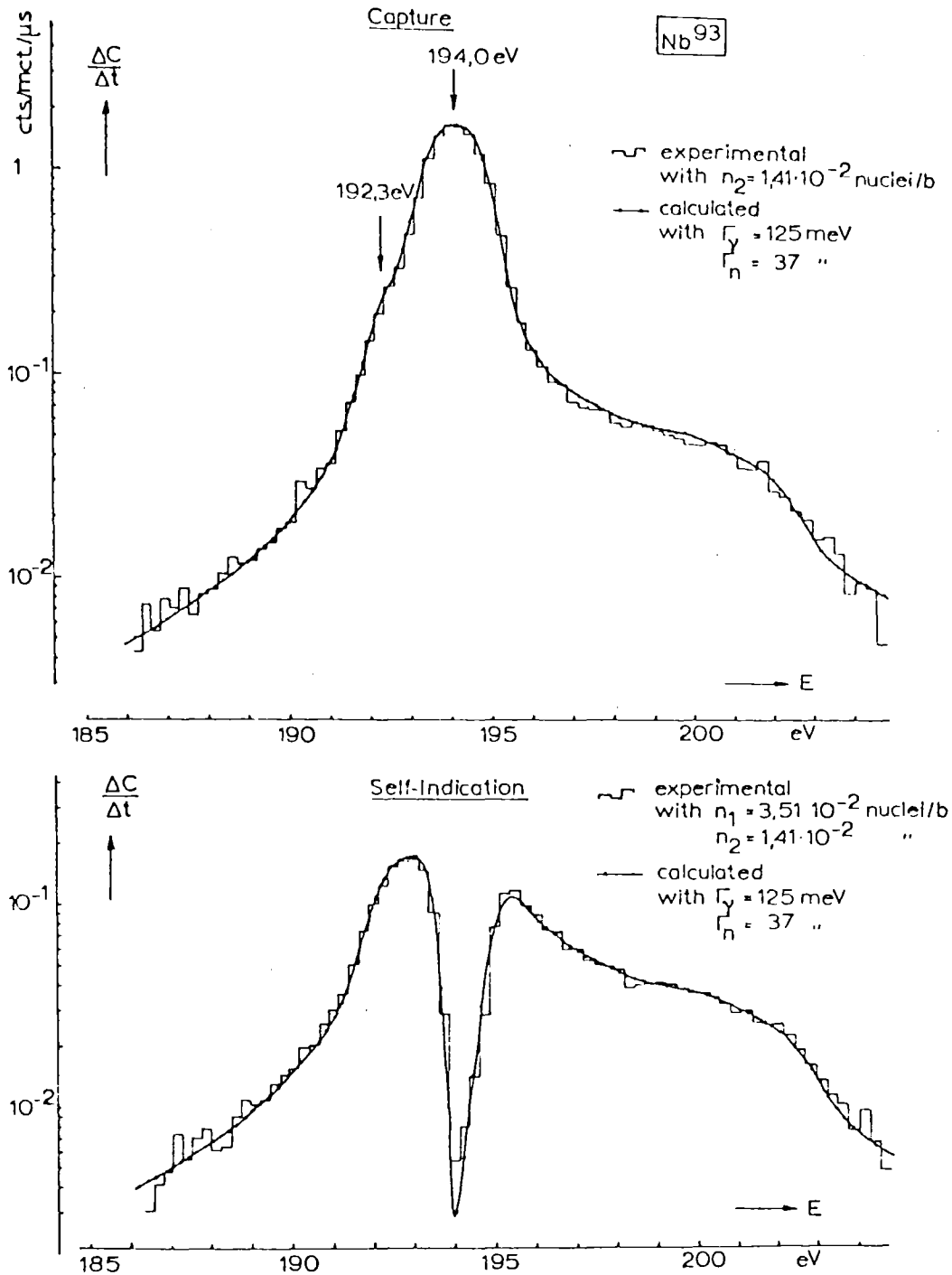


Fig. 10 - Measured (histograms) and calculated (smooth curves) capture and self-indication count rates near the 194 eV resonance of $^{93}\text{Nb}+n$. The enhancement around 200 eV is due to multiple scattering: The low-energy maximum of the self-indication curve is higher than the high-energy one because of the "window" produced by interference between potential and resonance scattering. The calculated curves were obtained with the TACASI code which actually fits the areas under the histograms but for checking purposes also prints the shapes in tabular form (Ref. 46).

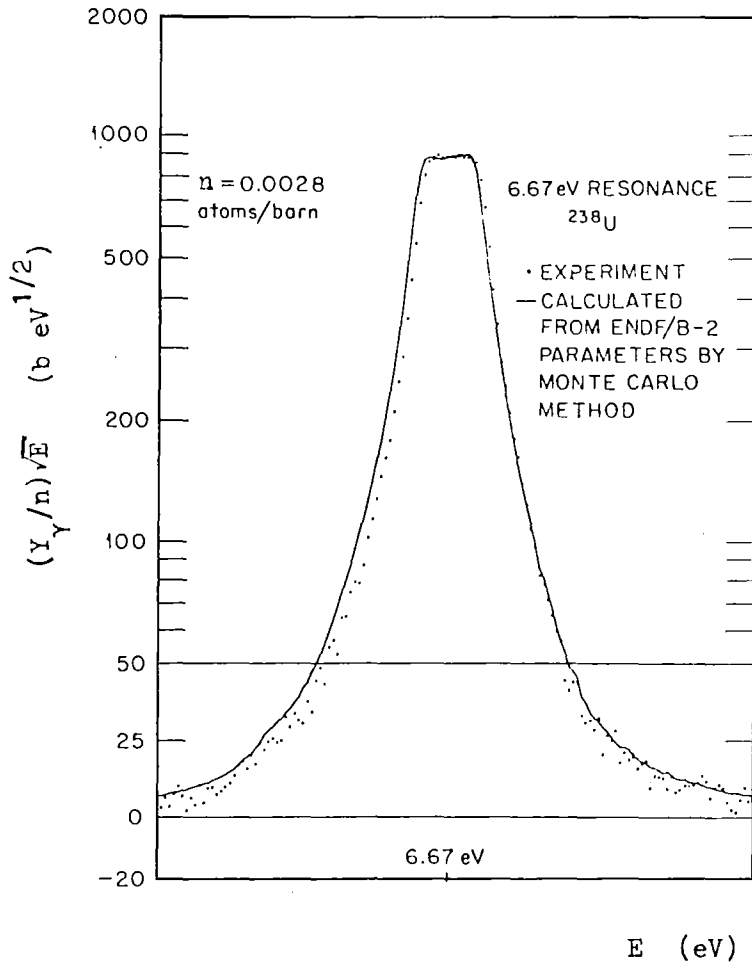


Fig. 11 - Thick-sample capture peak suitable for $\epsilon\phi$ determination with the saturated-resonance calibration technique. The flat top is typical for thick-sample yield data and indicates the region where the sample is black so that, apart from multiple scattering, $\sigma_\gamma/\sigma \approx \Gamma_\gamma/\Gamma$ (from Ref. 89).

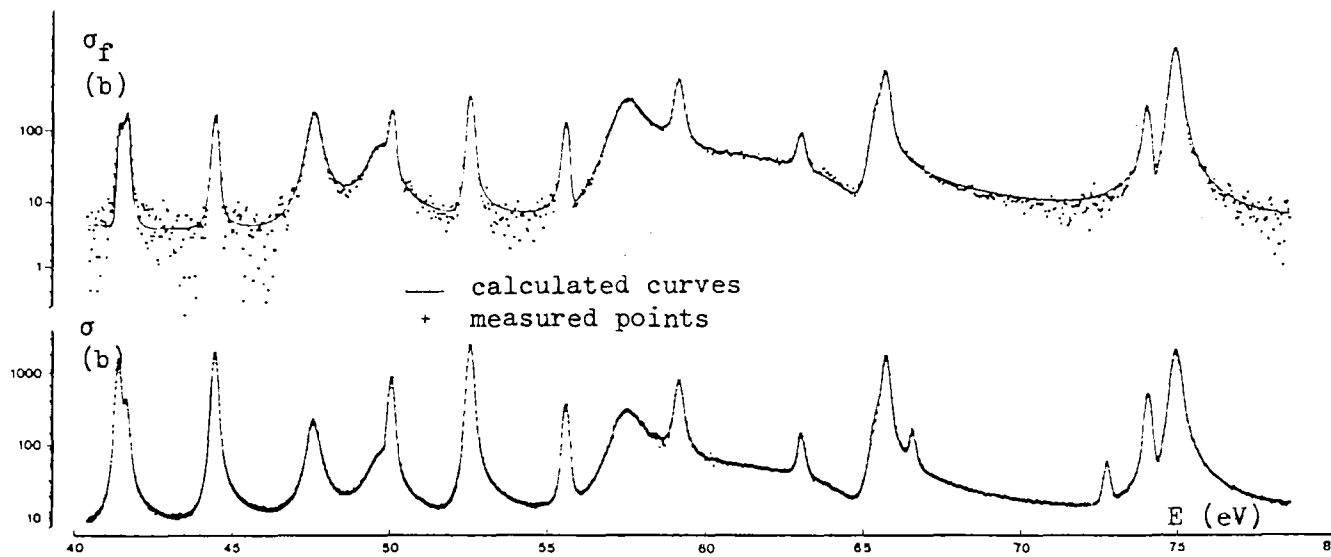


Fig. 12 - Fission and total cross section data for ^{239}Pu measured by time of flight. The smooth curves are least-squares fits obtained with Derrien's three-channel Reich-Moore shape analysis code (Ref. 50).

AUTOMATIC CROSS SECTION ANALYSIS PROGRAM

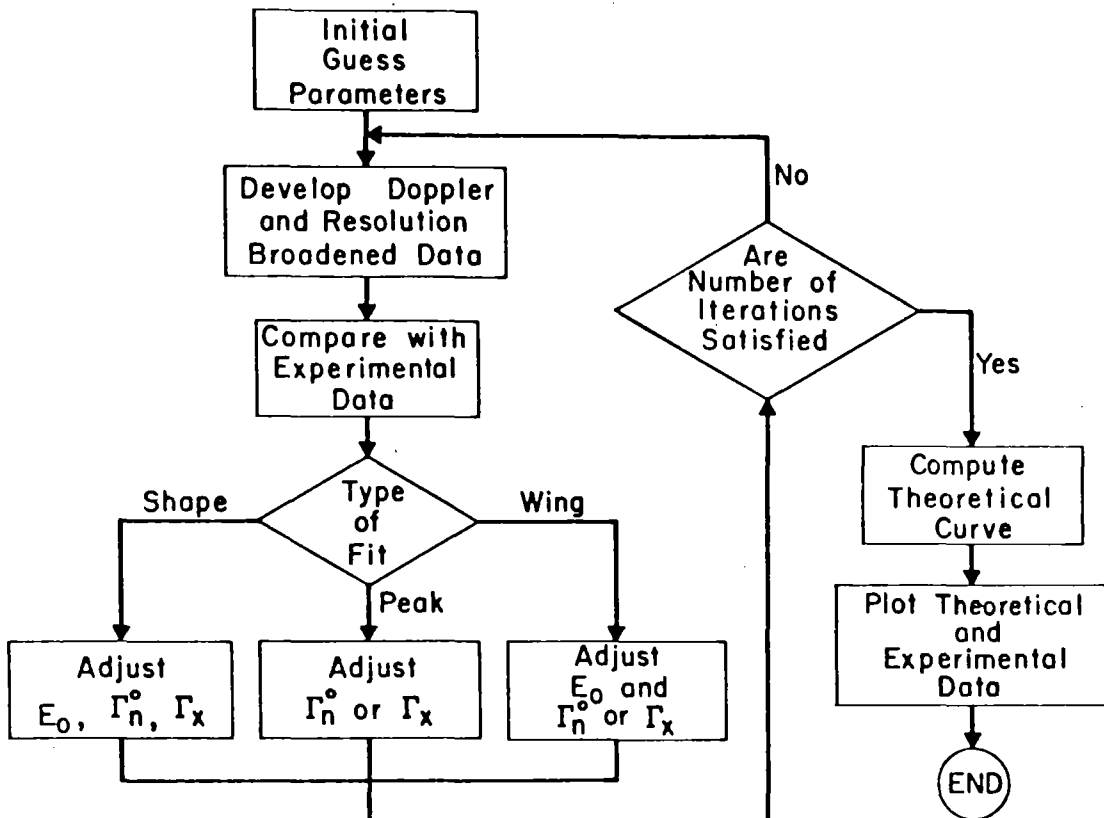


Fig. 13 - Flow diagram of the shape analysis program ACSAP. Theoretical cross section data are computed from initial guess parameters, then Doppler and resolution broadened, finally compared with the input data. After adjusting the desired parameters the program reiterates a specified number of times before producing an output listing and plot of the results (from Ref. 51).

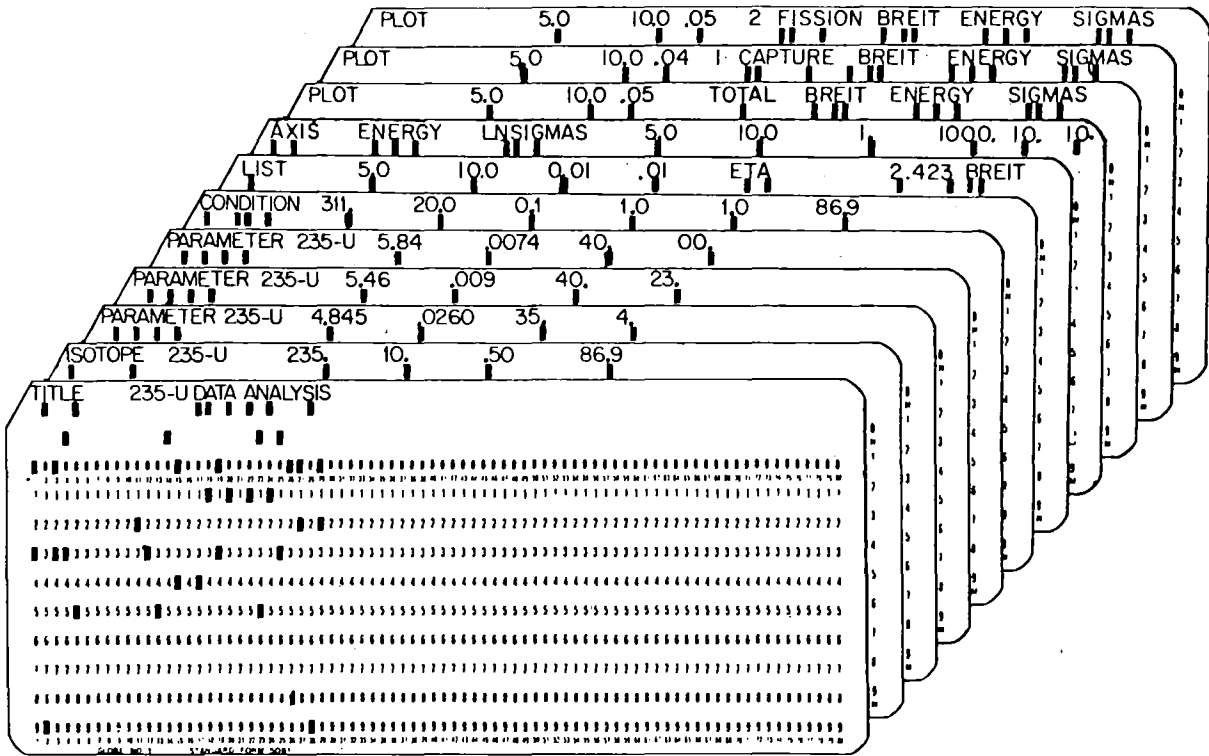


Figure 14 - Input function cards for a short ACSAP run. Key words at the first of each card provide programmability. (from Ref. 51)

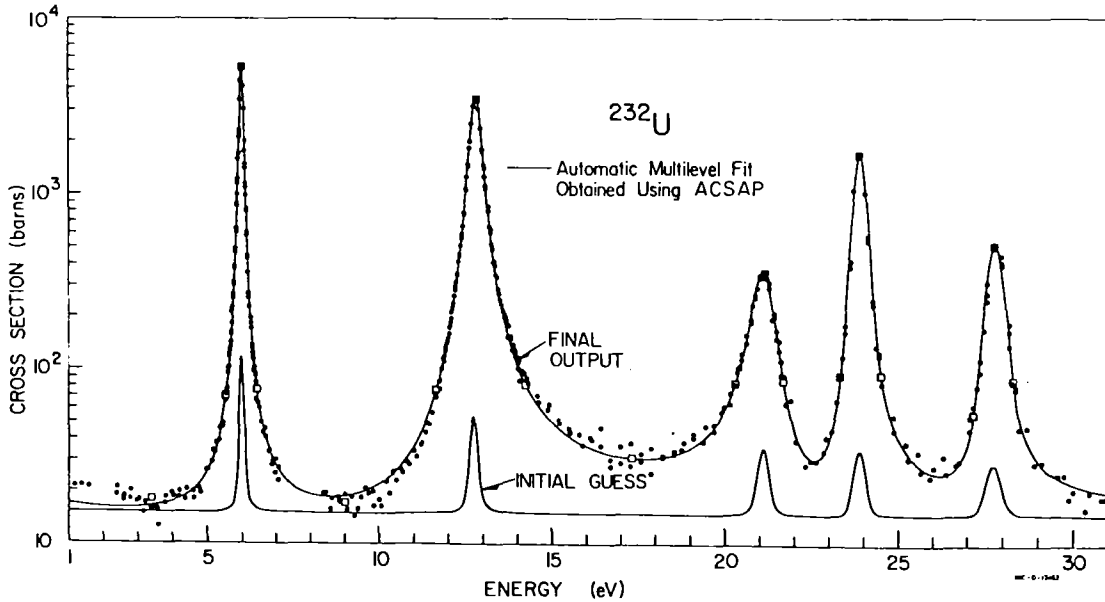


Figure 15 - A theoretical fit to the ²³²U cross section using ACSAP. Initial guess parameters were deliberately chosen "far from correct" to emphasize power of ACSAP algorithms (from Ref. 51).

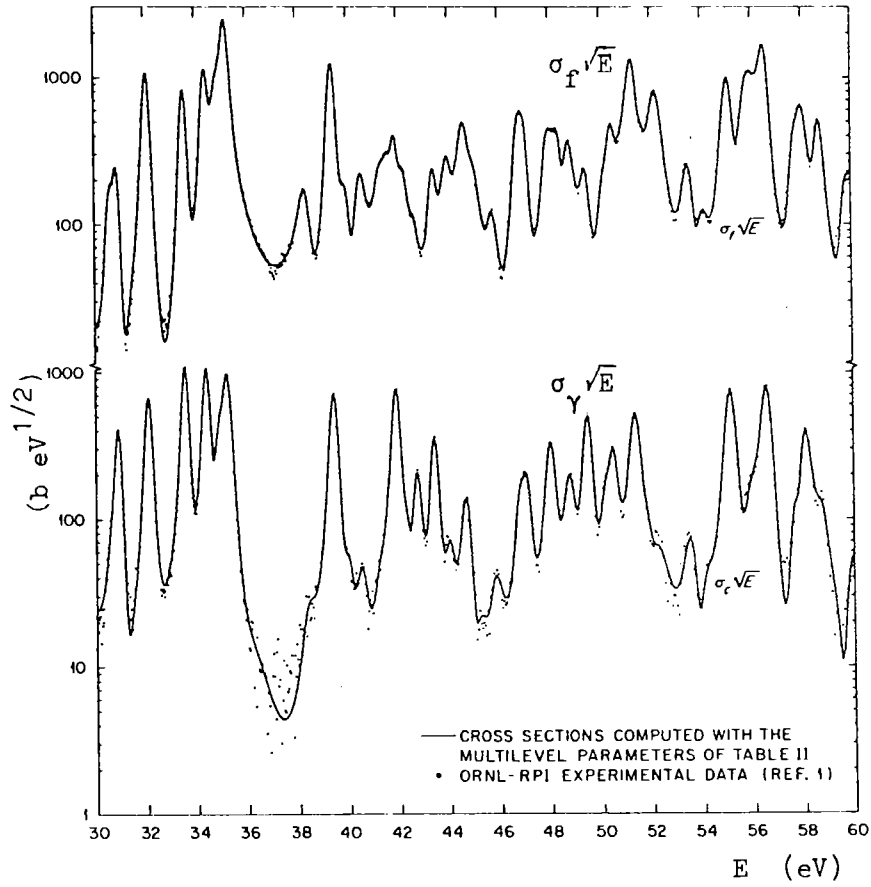


Fig. 16 - Fission and capture cross sections of ^{235}U from 30 to 60 eV. The curves are obtained in a simultaneous fit with the Adler-Adler formalism (Ref. 89).

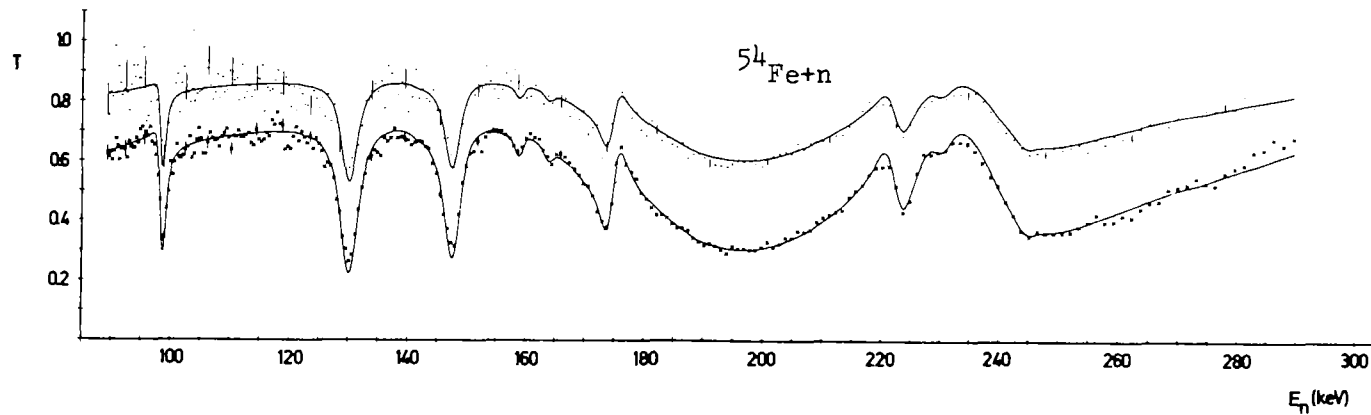


Fig. 17 - Two sets of transmission data on ^{54}Fe and a simultaneous fit obtained with the transmission shape analysis code FANAL (Ref. 36). Note the very severe level-level interference caused by the unusually broad s-wave resonances at 191 and 246 keV. As a consequence the resonance shapes above 120 keV are quite unlike single-level Breit-Wigner shapes. Nevertheless they are properly described by the employed Reich-Moore formalism (from Ref. 90).

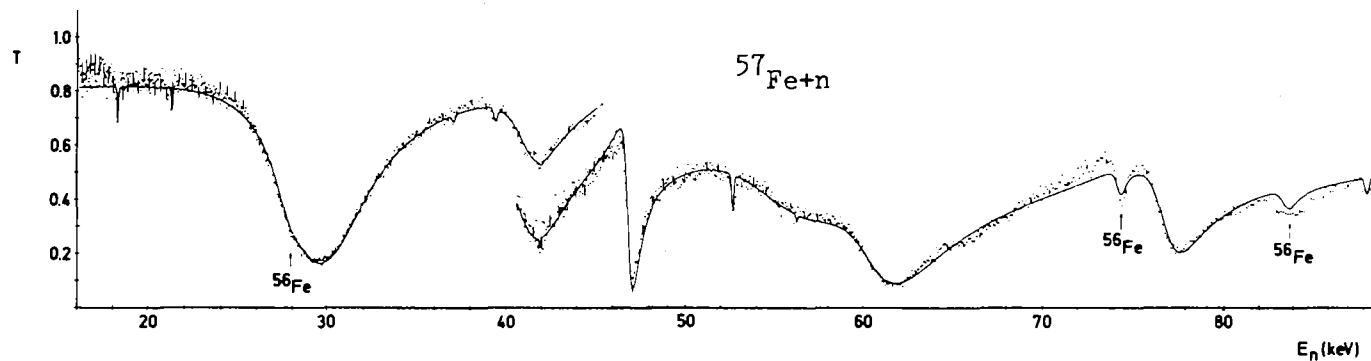


Fig. 18 - Two sets of transmission data on ^{57}Fe and a simultaneous fit obtained with the transmission shape analysis code FANAL (Ref. 36). The interpretation here is complicated by the fact that no less than three s-wave channels are open, two elastic ($J = 0$ and $J = 1$) and one inelastic channel ($J = 1$). Additional elastic and especially inelastic scattering data would have been helpful to resolve the many ambiguities (from Ref. 90).

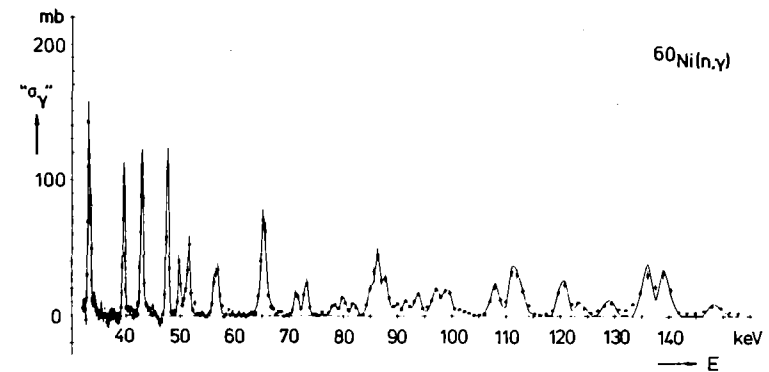
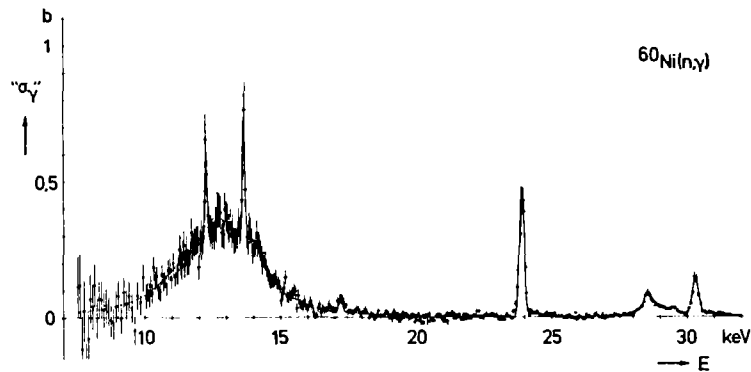
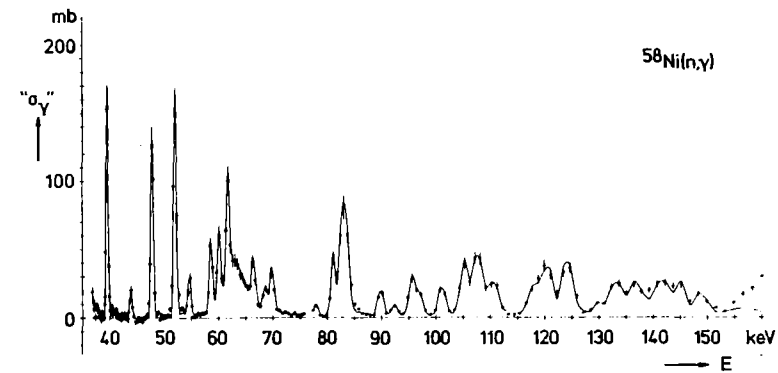
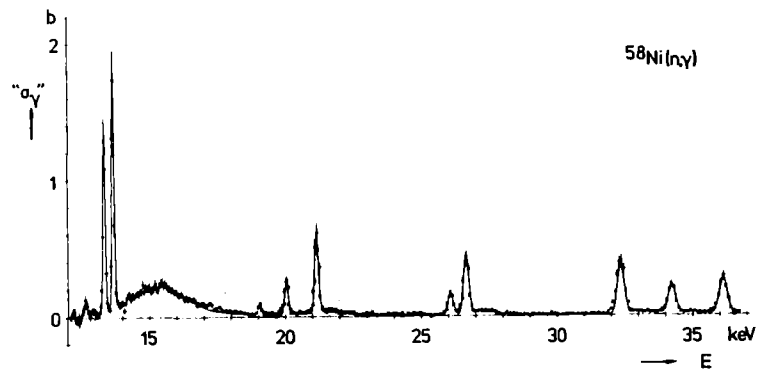
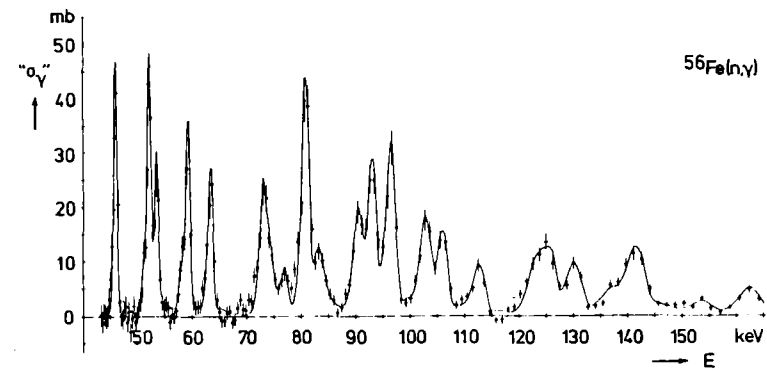
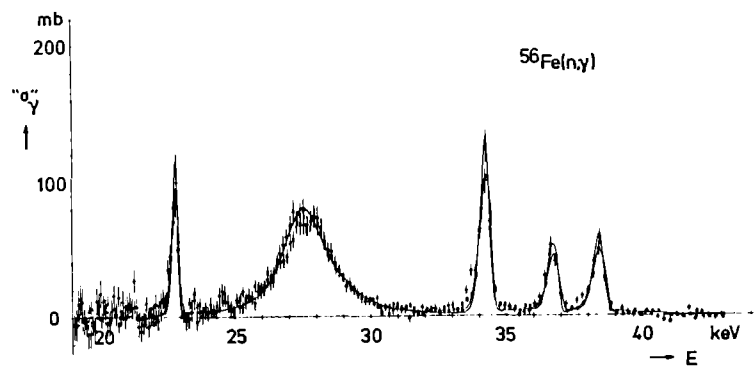


Fig. 19 - Capture yield data on structural-material isotopes and automatic fits obtained with the capture shape analysis program FANAC (Ref. 38). Most of the resonances seen here are p- and d-wave levels. The two curves for the low-energy data on ^{56}Fe correspond to the two data sets taken with slightly different resolution. (From Ref. 40c)

$$\int dE (\sigma - \sigma_p) = 2\pi^2 \lambda_c^2 g \Gamma_n \cos 2\phi_c, \quad (199)$$

$$\int dE \sigma_x = 2\pi^2 \lambda_c^2 g \frac{\Gamma_n x}{\Gamma}, \quad (200)$$

which do not depend on resolution or Doppler broadening.

2.8.2 Distant levels

So far we glossed over the problems associated with the infinite number of eigenvalues E_λ . In practice one knows only a finite number Λ of them and splits the R-matrix or reduced R-matrix in a smooth part R^0 due to the "distant" levels outside a given energy range and a resonant part R^1 due to the levels explicitly considered,

$$R_{cc'} = R_{cc'}^0 + R_{cc'}^1 = R_{cc'}^0 + \sum_{\lambda=1}^{\Lambda} \frac{\gamma_{\lambda c} \gamma_{\lambda c'}}{E_\lambda - E}. \quad (201)$$

In SLBW approximation the sum contains one term only, in Reich-Moore approximation E_λ is to be replaced by $E_\lambda + \Delta_\lambda - i\Gamma_\lambda/2$ (see Sect. 2.3.7). In the resonance region non-resonant, i.e. "direct" transitions between channels can usually be neglected and so can off-diagonal elements of R^0 which represent such transitions. We write therefore

$$[1 - R^0 L^0]_{cc'} = (1 - R_{cc'}^0 L_c^0) \delta_{cc'} = q_{cc'} e^{i\xi_c} \quad (202)$$

with $q_{cc'} = |1 - R_{cc'}^0 L_c^0| \delta_{cc'}$, $\xi_c = \arg(1 - R_{cc'}^0 L_c^0)$ (203)(204)

and get $[(1 - RL^0)^{-1}]_{cc'} = e^{-i\xi_c} [(1 - q^{-1} R_q^{-1} (1 - R^0 L^{0*}) L^0)^{-1}]_{cc'} \frac{1}{q_{c'c}}$ (205)

$$[1 - RL^{0*}]_{cc'} = q_{cc'} [1 - q^{-1} R_q^{-1} (1 - R^0 L^0) L^{0*}]_{cc'} e^{-i\xi_c} \quad (206)$$

Inserting this in the expression (17) for U we see that all R-matrix equations are preserved if we redefine as follows,

$$\gamma_{\lambda c} \rightarrow \frac{\gamma_{\lambda c}}{|1 - R_{cc'}^0 L_c^0|} \equiv \alpha_{\lambda c} \quad \text{affecting } R_{cc'}, \Gamma_{\lambda c}, \Delta_\lambda, (A^{-1})_{\lambda\mu} \quad (207)$$

$$\phi_c \rightarrow \phi_c + \arg(1 - R_{cc'}^0 L_c^0), \quad " \quad \sigma_p, \quad (208)$$

$$\gamma_{\lambda c} L_c^0 \gamma_{\mu c} \rightarrow \alpha_{\lambda c} (L_c^0 - R_{cc'}^0 |L_c^0|^2) \alpha_{\mu c} \quad " \quad \Delta_\lambda, (A^{-1})_{\lambda\mu}. \quad (209)$$

We can use level statistics to estimate $R_{cc'}^0$. Denoting length and midpoint of the interval of explicitly given levels by I and \bar{E} we have

$$R_{cc'}^0 = \sum_{\lambda} \frac{\gamma_{\lambda c}^2}{E_\lambda - E} - \sum_{\lambda=1}^{\Lambda} \frac{\gamma_{\lambda c}^2}{E_\lambda - E} = \int_{-\infty}^{\infty} dE' \frac{s_c(E')}{E' - E} - \int_{\bar{E}-I/2}^{\bar{E}+I/2} dE' \frac{s_c(E')}{E' - E}, \quad (210)$$

where we replaced sums by integrals and introduced the strength function s_c , Eq.50. With the definition of the distant-level parameter R_c^{∞} (Eq. 51) and the assumption that neither R_c nor s_c varies significantly over the c interval I one gets

$$R_{cc}^0 = R_c^{\infty}(\bar{E}) - 2s_c(\bar{E}) \operatorname{ar} \tanh \frac{E-\bar{E}}{I/2}, \quad (211)$$

a result which in practice is only needed for neutron channels ($c \in n$). Usually derived from a picket fence model (e.g. in Refs. 36, 55) it is seen to be quite general. It has the great advantage over expansions in powers of $E-\bar{E}$ with adjustable coefficients (e.g. Refs. 54, 56) that only two parameters with a clear physical meaning are involved, R_c^{∞} (or R_c' , cf. Eq. 53) and s_c (or S_{JJ} , cf. Eq. 54). Both are tabulated extensively (e.g. in Ref. 4) or can be estimated with the optical model. Only slight adjustment (if any) is usually needed for a very satisfactory reproduction of potential scattering over very wide energy ranges. As an example Fig.20 shows R_c' vs. A as calculated from an optical model (Ref. 59) and R_c' values for medium-mass nuclei obtained empirically by adjusting R_c^{∞} (together with s_c and the resonance parameters) in shape fits to transmission data in the range 10 to 300 keV (Refs. 57, 58), see also Figs.17,18). Since Eq. 211 is valid on the average but not in cases where untypically weak or strong levels are located just outside the interval I it is good practice to include such "nearby" levels explicitly in R_c' and to use Eq. 211 only for the more distant levels. This means that the interval I is chosen wider than the interval in which one actually wants to calculate cross sections.

2.8.3 Subthreshold ("negative") levels

An example of the "nearby" levels just mentioned are levels with $E_{\lambda} < 0$ ("negative" levels) corresponding to compound states just below the neutron binding energy. Although low-energy cross sections are mainly determined by the "positive" levels their exact description frequently requires one or at most two additional levels with $E_{\lambda} < 0$. Let us assume that for a non-fissile target nucleus ($\Gamma = \Gamma_n + \Gamma_{\gamma}$) we know the positive levels up to a certain energy and want to determine the parameters E_{λ} , $\Gamma_{\lambda n}$, $\Gamma_{\lambda \gamma}$ for one negative level so that the thermal cross sections are reproduced. At thermal energies the P_{λ} for $\lambda > 1$ are so small that only s-wave interaction need be considered. With the usual choice $B_c = 0$ the Reich-Moore collision function for a given s-wave channel is given by

$$U_{cc} = e^{-2i\phi_c} \frac{1+i \sum_{\lambda} \frac{\Gamma_{\lambda n}/2}{E_{\lambda} - E - i\Gamma_{\lambda \gamma}/2}}{1-i \sum_{\lambda} \frac{\Gamma_{\lambda n}/2}{E_{\lambda} - E - i\Gamma_{\lambda \gamma}/2}} \quad (c \in n). \quad (212)$$

The resonance parameters for all positive levels and the one negative level are contained in the sum, and in this way they enter into all cross section expressions. The explicit relationship between the sum and the cross sections is obtained if we solve Eq. 212 for the sum and eliminate U_{cc} by means of

$$\operatorname{Re} U_{cc} = 1 - \frac{\sigma_c}{2\pi\lambda_c^2 g_c}, \quad \operatorname{Im} U_{cc} = \pm \sqrt{\frac{\sigma_{cc}}{\pi\lambda_c^2 g_c} - \left(\frac{\sigma_c}{2\pi\lambda_c^2 g_c}\right)^2}, \quad (213)(214)$$

which follows from Eqs. 14 and 15. The resulting expression can then be specialised to the thermal energy, $E = 25.3$ meV, for which $\phi_c = k R_c' = k a_c (1-R_c^{\infty}) \ll 1$ (cf. Eqs. 53, 208, 211). Furthermore we assume that no resonance is very close to E which means $\sigma_c \ll 4\pi\lambda_c^2 g_c$, $E \ll |E_{\lambda}|$ and $\Gamma_{\lambda \gamma}^2 \ll E_{\lambda}^2$ for all λ . Under these conditions we get from the real and imaginary part

$$\frac{\Gamma_n}{E_0} = - \sum_{\lambda \neq 0} \frac{\Gamma_{\lambda n}}{E_\lambda} \pm \sqrt{\frac{\sigma_{cc}}{\pi \chi_c^2 g_c} + 2k_c R'_c} \quad , \quad (215)$$

$$\frac{\Gamma_Y \Gamma_n}{E_0^2} = - \sum_{\lambda \neq 0} \frac{\Gamma_{\lambda Y} \Gamma_{\lambda n}}{E_\lambda^2} + \frac{\sigma_{Yc}}{\pi \chi_c^2 g_c} \quad , \quad (216)$$

where $\sigma_{Yc} = \sigma_c - \sigma_{cc}$ is the capture cross section for channel c, and where we placed the unknown sum terms on the left-hand sides, the known positive-level terms together with the other known quantities on the right-hand sides. The sign ambiguity is due to the fact that the cross sections depend on $(\text{Im } U_{cc})^2$ rather than $\text{Im } U_{cc}$. In most cases the positive sign can be immediately discarded because it would make Γ_n/E_0 positive contrary to the assumption $E_0 < 0$. If this criterion fails one chooses the sign that gives better overall results in the thermal region.

With only two equations for the three unknown quantities E_0 , Γ_n , Γ_Y we can choose one of the three and then calculate the other two. The fact that radiation widths do not fluctuate much from level to level suggests to take Γ_Y as the mean radiation width obtained from the positive resonances. Note that in Eqs. 215 and 216 all neutron widths must be calculated at the (thermal) energy E, by specialisation of the general relationship

$$\Gamma_n(E) = \Gamma_n(|E_0|) \frac{P_\ell(E)}{P_\ell(|E_0|)} = \Gamma_n^\ell \sqrt{\frac{E}{1\text{eV}}} \frac{v_\ell(E)}{v_\ell(|E_0|)} \quad (217)$$

(with $v_\ell \equiv P_\ell/P_0$) to $\ell=0$. The energy-independent quantity $\Gamma_{\lambda n}^\ell$ is the reduced neutron width. In many resonance parameter tables it is listed together with, or instead of, the nominal neutron width $\Gamma_{\lambda n}(|E_\lambda|)$.

For target spin $I=0$ only one elastic s-wave channel ($J=1/2$) is open, and $\sigma_c = \sigma$, $\sigma_{cc} = \sigma_n$, $\sigma_{cy} = \sigma_Y$. Otherwise one has to consider both elastic channels ($J=I \pm 1/2$) separately which may be problematic since the two σ_c , σ_{cc} , σ_{cy} are usually not known separately but only their sum σ , σ_n , σ_Y . Only in rare cases is one negative level per channel not enough to fit known low-energy cross sections. One can then replace the left-hand sides of Eqs. 215, 216 by appropriate sums over negative levels and determine the parameters by a regular shape fit.

3. EVALUATION OF RESONANCE DATA

We shall now briefly discuss some of the problems encountered by the evaluator. He has to construct complete resonance parameter sets from published resonance parameter data and to determine the level-statistical parameters needed for interpretation and prediction of average cross section data in the region of unresolved resonances.

3.1 Intercomparison of resonance parameter sets

The following discussion will be restricted to the intercomparison of resonance parameters of the R-matrix type. It is very rare that different authors use the same potential-scattering parameters (e.g. nuclear radii) in their resonance fits. One should therefore put all available resonance parameter information on a common basis before a detailed comparison and evaluation is started.

3.1.1 Different potential-scattering parameters

Such a common basis can be established by means of the expressions for level shifts and partial widths

$$\Delta_{\lambda} = \sum_c \frac{\gamma_{\lambda c}^2}{|1-R_{cc}^0 L_c^0|^2} (B_c - S_c + R_{cc}^0 |L_c^0|^2), \quad (218)$$

$$\Gamma_{\lambda c} = \frac{2P_c \gamma_{\lambda c}^2}{|1-R_{cc}^0 L_c^0|^2}, \quad (219)$$

which follow from Eqs. 64, 207, 209. With a given author's information on his treatment of potential scattering, e.g. his choice of R' as a function of E , we can calculate $\phi_{\ell}(k R'_c)$ at each resonance and compare it to $\phi_{\ell}(k a_c)$ where a_c is the nuclear radius to which we want to refer all resonance parameters, defined e.g. by $a_c = 1.4 \text{ fm } A^{1/3}$ or (ENDF, Ref. 12) $a_c = 1.23 \text{ fm } A^{1/3} + 0.8 \text{ fm}$. The difference between $\phi_{\ell}(k R'_c)$ and $\phi_{\ell}(k a_c)$ can be formally ascribed to a certain value of R_c , i.e. R_{cc}^0 , which in turn can be inserted in Eqs. 218, 219. Thus one gets from the author's resonance energies and widths those which correspond to the adopted a_c convention, with the influence of distant levels removed. These effects are usually negligible at eV energies but can be important in the higher keV region.

3.1.2 Different boundary parameters B_c

Less frequent is the choice of different boundary parameters by different authors. Nevertheless we shall treat this problem in some detail because a very simple method for conversion between the Wigner-Eisenbud (or Reich-Moore) and the Kapur-Peierls representation can be derived from it.

We consider two choices of the boundary parameters, B and B' , and the corresponding quantities R , L^0 and R' , $L^{0'}$. Now the collision matrix does not depend on a particular choice, so that (cf. Eq. 17)

$$(1-RL^0)^{-1}R = R(1-L^0R)^{-1} = (1-R'L^{0'})^{-1}R', \quad (220)$$

whence $(1-R'L^{0'})R = R'(1-L^0R) \quad (221)$

or $R' = (1-\delta B \cdot R)^{-1}R \quad (222)$

with $\delta B \equiv B' - B = L^0 - L^{0'}. \quad (223)$

The poles and residues of R are the E_{λ} and $\gamma_{\lambda c} \gamma_{\lambda c}'$, those of R' will be denoted by E'_{λ} , $\gamma'_{\lambda c} \gamma'_{\lambda c}'$. Eq. 222 shows that the poles of R' are the solutions of

$$\det [1 - \delta B \cdot R(E'_{\lambda})] = 0. \quad (224)$$

The residues can be obtained as follows. From Eq. 222 we get

$$\frac{\partial}{\partial E}(R'^{-1}) = \frac{\partial}{\partial E}(R^{-1} - \delta B), \quad (225)$$

or, denoting differentiation with respect to E by a dot,

$$-R'^{-1} \dot{R}' R'^{-1} = -R^{-1} \dot{R} R^{-1} - \dot{\delta B}. \quad (226)$$

Multiplying from both sides with $R' = (1+R'\delta B)R$, which follows from Eq. 221, and going so close to the pole E'_λ of R' that $R' \approx \gamma'_{\lambda c} \gamma'_{\lambda c} / (E'_\lambda - E)$, $E \approx E'_\lambda$, we find

$$1 = \sum_{c,c'} \gamma'_{\lambda c} \delta B_c \dot{R}_{cc'}(E'_\lambda) \delta B_{c'} \gamma'_{\lambda c'} + \sum_c \gamma'_{\lambda c} \delta \dot{B}_c \gamma'_{\lambda c}$$

$$= \sum_{\mu c} \left(\sum_c \frac{\gamma'_{\lambda c} \delta B_c \gamma'_{\mu c}}{E_\mu - E'_\lambda} \right)^2 + \sum_c \gamma'^2_{\lambda c} \delta \dot{B}_c. \quad (227)$$

Especially simple expressions are obtained from Eqs. 224 and 227 if the boundary parameter is changed for one channel only, namely

$$1 = \delta B_c \sum_{\mu} \frac{\gamma'^2_{\mu c}}{E_\mu - E'_\lambda}, \quad (228)$$

$$1 = \gamma'^2_{\lambda c} (\delta B_c^2 \sum_{\mu} \frac{\gamma'^2_{\mu c}}{(E_\mu - E'_\lambda)^2} + \delta \dot{B}_c). \quad (229)$$

Eq. 228 can easily be solved for E'_λ by iteration (see below) whereupon Eq. 229 yields $\gamma'_{\lambda c}$. If δB_c does not depend on energy, as in the Wigner-Eisenbud representation, $\delta \dot{B}_c$ vanishes, of course.

3.2 Conversion from Wigner-Eisenbud to Kapur-Peierls resonance parameters

The results of the preceding section can be applied to the special case $B_c = S_c$, $B_{c'} = L_c$, i.e. $\delta B_c = iP_c$, which corresponds to conversion from Wigner-Eisenbud (s-wave or locally defined p-, d-...wave) parameters to Kapur-Peierls parameters or vice versa (Ref. 48). With the notation introduced in Sect. 2.3 for Kapur-Peierls parameters ($E'_\lambda = \mathcal{E}_\lambda$, $\gamma'_{\lambda c} = g_{\lambda c}$, $2P_c \gamma'^2_{\lambda c} = G_{\lambda c}$) we get from Eqs. 228 and 229

$$\mathcal{E}_\lambda = E_\lambda - \frac{i\Gamma_{\lambda c}/2}{1 - \sum_{\mu \neq \lambda} \frac{i\Gamma_{\mu c}/2}{E_\mu - \mathcal{E}_\lambda}}, \quad (230)$$

$$\frac{iG_{\lambda c}}{2} = \left(\sum_{\mu} \frac{i\Gamma_{\mu c}/2}{(E_\mu - \mathcal{E}_\lambda)^2} \right)^{-1} \quad (231)$$

or

$$G_{\lambda c}^{1/2} = \frac{\Gamma_{\lambda c}^{1/2}}{\sqrt{\left(1 - \sum_{\mu \neq \lambda} \frac{i\Gamma_{\mu c}/2}{E_\mu - \mathcal{E}_\lambda}\right)^2 - \sum_{\mu \neq \lambda} \frac{\Gamma_{\lambda c} \Gamma_{\mu c}/4}{(E_\mu - \mathcal{E}_\lambda)^2}}} \quad (232)$$

where the square root is taken with the positive sign so that for isolated levels $G_{\lambda c}^{1/2} = \Gamma_{\lambda c}^{1/2}$. The term with δB_c has been omitted since we consider the dependence of δB_c as parametric rather than functional so that the argument of $\delta B_c = iP_c(E)$ coincides only "accidentally" with the bombarding energy. As a consequence all widths ($\Gamma_{\mu c}$, $G_{\lambda c}$) are to be calculated at the energy E for which we want to calculate the Kapur-Peierls parameters (rather than at \mathcal{E}_λ).

Eq. 230 is convenient for iteration starting from $\mathcal{E}_\lambda = E_\lambda - i\Gamma_{\lambda c}/2$. Convergence is rapid even with severe level overlap (Ref. 48). Having determined \mathcal{E}_λ with sufficient accuracy one can calculate $G_{\lambda c}$ as a simple sum over levels (Eq. 231). The method is formally simpler than the conversion techniques based on matrix inversion (Ref. 17)

or on partial-fraction expansion of the determinant in Eq. 224 (Refs. 20,22). In particular large numbers of resonances are easily dealt with. Computation of determinants and matrix inversion are replaced by a perturbation approach which clearly exhibits the influence of interfering levels. Their importance is essentially proportional to $\Gamma_{\mu c} / (E_{\lambda} - E_{\mu})$. In SLBW approximation the sums in Eqs. 230 and 231 vanish and one gets immediately, for conversion in all channels,

$$\mathcal{E}_{\lambda} = E_{\lambda} - i \sum_c \Gamma_{\lambda c} / 2 = E_{\lambda} - i \Gamma_{\lambda} / 2, \quad G_{\lambda c}^{1/2} = \Gamma_{\lambda c}^{1/2}. \quad (233)(234)$$

In the two-channel case iteration of Eq. 230 produces the continued-fraction representation of the tangent,

$$\begin{aligned} \mathcal{E}_{\lambda} &= E_{\lambda} - \frac{i \Gamma_{\lambda c}}{2} \left(1 + \frac{\Gamma_{\mu c}^{1/2}}{\Gamma_{\lambda c}^{1/2}} \frac{x/2}{1 - \frac{(x/2)^2}{1 - \frac{(x/2)^2}{1 - \dots}}} \right) \\ &= E_{\lambda} - \frac{i \Gamma_{\lambda c}}{2} \left(1 - \frac{\Gamma_{\mu c}^{1/2}}{\Gamma_{\lambda c}^{1/2}} \tan \alpha \right) \end{aligned} \quad (235)$$

where

$$\sin 2\alpha \equiv x \equiv \frac{\Gamma_{\lambda c}^{1/2} \Gamma_{\mu c}^{1/2}}{(E_{\mu} - i \Gamma_{\mu c} / 2) + (E_{\lambda} - i \Gamma_{\lambda c} / 2)}, \quad (\lambda, \mu = 1, 2). \quad (236)$$

This is what one also obtains as solution of the characteristic equation (224) in the diagonalisation of the part $(E_{\lambda} - E) \delta_{\lambda \mu} - i \Gamma_{\lambda c}^{1/2} \Gamma_{\mu c}^{1/2} / 2$ of the inverse level matrix, Eq. 22. We shall not go further into details. It should be sufficiently clear by now that our perturbation approach is most useful for many levels and few channels, that is for the Reich-Moore formalism. With the Kapur-Peierls choice $L_c^0 = 0$ for all particle channels the essential Reich-Moore formulae assume the simple form

$$U_{cc'} = e^{-i(\phi_c + \phi_{c'})} \left(\delta_{cc'} + \sum_{\lambda} \frac{i G_{\lambda c}^{1/2} G_{\lambda c'}^{1/2}}{\mathcal{E}_{\lambda} - E - i \Gamma_{\lambda \gamma} / 2} \right) \quad (c, c' \notin \gamma), \quad (237)$$

$$\sigma_{c\gamma} = \sum_{c' \in \gamma} \sigma_{cc'} = \pi \lambda_c^2 g_c \sum_{\lambda} \frac{|G_{\lambda c}| |\Gamma_{\lambda \gamma}|}{|\mathcal{E}_{\lambda} - E - i \Gamma_{\lambda \gamma} / 2|^2}, \quad (238)$$

where \mathcal{E}_{λ} , $G_{\lambda c}^{1/2}$ are the conversion results for the particle channels ($\mathcal{E}_{\lambda} - i \Gamma_{\lambda \gamma} / 2 \approx E_{\lambda} - i \Gamma_{\lambda} / 2$ for relatively isolated levels).

In this way one can convert Reich-Moore to Kapur-Peierls parameters. The corresponding cross sections can be Doppler broadened by means of the Voigt profiles (see Sect. 2.4.3), but we stress again that the price for this is heavy: One must convert parameters for each energy grid point and then calculate complicated coefficients for the Voigt profiles involving double sums over levels (Eqs. 69, 70, 72) which is time-consuming if many levels are involved. Direct numerical broadening of Reich-Moore cross sections is usually simpler, faster and more accurate.

3.3 Applied level statistics

It was already mentioned that one of the reasons for parametrisation of resonance cross section data is the need to determine level-statistical parameters such as mean level spacings, average widths and strength functions which permit extrapolation of average cross sections and simulation of cross section fluctuations in the unresolved-resonance region. As in resonance theory we shall need only very few formulae from the impressive but often still speculative edifice of the statistical theory of spectra (Refs. 60, 61).

3.3.1 The Porter-Thomas hypothesis

The reduced width amplitudes $\gamma_{\lambda c}$ of Wigner-Eisenbud R-matrix theory are essentially values of the internal wave function taken at the channel radius a_c , as our little single-particle exercise (Sect. 2.3.3, Eq. 42) showed. They can be expressed by the overlap between the λ -th eigenfunction and the channel wave function at the channel entrance ($r = a_c$). In the multi-channel (A+1)-nucleon case this is a (3A+2)-dimensional configuration space integral over the surface of the interaction sphere. The very complicated integrand oscillates rapidly so that negative and positive contributions nearly cancel. The integral is thus almost equal to zero and is positive or negative with presumably equal probabilities depending on the particulars of the λ -th eigenstate. Under these circumstances a Gaussian distribution of the $\gamma_{\lambda c}$ for given c is a reasonable guess. Omitting the level subscript we write

$$p(\gamma_c) d\gamma_c = \frac{1}{\sqrt{\pi}} e^{-x^2} dx, \quad -\infty < x \equiv \frac{\gamma_c}{\sqrt{2\langle\gamma_c^2\rangle}} < \infty. \quad (239)$$

This is the Porter-Thomas hypothesis (Ref. 62) which, with $d\gamma_c^2 = 2\gamma_c d\gamma_c$, $p(\gamma_c) d\gamma_c \equiv p(\gamma_c^2) d\gamma_c^2$ immediately yields the famous Porter-Thomas distribution

$$p(\gamma_c^2) d\gamma_c^2 = \frac{e^{-y}}{\sqrt{\pi y}} dy, \quad 0 < y \equiv \frac{\gamma_c^2}{2\langle\gamma_c^2\rangle} < \infty. \quad (240)$$

It applies to reduced neutron widths whenever the resonances are excitable only via one channel so that $\Gamma_n^l / \langle\Gamma_n^l\rangle = \gamma_c^2 / \langle\gamma_c^2\rangle$ (e.g. for $l=0$ or $l=1$, see Table 1), but also to partial radiation widths for single radiative transitions, not only in nuclear but also in atomic and molecular resonance spectroscopy. Many observable widths, however, are sums of single-channel widths, for instance many reduced neutron widths for $l>0$ and $l>1$, or the total radiation width or fission widths. If the averages $\langle\gamma_c^2\rangle$ were the same for all ν contributing channels one would get the generalised Porter-Thomas distribution, a χ^2 -distribution with ν degrees of freedom,

$$p(\gamma_x^2) d\gamma_x^2 = \Gamma(\frac{\nu}{2})^{-1} e^{-y} y^{\nu/2-1} dy, \quad 0 < y \equiv \frac{\nu\gamma_x^2}{2\langle\gamma_x^2\rangle} < \infty, \quad (241)$$

where $\Gamma(\nu/2)$ is the gamma function and

$$\gamma_x^2 \equiv \sum_{c \in x} \gamma_c^2, \quad \langle\gamma_x^2\rangle = \nu \langle\gamma_c^2\rangle. \quad (242)(243)$$

The single-channel Porter-Thomas distribution ($\nu=1$) agrees well with observed distributions of single-channel reduced neutron widths (Ref. 63) and partial radiation widths (Ref. 64). The general χ^2 distribution is useful for two-channel reduced neutron widths ($\nu=2$, exponential distribution) and, with an effective number ν of channels, also for fission widths (ν small) and total radiation widths (ν very large). That ν is large for total radiation widths could be expected

because usually there is a huge number of allowed radiative transitions to lower-lying compound states, each giving rise to a sum term in Eq. 242. That ν is small for fission widths, however, surprises at first sight. The hundreds of possible pairs of fission fragments, each with many possible excitations, would seem to imply equally many reaction channels or partial fission widths, and a correspondingly large ν .

The puzzle was solved by A. Bohr (Ref. 65). He pointed out that before scission can occur the compound system must cross the saddle point of the potential-energy surface (in deformation parameter space) beyond which Coulomb repulsion prevails over nuclear cohesion. At the saddle point most energy is tied up as deformation energy, only little being available for other modes of excitation whose spectrum resembles somewhat the low-lying (collective) states observed for the ground-state deformation. Energy, angular momentum and parity requirements allow access to only very few of these transition states. This introduces quite rigid correlations between partial widths for the many different fission fragment channels in such a way that the fission width can be approximated as a sum of terms, one for each accessible transition state (or "saddle-point channel"), each term being governed by a single-channel Porter-Thomas distribution (Ref. 66). For fission, therefore, ν is the number of saddle-point channels rather than reaction channels in the usual sense.

This illustrates that the level-statistical "laws" are nowhere as rigid as the formal resonance theory discussed in previous sections. They hold mainly for typical compound levels where all single-particle, collective or other simplicity has been lost. Reflecting more our ignorance than truly statistical phenomena they may fail if the states considered are simple and well understood. Thus the collective transition states of a fissioning nucleus enabled us to modify and, in fact, to simplify the reaction channel concept. In the single-particle exercise with square-well complex potential, Sect. 2.3.3, nothing at all was random or unspecified, and the reduced neutron widths, Eqs. 58, turned out to obey a δ -distribution instead of the Porter-Thomas "law".

3.3.2 Wigner's surmise and Hamiltonian ensemble theory

To find the distribution $p(D)dD$ of nearest-neighbour spacings, $D_\lambda = E_{\lambda+1} - E_\lambda$, in a $J\pi$ level sequence turned out to be much more difficult than to find the width distributions. Very early Wigner tried a bold guess ("Wigner's surmise", Ref. 67). He took issue with the exponential distribution tried by others which is obtained if the probability to find a level in a small energy interval dD is just $dD / \langle D \rangle$, independent of its distance D from the preceding level. He asserted that because of "level repulsion" at least for small D this probability should be proportional to DdD and assumed tentatively that this is true also for large D so that

$$p(D)dD = \exp(-c \int_0^D dD') c D dD = e^{-cD^2/2} c D dD \quad (244)$$

Expressing the proportionality constant c by the mean level spacing $\langle D \rangle$ one can write the Wigner distribution as

$$p(D)dD = 2e^{-x^2} x dx, \quad 0 < x \equiv \frac{\sqrt{\pi}}{2} \frac{D}{\langle D \rangle} < \infty. \quad (245)$$

Wigner illustrated the level repulsion by pointing to the spacing $D = \sqrt{(H_{11} - H_{22})^2 + 4H_{12}^2}$ between the eigenvalues of a two-dimensional (real, symmetric) Hamiltonian matrix H which can be visualised as the distance of a point with coordinates $H_{11} - H_{22}$ and $2H_{12}$ from the origin. If the H_{ij} are considered as random variables the probability to obtain a given D within dD is proportional to the two-dimensional area element $2\pi D dD$, at least in a small domain around the origin in which nonuniformity of the unknown probability distributions of the $H_{\lambda\mu}$ can be neglected. $D=0$ is seen

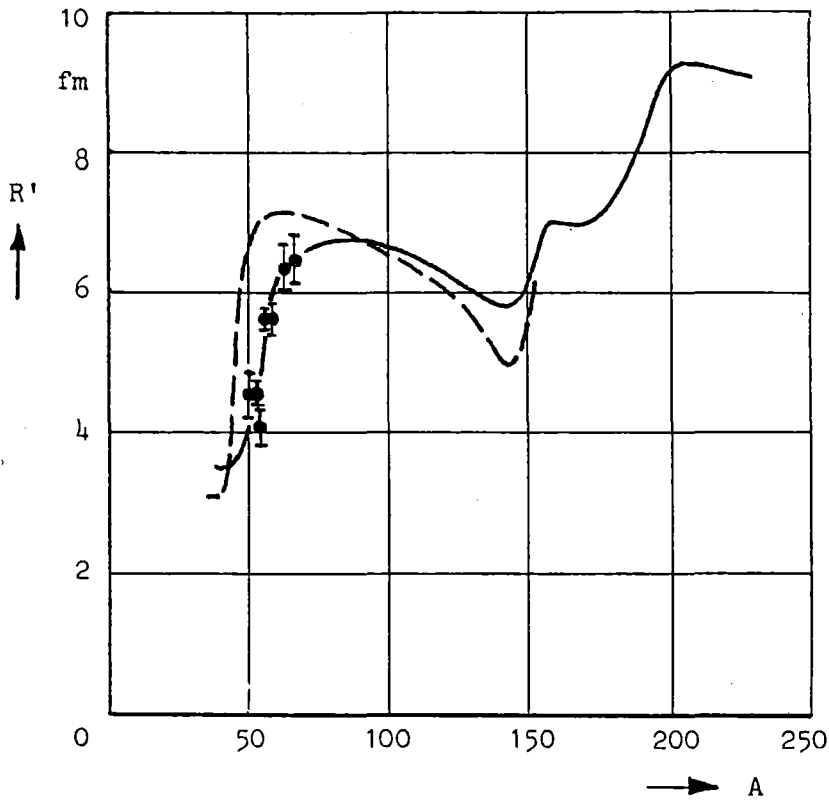


Fig. 20 - Effective radii obtained for Cr, Fe and Ni isotopes by shape fits to transmission data below 300 keV (see Figs. 17 and 18) with the FANAL code (Ref. 36, 57, 58). The broken curve was calculated by Moldauer (Ref. 91) for a complex spherical potential, the solid curve by Jain (Ref. 59) for a complex potential with vibrational and rotational coupling.

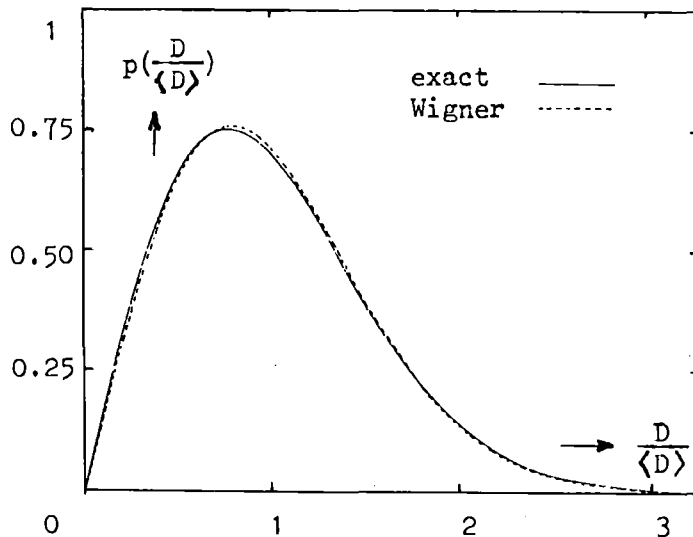


Fig. 21 - Next-neighbour spacing distributions for the Gaussian orthogonal ensemble. Solid line: very large $N \times N$ matrices, limit $N \rightarrow \infty$ (Gaudin, Ref. 69). Broken line: 2×2 matrices (Wigner distribution). From Ref. 69.

to be infinitely unlikely, which is related to the fact that two conditions, $H_{11}=H_{22}$ and $H_{12}=0$, must be fulfilled instead of one as for $D \neq 0$. This latter argument is also true for 3-, 4- ... dimensional Hamiltonian matrices, coincidence of two characteristic values always requiring two conditions instead of one.

A more rigorous theory of statistical ensembles of Hamiltonians was developed in a brilliant mathematical tour de force by Wigner, Porter, Mehta, Dyson and others (Refs. 60, 61) in an attempt to establish a kind of statistical thermodynamics of quantum systems. First the so-called Gaussian orthogonal ensemble was studied which consists of real symmetric Hamiltonian matrices H whose elements $H_{\lambda\mu}$ are uncorrelated and whose density function $p(H)$ is invariant under rotations in Hilbert space (so that all representations including the diagonal form are put on an equal footing). For 2×2 matrices the Wigner distribution was obtained. For very large matrices Mehta and Gaudin (Refs. 68, 69) found expressions that are fairly complicated but, as Fig. 21 shows, differ only slightly from the 2×2 curve, i.e. Wigner's surmise.

A major difficulty with the Gaussian ensemble is that it leads to a rather unrealistic level density formula, viz. Wigner's semi-circle law for $N \times N$ matrices with very large N ,

$$\rho(E) = \begin{cases} \frac{4N}{\pi I} \sqrt{1 - \left(\frac{E - \bar{E}}{I/2}\right)^2} & \text{for } (E - \bar{E})^2 < I^2/4 \\ 0 & \text{otherwise} \end{cases} \quad (N \text{ large}) \quad (246)$$

where \bar{E} and I are midpoint and length of the energy interval in which the eigenvalues occur. This is quite different from the exponentially rising level densities obtained for instance from the Fermi gas independent-particle model.

Dyson gave up the hypothesis of statistically independent matrix elements $H_{\lambda\mu}$ and introduced the circular orthogonal ensembles (Ref. 70). He could show that with these one could reproduce any reasonable energy dependence of the level density ρ apparently without changing less global results such as the spacing distribution obtained with the Gaussian ensembles.

Recently French, Wong and others studied the statistical shell model where not the elements $H_{\lambda\mu}$ but only those of the residual interaction are considered as random variables (cf. Ref. 71). This model, more physical than the Gaussian and circular orthogonal ensembles, nevertheless confirmed their results for nearest-neighbor level spacings, whereas $\rho(E)$ turned out to be Gaussian instead of semi-circular.

Both the orthogonal ensembles and the statistical shell model indicate that nuclear (or atomic) level sequences have a nearly "crystalline" regularity in the sense that the familiar staircase diagram (number of levels vs. energy) follows very closely the practically straight line with slope $\rho(E)$, deviations by more than one unit being extremely unlikely (Ref. 72). This implies that adjacent nearest-neighbour spacings are correlated in such a way that a large spacing is followed by a short spacing more often than not and vice versa. In fact, for orthogonal ensembles the expected correlation coefficient is

$$C(D_\lambda, D_{\lambda+1}) \equiv \frac{\text{cov}(D_\lambda, D_{\lambda+1})}{\sqrt{\text{var}(D_\lambda)\text{var}(D_{\lambda+1})}} \approx -0.27 \quad (247)$$

for large matrices. The exact value $(8\pi - 27)/(11\pi - 27) \approx -0.253$ for the simplest case of 3×3 matrices (Ref. 73) is already a good approximation. Empirical evidence from long and pure sequences of s-wave neutron resonances supports these theoretical results (Ref. 74).

The Porter-Thomas distribution of single-channel widths, the Wigner distribution of level spacings and the quasi-crystalline long-range regularity of level sequences is about all the level statistics we need for applications.

3.3.3 Maximum-likelihood estimation of $\langle \Gamma_n^k \rangle$ and $\langle D \rangle$ from perfect samples

Suppose we know all level energies E_λ and reduced neutron widths Γ_λ^k for a pure $J\Pi$ level sequence in a given energy range. What can we infer about the true mean values $\langle D \rangle$ and $\langle \Gamma_n^k \rangle$, and about their ratio, the strength function $S_n^k \equiv \langle \Gamma_n^k \rangle / \langle D \rangle$? This is the typical Statistical problem of parameter estimation. It was tackled by Slavinskis and Kennett (Ref. 75) with the maximum-likelihood method. Consider first the reduced neutron widths which we shall write here simply as Γ_λ . The probability to find Γ_1 in $d\Gamma_1$, Γ_2 in $d\Gamma_2$, ..., Γ_N in $d\Gamma_N$ is a product of Porter-Thomas probabilities (we consider here the single-channel case, $v=1$, e.g. s-wave resonances),

$$\prod_{\lambda=1}^N p(\Gamma_\lambda) d\Gamma_\lambda = (2\pi \langle \Gamma \rangle)^{-N/2} \exp\left(-\frac{1}{2\langle \Gamma \rangle} \sum_{\lambda=1}^N \Gamma_\lambda\right) \prod_{\mu=1}^N \frac{d\Gamma_\mu}{\sqrt{\Gamma_\mu}}. \quad (248)$$

The value of the true average $\langle \Gamma \rangle$ that leads with greatest probability to the experimental result obviously maximises the likelihood function $L \equiv \prod_{\lambda} p(\Gamma_\lambda)$. From $\partial L / \partial \langle \Gamma \rangle = 0$ or, more conveniently, from $\partial \ln L / \partial \langle \Gamma \rangle = 0$, one finds the maximum-likelihood estimator

$$\langle \Gamma \rangle = \frac{1}{N} \sum_{\lambda=1}^N \Gamma_\lambda. \quad (249)$$

This is just the sample average $\bar{\Gamma}$. In the language of mathematical statistics $\bar{\Gamma}$ is a minimal sufficient statistic, i.e. a quantity that can be calculated from the sample $\Gamma_1, \dots, \Gamma_N$, contains all information about $\langle \Gamma \rangle$ that the sample itself contains, and has the smallest variance of all possible estimators. It is an unbiased estimator for $\langle \Gamma \rangle$ because for very large samples it tends towards $\langle \Gamma \rangle$.

In order to assign confidence limits we need the probability distribution of the random variable $\bar{\Gamma}$. This we know already from the discussion of sums of partial widths to be a χ^2 -distribution with N degrees of freedom (compare Eq. 241),

$$p(\bar{\Gamma}) d\bar{\Gamma} = \Gamma \left(\frac{N}{2}\right)^{-1} e^{-y} y^{N/2-1} dy, \quad 0 < y \equiv \frac{N\bar{\Gamma}}{2\langle \Gamma \rangle} < \infty. \quad (250)$$

Confidence limits y_- and y_+ can now be assigned for instance at the 68 % confidence level, in analogy to the standard deviation of a Gaussian distribution. One demands that y lie with $\text{erf}(1/\sqrt{2}) \approx 68\%$ probability within the interval $(y_- \dots y_+)$, and with equal probability below and above,

$$\Gamma \left(\frac{N}{2}\right)^{-1} \int_0^{y_-} e^{-y} y^{N/2-1} dy \equiv \Gamma \left(\frac{N}{2}\right)^{-1} \int_{y_+}^{\infty} e^{-y} y^{N/2-1} dy \equiv \frac{1}{2} \text{erfc} \frac{1}{\sqrt{2}}. \quad (251)$$

The confidence limits y_- , y_+ thus defined depend only on the sample size N and can be found e.g. in tables of χ^2 -distributions or numerically from Eqs. 251. One knows now that with 68 % probability $y_- < y < y_+$ and thus

$$\frac{N}{2y_+} \bar{\Gamma} < \langle \Gamma \rangle < \frac{N}{2y_-} \bar{\Gamma}. \quad (252)$$

For very large samples the χ^2 distribution is nearly Gaussian so that

$$y_\pm = \langle y \rangle \pm \sqrt{\text{var}(y)} = \frac{N}{2} (1 \pm \sqrt{\frac{2}{N}}) \quad \text{for } N \gg 1. \quad (253)$$

So far we neglected experimental errors $\delta\Gamma_\lambda$ of the Γ_λ which cause an uncertainty $\delta\bar{\Gamma} = \sqrt{\sum_\lambda (\delta\Gamma_\lambda)^2}/N$ of $\bar{\Gamma}$. They are usually accounted for in sufficient approximation if the confidence limits are extended so that the squares of the statistical and experimental errors are added,

$$y_\pm \rightarrow y_\pm \pm [\sqrt{\text{var}(y) + (\delta\bar{\Gamma})^2} - \sqrt{\text{var}(y)}]. \quad (254)$$

Slayinskas and Kennett found maximum-likelihood estimators also for $\langle D \rangle$ and $\langle \Gamma_n^k \rangle / \langle D \rangle = S_k$ but we shall not follow their derivation because they neglected the level-spacing correlations, Eq. 247, cf. Ref. 76. Dyson and Mehta (Ref. 72) showed that due to the regularity of level sequences the number N of levels in a given energy interval is already a rather good statistic for the estimation of the average level density, and that the optimum statistic for the orthogonal ensemble is

$$\rho = \frac{1}{\langle D \rangle} = \frac{4}{\pi I} \sum_{\lambda=1}^N \sqrt{1 - \left(\frac{E_\lambda - \bar{E}}{I/2} \right)^2} \quad (255)$$

where I and \bar{E} are length and midpoint of the energy interval from which the energy sample comes. This statistic may be considered as a kind of level count with semicircle weighting. Its variance is

$$\text{var } \rho = \frac{1}{2} \left(\frac{4}{\pi I} \right)^2. \quad (256)$$

3.3.4 Maximum-likelihood estimation of $\langle \Gamma_n^k \rangle$ and $\langle D \rangle$ in the case of missed levels

The estimators for $\langle \Gamma_n^k \rangle$ and $1/\langle D \rangle$ presented so far are not very useful in practice because they are applicable only to perfect samples from which no levels are missing. In practice the smallest, but according to the Porter-Thomas distribution most frequent, widths are always missing. As a consequence all observed width and especially spacing distributions are badly distorted. It is therefore best to use the width distribution to estimate $\langle \Gamma_n^k \rangle$ which then permits estimation of the number of missing levels and thus of $\langle D \rangle$ and S_k .

Let us assume that levels with reduced widths $\Gamma_\lambda < \Gamma_0 \equiv 2x_0 \langle \Gamma \rangle$ are undetectable and missing from the sample. The distribution of detectable widths is then the truncated Porter-Thomas distribution

$$p(\Gamma_\lambda) d\Gamma_\lambda = \frac{1}{\text{erfc } \sqrt{x_0}} \frac{e^{-x}}{\sqrt{\pi x}} dx, \quad x_0 < x \equiv \frac{\Gamma_\lambda}{2\langle \Gamma \rangle} < \infty, \quad (257)$$

properly normalised to unity by the complementary error function. Maximising the corresponding likelihood function one gets

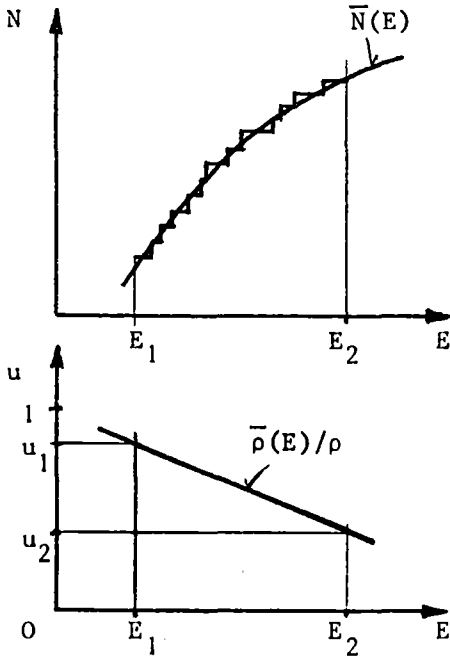
$$\langle \Gamma \rangle \left(1 + \frac{2}{\sqrt{\pi}} \frac{e^{-x_0} \sqrt{x_0}}{\text{erfc } \sqrt{x_0}} \right) = \frac{1}{N} \sum_{\lambda=1}^N \Gamma_\lambda = \bar{\Gamma}. \quad (258)$$

The term in brackets is clearly a missing-level correction factor depending on $\langle \Gamma \rangle$. The equation is readily solved by iteration starting from $\langle \Gamma \rangle = \bar{\Gamma}$. This simple approach works well whenever the detectability threshold Γ_0 can be considered as constant and is sufficiently well known.

Often Γ_0 varies significantly over the energy range from which the width sample is taken. The truncation of the Porter-Thomas distribution is then not sharp but fuzzy. Fuketa and Harvey (Ref. 77) developed a widely used estimation procedure for $\langle \Gamma \rangle$ with an energy dependence of the form $\Gamma_0 = aE^b$, where a is an adjustable constant and b is determined by the experimental details ($b \approx 2$ in many experiments).

Of course the observed level density reflects the energy dependence of Γ_0 , and in fact one can devise a procedure which utilises the level energies E_1, \dots, E_N as well as the reduced widths $\Gamma_1, \dots, \Gamma_N$ and obviates the need to know anything about the detection threshold and experimental details. This is especially useful if the latter are not known or if the resonance parameter data stem from many different experiments. Due to the regularity of level sequences and smooth behaviour of $\Gamma_0(E)$ (at least for single experiments) the typical level density staircase curve (number of levels versus energy) fluctuates but little around a smooth curve which usually can be taken as a parabola,

$$\bar{N}(E) = c_0 + c_1 E + c_2 E^2. \quad (259)$$



The coefficients can be determined in a least-squares fit and will be considered as known. The energy derivative is the apparent level density,

$$\bar{\rho}(E) = c_1 + 2c_2 E, \quad (260)$$

which is smaller than the true level density $\rho \equiv 1/\langle D \rangle$, whose energy dependence we shall neglect as well as that of $\langle \Gamma \rangle$. The detectable fraction of levels (on the average) is then

$$u \equiv \frac{\bar{\rho}(E)}{\rho} = (c_1 + 2c_2 E)\langle D \rangle = \text{erfc}\sqrt{x_0}, \quad (261)$$

where the complementary error function has the same meaning as in Eq. 255: it is the integral over the Porter-Thomas distribution above the detectability threshold $x_0 = \Gamma_0/(2\langle \Gamma \rangle)$. We have thus found from the observed level energies the energy dependence of Γ_0 , at least in implicit form and in terms of $\langle \Gamma \rangle$ and $\langle D \rangle$.

Fig. 22

The parabolic fit to the staircase diagram is seen to be equivalent to a linear decrease of the detectable fraction from $u_1 = u(E_1)$ to $u_2 = u(E_2)$. The probability that at some unspecified energy within the interval $(E_1 \dots E_2)$ the detectable fraction has the value u is therefore a constant between u_1 and u_2 and vanishes elsewhere. We can thus write the width distribution with fuzzy truncation edge as

$$p(\Gamma_\lambda) d\Gamma_\lambda = \frac{p_1 p_2 d\Gamma_\lambda}{\int_0^\infty p_1 p_2 d\Gamma_\lambda}, \quad (262)$$

where $p_1 d\Gamma_\lambda$ is the (a priori) Porter-Thomas probability for a reduced width Γ_λ in $d\Gamma_\lambda$, and p_2 the conditional probability that Γ_λ , for unspecified E_λ , exceeds the detection threshold,

$$p_2 = \begin{cases} 1 & \text{if } \text{erfc}\sqrt{x_\lambda} \leq u_2 \\ \frac{u_1 - \text{erfc}\sqrt{x_\lambda}}{u_1 - u_2} & \text{if } u_2 \leq \text{erfc}\sqrt{x_\lambda} \leq u_1 \\ 0 & \text{if } \text{erfc}\sqrt{x_\lambda} \geq u_1 \end{cases} \quad (263)$$

$$\text{with } u_i = u(E_i) = (c_1 + 2c_2 E_i) \langle D \rangle \quad (i=1,2) \quad (264)$$

and $x_\lambda \equiv \Gamma_\lambda / (2 \langle \Gamma \rangle)$. The denominator in Eq. 262 is equal to the average observable fraction in the interval $(E_1 \dots E_2)$, $\bar{u} = u(\bar{E}) = [c_1 + c_2(E_1 + E_2)] \langle D \rangle$. The likelihood function $L = \prod_\lambda p(\Gamma_\lambda)$ depends on the (known) fit parameters and the unknown level-statistical parameters $\langle \Gamma \rangle$ and $\langle D \rangle$. Thus its maximum is obtained for $\partial L / \partial \langle \Gamma \rangle = 0$ and $\partial L / \partial \langle D \rangle = 0$, whence

$$\langle \Gamma \rangle \left(1 + \frac{1}{N} \sum'_\lambda \frac{2}{\sqrt{\pi}} \frac{e^{-x_\lambda \sqrt{x_\lambda}}}{u_1 - \text{erfc} \sqrt{x_\lambda}} \right) = \bar{\Gamma}, \quad (265)$$

$$\frac{1}{N} \sum'_\lambda \frac{\text{erfc} \sqrt{x_\lambda}}{u_1 - \text{erfc} \sqrt{x_\lambda}} = 1. \quad (266)$$

The primes indicate that the sums contain only terms from the "fuzzy edge" of the width distribution, for which $u_2 < \text{erfc} \sqrt{x_\lambda} < u_1$ with $u_1 = (c_1 + 2c_2 E_1) \langle D \rangle$, $u_2 = (c_1 + 2c_2 E_2) \langle D \rangle$, $x_\lambda = \Gamma_\lambda / (2 \langle \Gamma \rangle)$. The equations are again convenient for iteration, starting e.g. from $\langle \Gamma \rangle \approx \bar{\Gamma}$, $\langle D \rangle \approx (E_2 - E_1) / N$. A program based on this approach (Ref. 78) yielded the results shown in Fig. 23.

So far we restricted the discussion to pure level sequences for a given $J\pi$. Some of the results remain approximately valid also for mixed sequences. Consider, for instance, the p-wave levels for target spin $I=0$. Their spin is either $J=1/2$ or $J=3/2$, i.e. they belong to two different sequences. It is consistent with empirical evidence to consider their strength functions as independent of J , so that $S_{1/2} = S_{3/2}$. The spin dependence of the level densities was derived by Bethe (Ref. 79, cf. also Ref. 80) from the Fermi-Gas model as

$$\rho_J \propto \exp\left[-\frac{J^2}{2\sigma^2}\right] - \exp\left[-\frac{(J+1)^2}{2\sigma^2}\right] \propto \sinh\left(\frac{J+1/2}{2\sigma^2}\right) \exp\left[-\frac{(J+1/2)^2}{2\sigma^2}\right] \quad (267)$$

The spin cut-off factor σ has values around 4 so that for small spins one has $\rho_J \propto 2J+1$. In this approximation and with $S_{1/2} = S_{3/2}$ one finds that the $g_n^{\Gamma_1}$ values of the combined p-wave sequences have the Porter-Thomas distribution, the average being

$$\langle g_n^{\Gamma_1} \rangle = \frac{S_1}{\rho_{1/2} + \rho_{3/2}} = \langle D \rangle_1 S_1, \quad (268)$$

where $\langle D \rangle_1$ is the average spacing of all p-wave levels and S_1 the strength function of each separate sequence. We can therefore employ, essentially the same estimation procedure as for pure sequences with $v=1$, with Γ_n conveniently replaced by $g_n^{\Gamma_1}$ so that the mostly unknown level spins are not needed.

Generalisation to $v=2$ (exponential distribution) is straightforward.

3.3.5 Spin assignment for given resonance areas with Bayes' theorem

It was already mentioned that resonance peak areas are sufficient for the calculation of average cross sections or zero-dilution group constants but not of Doppler effect or self-shielding. For these one requires spins. Level statistics can give us a handle to assign unknown spins if the area parameters $g_n^{\Gamma_n}$, $g_n^{\Gamma_n} \Gamma_n / \Gamma$ are known, at least in the sense that the resulting average spin distribution over many levels is realistic. Let us consider the typical case that enough information on s-wave resonance parameters is available to permit estimation (including missing-level correction) of $\langle D \rangle_0$ and S_0 , and that S_1, S_2, \dots are known from analysis of average cross sections and optical-model calculations. All required mean level spacings $\langle D_J \rangle$ can then be found from the s-wave spacing with

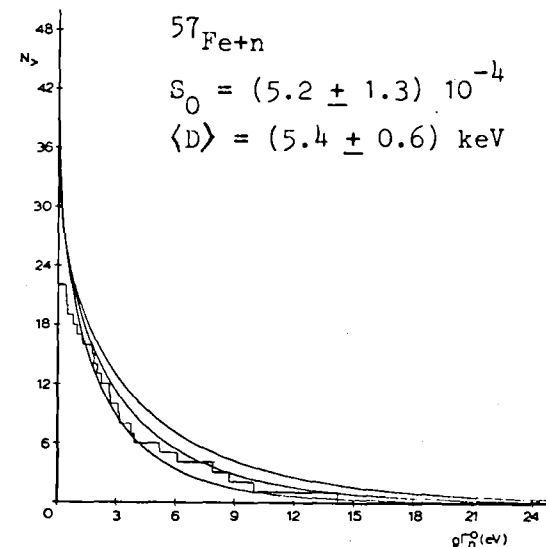
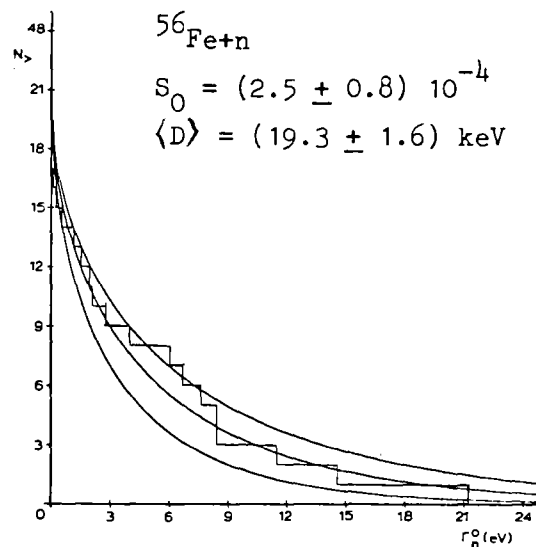
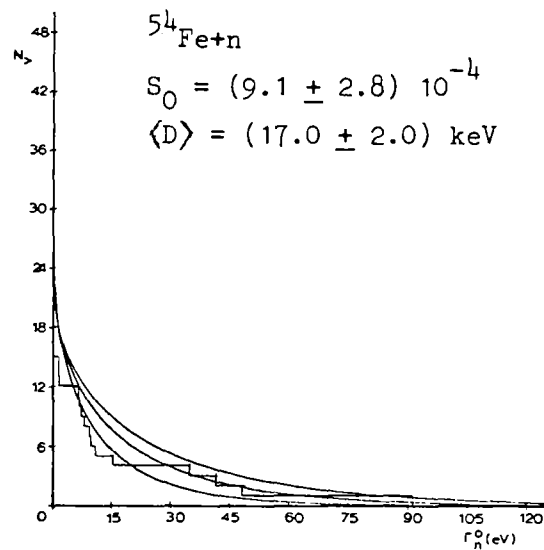


Fig. 23 - Results of statistical resonance analysis for iron isotopes obtained with the maximum-likelihood code STARA (Ref. 78). The histograms are observed integral width distributions for s-wave levels below 400 keV (below 200 keV for ^{57}Fe). The curves are the most likely distributions and the 68% confidence limits. Note that the curves are no fits to the histograms but correspond to the solution $\langle \Gamma_n^0 \rangle$ of Eqs. 265, 266.

the help of Eq. 267, and the average neutron widths from $\langle \Gamma_{n,\ell J} \rangle = v_{\ell J} \langle D_J \rangle S_{\ell} \sqrt{E/1eV} v_{\ell}(E)$, where $v_{\ell J}$ is the number of channel spins (1 or 2) compatible with ℓ and J . We can now calculate the probabilities

$$p_{\ell J} d(g\Gamma_n) = \Gamma \left(\frac{v_{\ell J}}{2}\right)^{-1} e^{-x} x^{v_{\ell J}/2-1} dx, \quad 0 < x \equiv \frac{v_{\ell J}}{2} \frac{g\Gamma_n}{g_J \langle \Gamma_{n,\ell J} \rangle} < \infty \quad (269)$$

with $\ell = 0, 1, 2, \dots$ for an observed value $g\Gamma_n$ in $d(g\Gamma_n)$. Bayes' theorem (see e.g. Ref. 41) tells us that we may take the probability for a given ℓJ combination as proportional to $p_{\ell J}$ if all combinations are equally probable a priori. The probability for a given spin J is then

$$p_J = \frac{\sum_{\ell} p_{\ell J}(g\Gamma_n)}{\sum_{\ell, J} p_{\ell J}(g\Gamma_n)}, \quad (270)$$

where the sum in the denominator is over all ℓ that are compatible with J . Often one sees immediately that a certain spin is probably correct, the others being too unlikely. In general one must make a probabilistic choice, for example with the Monte Carlo technique.

If additional types of resonance areas are known one can utilise this information also. Let us take, for instance, the capture peak areas $2\pi^2 \lambda(E_0)^2 g\Gamma_n \Gamma_{\gamma} / \Gamma$ with $\Gamma = \Gamma_n + \Gamma_{\gamma}$ (non-fissile target nucleus). From $g\Gamma_n$ and $g\Gamma_n \Gamma_{\gamma} / \Gamma$ we get $g\Gamma_{\gamma}$, for which an expression similar to Eq. 277 holds. If we know the effective degree of freedom and the average width for the (n, γ) reaction we can calculate the probability $p_{\ell J}(g\Gamma_{\gamma})$ and base the spin selection on the joint probabilities $p_{\ell J}(g\Gamma_n) p_{\ell J}(g\Gamma_{\gamma})$. Unfortunately $g\Gamma_n$ is often unknown. One must then consider the probability (for each allowed ℓJ)

$$p(\zeta) d\zeta = \int \int_{\zeta \text{ in } d\zeta} d\xi d\eta p_1(\xi) p_2(\eta) \quad (271)$$

$$= d\zeta \int_{\zeta}^{\infty} d\xi p_1(\xi) p_2\left(\frac{\xi\zeta}{\xi-\zeta}\right) \left(\frac{\xi}{\xi-\zeta}\right)^2 \quad (271)$$

where we omitted the subscripts ℓ, J and simplified the notation with $\xi \equiv g\Gamma_n$, $\eta \equiv g\Gamma_{\gamma}$, $\zeta \equiv g\Gamma_n \Gamma_{\gamma} / \Gamma$, p_1 and p_2 being the χ^2 -distributions for $g\Gamma_n$ and $g\Gamma_{\gamma}$.

The effective degree of freedom ν for a width distribution can again be estimated with the maximum-likelihood method from a width sample $\Gamma_1, \Gamma_2, \dots, \Gamma_N$ if the average $\langle \Gamma \rangle$ is sufficiently well known. The likelihood function is maximised if ν is chosen as the solution of

$$\psi\left(\frac{\nu}{2}\right) - \ln \frac{\nu}{2} = \frac{1}{N} \sum_{\lambda} \ln \frac{\Gamma_{\lambda}}{\langle \Gamma \rangle} = \overline{\ln \Gamma} - \ln \langle \Gamma \rangle \quad (272)$$

where $\psi(\)$ is the logarithmic derivative of the gamma function $\Gamma(\)$ and the bar denotes the sample average as before (Ref. 62). Curves for the function on the right-hand side and for the asymptotic variance of the maximum-likelihood estimate ν are given in Ref. 56.

3.3.6 Monte Carlo generation of level sequences

There are situations in applied neutron physics where the resonance structure of the cross sections is important but unobservable due to finite instrumental resolution. For instance the average transmission in a given energy (group) interval can be written as

$$\langle e^{-n\sigma} \rangle = e^{-n\langle\sigma\rangle} \langle e^{-n(\sigma - \langle\sigma\rangle)} \rangle = e^{-n\langle\sigma\rangle} \left(1 + \frac{n^2}{2} \text{var}(\sigma) + \dots \right). \quad (273)$$

The variance and the higher-order terms are mainly due to the resonances in the interval. The reduction of raw transmission or yield data to average cross sections requires thus information on the resonance structure, the corresponding corrections being especially large for thick samples and for wildly fluctuating cross sections. Enhanced temperature, i.e. Doppler broadening, implies less fluctuation, hence less variance, so that average transmission and self-shielding of yields are reduced, reaction rates increased.

In the region of unresolved resonances (typically above a few keV for heavy, above a few hundred keV for medium-mass nuclei) these effects must be calculated from level statistics. One can sample the Wigner distribution to build up ladders of resonances, then find their widths from the Porter-Thomas or other appropriate χ^2 distributions, and finally obtain Doppler-broadened cross section values at equidistant or randomly chosen energy points along the ladder. Sorting the results into cross section bins one gets a histogram representation or tables of the cross section probability distributions $p(\sigma_x) d\sigma_x$, from which one can calculate the needed cross section functionals, e.g. the average, the variance etc., e.g.

$$\langle e^{-n\sigma} \rangle = \int_0^{\infty} d\sigma p(\sigma) e^{-n\sigma} = \sum_i \Delta\sigma p(\sigma_i) e^{-n\sigma_i}. \quad (274)$$

This is the principle of the so-called probability table method (Ref. 81).

A more direct but somewhat slower method is the generation of "resonance environments" or "mini-ladders" (Ref. 82, 83) for each energy required in a Monte Carlo calculation (e.g. simulation of multiple-collision events). One samples, for each relevant J π level sequence, the distribution of "central" spacings,

$$p(D)dD \propto D p_w(D)dD, \quad (275)$$

where $p_w dD$ is the Wigner distribution and the extra factor D accounts for the fact that the probability for a randomly selected energy to fall in a given energy interval is proportional to the interval size. Then one samples the (uniformly distributed) actual position of E within the central interval D which fixes the distance to the nearest two levels. Sampling the (bare) Wigner distribution one can generate further resonance energies above and below. Then the widths are sampled from the appropriate χ^2 -distributions, and the cross section at E is calculated. With a reasonable level-statistical representation of distant levels (cf. Sect. 2.8.2) two to three levels below and above are usually enough to yield adequate cross section distributions. Addition of more distant levels does not change the results significantly, as experience with the SESH code (Ref. 82) for self-shielding and multiple-scattering correction of yield data showed (Ref. 83).

It should be noticed that in these Monte Carlo calculations the level spacing correlations as given by Eq. 247 were always neglected because there seems to be no simple recipe to produce them. The methods employed in theoretical studies of level spacings and their correlations, namely diagonalisation of Hamiltonian matrices belonging to the orthogonal ensemble etc., are by far too complicated for applied Monte Carlo calculations. The practical importance of the correlations is not very clear either, no systematic studies being available.

3.3.7 Test statistics for purity of level sequences

The theory of the orthogonal ensemble predicts that the level-density staircase curve $N(E)$ of a pure sequence deviates very little from a straight line with slope $\rho=1/\langle D \rangle$. The mean-square deviation from a best-fit straight line $\bar{N}(E)=c_0+c_1E$ in the interval $(E_1 \dots E_2)$, called the Δ_3 statistic by Dyson and Mehta,

$$\Delta_3 = \frac{1}{E_2-E_1} \int_{E_1}^{E_2} [N(E) - \bar{N}(E)]^2 dE, \quad (276)$$

was shown (Ref. 77) to have the expectation value

$$\Delta_3 = \frac{1}{\pi^2} \left[\ln(2\pi N) + \gamma - \frac{\pi^2}{8} - \frac{5}{4} \right] = \frac{1}{\pi^2} (\ln N - 0.0687) \quad (277)$$

($\gamma = 0.5772 \dots$ is Euler's constant) and the variance

$$\text{var}(\Delta_3) = \frac{1}{\pi^4} \left[\frac{4\pi^2}{45} + \frac{7}{24} \right] = \frac{1.1690}{\pi^4}. \quad (278)$$

Absence of mixed levels or presence of spurious levels from other sequences obviously increases Δ_3 . One has therefore tried to use Δ_3 as a test statistic for the purity of levels, see Refs. 84, 86.

An optimum statistic for the presence of spurious or missing levels is, according to Dyson (see Refs. 84, 85),

$$F_\lambda = \sum_{\mu \neq \lambda} \arccosh \frac{I/2}{E_\mu - E_\lambda} \quad (279)$$

where μ runs through all levels between $E_\lambda - I/2$ and $E_\lambda + I/2$ and I is an arbitrary fixed interval (for instance 20 times $\langle D \rangle$). Expectation value and variance are, with $n \equiv \pi I / (2 \langle D \rangle)$,

$$\langle F_\lambda \rangle = n - \ln n - \gamma + 2 \approx n - \ln n - 0.656 \quad (280)$$

$$\text{var}(F_\lambda) \approx \ln n, \quad (281)$$

if E_λ is a true member of the sequence. If E_λ is the energy of a spurious level in an otherwise pure sequence one gets

$$\langle F_\lambda \rangle = n, \quad (282)$$

so that a spurious or missing level produces, on the average, a peak or a dip in F_λ of magnitude $\sim \ln n$. The catch lies in the words "on the average" (see Ref. 84). It should be stressed that none of these tests permits unambiguous identification of spurious or missed levels but, as the Columbia group demonstrated (Refs. 84, 86), by combining all available tests one can purify almost pure level sequences further, to a degree which is wholly satisfactory for applied purposes.

4. CONCLUDING REMARKS

We reviewed those aspects of neutron resonance theory, including level statistics, that are most important for applications in neutron cross section metrology and nuclear technology. Among the topics which were not treated are the double-humped fission barrier and its consequences, and resonance-averaged cross sections. These are treated by J.E. Lynn and P. Moldauer in

special parts of this course. For other recent developments in the area of level statistics or rather limitations of it caused by phenomena such as doorway states, valence nucleon transitions, precompound reactions we refer the reader to Refs. 87 and 88. We close by restating a few main points:

1. Multi-level cross sections should be calculated from the collision matrix rather than from explicit cross section expressions. This avoids double sums over levels that are very time-consuming when many levels are involved.
2. If explicit cross section expressions must be used the total cross section is the easiest, the elastic-scattering cross section the most difficult to calculate. The latter is therefore best obtained as difference.
3. The Reich-Moore formalism requires a minimum of real parameters, is virtually exact and not slower than the other multi-level approximations.
4. The applicability of the Voigt profiles ψ and χ to Doppler broadening of MLBW or Adler-Adler cross sections should not be overestimated in view of the necessary preparatory work and the inferior accuracy obtained. Numerical broadening of Reich-Moore cross sections need not be slower, on the contrary, and avoids consistency and accuracy problems. Adler-Adler parametrisation is restricted to relatively small energy intervals, i.e. to heavy nuclei.
5. Partial cross section (yield) data cannot be analysed properly without transmission data of comparable energy resolution and detection power for narrow levels.
6. Measurers and analysts of resonance data should state the errors as clearly as possible, with statistical and systematic components separated, and at least some indication of correlations between deduced resonance parameters.
7. To state resonance parameters without the corresponding channel radii and other potential-scattering or distant-level parameters is a cardinal sin.
8. The Porter-Thomas distribution is the most efficient tool for missing-level corrections. The Wigner distribution is less important for data analysis than for generation of artificial (mock) cross sections for the calculation of resonance effects in the unresolved-resonance region.

References

1. Winter Courses on Nuclear Physics and Reactors, Part I: Nuclear Theory for Applications, Trieste, 16 January - 10 February 1978, to be published
2. J.J. Schmidt, contribution to Ref. 1
3. CINDA 76/77, An Index to the Literature on Microscopic Neutron Data, IAEA Vienna, 1977
4. S.F. Mughabghab and D.I. Garber, BNL 325, 3rd ed., vol.I (1973), vol. II (1976)
5. A.M. Lane and R.G. Thomas, Rev. Mod. Phys. 30 (1958) 257
6. J.M. Blatt and L.C. Biedenharn, Rev. Mod. Phys. 24 (1952) 258
7. U. Fano and G. Racah, Irreducible Tensorial Sets, New York, 1959; cf. also A de-Shalit and I. Talmi, Nuclear Shell Theory, New York-London, 1963, ch. 15 and Appendix
8. L.C. Biedenharn, Report ORNL-1501 (1953)
9. E.P. Wigner and L. Eisenbud, Phys. Rev. 72 (1947) 29, E.P. Wigner, J. Am. Phys. Soc. 17 (1949) 99
10. P.L. Kapur and R.E. Peierls, Proc. Roy. Soc. (London) A166 (1938) 277; R.E. Peierls, Proc. Cambridge Phil. Soc. 44 (1947) 242
11. T. Teichmann and E.P. Wigner, Phys. Rev. 87 (1952) 123
12. M.K. Drake (ed.), Report ENDF 102 (1970)
13. D.R. Harris, Report LA-4327 (1970)
14. J. Krebs, G. le Coq, J.P. l'Hériveau, P. Ribon, Nuclear Data for Reactors, IAEA Vienna, 1970, p. 789
15. C.W. Reich and M.S. Moore, Phys. Rev. 111 (1958) 929
16. D.R. Harris, Neutron Cross Sections and Technology, Washington D.C., 1966 (CONF 660303), p. 833
17. D.B. Adler and F.T. Adler, Proc. Conf. Breeding Economics and Safety in Large Fast Power Reactors, Argonne, 1963, p. 695; F.T. Adler and D.B. Adler, Neutron Cross Section Technology, Washington D.C., 1966, vol. II, p. 873; F.T. Adler and D.B. Adler, Nucl. Data for Reactors, IAEA Vienna, 1970, p. 777
18. A.J.F. Siegert, Phys. Rev. 56 (1939) 750
19. J. Humblet and L. Rosenfeld, Nucl. Phys. 26 (1961) 529
20. G. de Saussure and R.B. Perez, Report ORNL-TM-2599 (1969); Nucl. Sc. Eng. 52 (1973) 412
21. G. de Saussure, R.B. Perez, H. Derrien, Nucl. Data for Reactors, IAEA Vienna, 1970, vol. II, p. 757
22. M. Segev, Report TNSD-R/462 (1977)
23. W.E. Lamb, Phys. Rev. 55 (1939) 190
24. F.H. Fröhner, unpublished
25. W. Voigt, Sitz-Ber. Bayer. Akad. Wiss. (1912) p. 603

26. M. Born, Optik, Berlin 1933
27. D.E. Cullen, C.R. Weisbin, Nucl. Sc. Eng. 60 (1976) 199
28. F.H. Fröhner, Nucl. Instr. Meth. 49 (1967) 89
29. L.P. Abagjan, N.O. Bazazjanc, I.I. Bondarenko, M.N. Nikolaev, Group Constants, KFK-tr-144 (German translation)
30. E.Kiefhaber et al., Report KFK 1572 (1972)
31. F.G. Perey, Specialist Meeting on Neutron Data of Structural Materials for Fast Reactors, Geel, 5-8 Dec. 1977
32. F.H. Fröhner, Specialist Meeting on Neutron Data of Structural Materials for Fast Reactors, Geel, 5-8 Dec. 1977
33. A. Arnaud, C. le Rigoleur, J.P. Marquette, Nuclear Cross Sections and Technology, NBS Spec. Publ. 425 (1975) vol. II, p. 961
34. M.C. Moxon, D.B. Gayther, M.G. Sowerby, KFK 2046 (1975) p. 73
35. B.J. Allen, A.R. de L. Musgrove, R. Taylor, R.L. Macklin, Specialist Meeting on Neutron Data of Structural Materials for Fast Reactors, Geel, 5-8 Dec. 1977, to be published
36. F.H. Fröhner, Report KFK 2129 (1976)
37. F.H. Fröhner and E. Haddad, Nucl. Phys. 71 (1965) 129
38. F.H. Fröhner, Report KFK 2145 (1978)
39. M.R. Bhat, R.E. Chrien, I.W. Cole, Neutron Cross Sections and Technology, Washington D.C. 1966, vol. 1, p. 522
40. A. Ernst, F.H. Fröhner and D. Kompe, Nuclear Data for Reactors, IAEA Vienna, 1970, vol. I, p. 633;
F.H. Fröhner, Report KFK 2046 (1975) p. 1;
F.H. Fröhner, Nuclear Cross Sections and Technology, NBS Spec. Publ. 425 (1975), vol. II, p. 929
41. J. Mathews and R.L. Walker, Mathematical Methods of Physics, New York-Amsterdam, 1965, p. 365
42. J.A. Harvey, Neutron Cross Sections and Technology, Washington D.C., 1966, vol. I, p. 31
43. F.H. Fröhner, E. Haddad, W.M. Lopez and S.J. Friesenhahn, Neutron Cross Sections and Technology, Washington D.C., 1966, vol. I, p. 55
44. D.J. Hughes, J. Nucl. Energy 1 (1955) 237; Progress in Nucl. Energy, Series I (1959) 1
45. S.E. Atta and J.A. Harvey, Report ORNL-3205 (1961)
46. F.H. Fröhner, Report GA-6909 (1966)
47. E.M. Cornelis, private communication
48. F.H. Fröhner, to be published
49. G. Rohr, private communication
50. H. Derrien, J. Blons, A. Michaudon, Nucl. Data for Reactors, IAEA Vienna, 1970, vol. I, p. 481
51. N.H. Marshall, J.W. Coddington, O.D. Simpson, J.R. Smith, Neutron Cross Sections and Technology, Knoxville, 1971, vol. I, p. 354
52. D.B. Adler and F.T. Adler, Report COO-1546-3 (1966)
53. G. de Saussure, private communication

54. M.C. Moxon, Proc. Specialist Meeting on Neutron Data of Structural Materials for Fast Reactors, Geel, Dec. 1977 (to be published)
55. G. de Saussure, D.K. Olsen, R.B. Perez, Nucl. Sci. Eng. 61 (1976) 496
56. J.E. Lynn, Neutron Resonance Reactions, Oxford, 1968, p. 278
57. H. Beer and R.R. Spencer, Nucl. Phys. A240 (1975) 29
58. H. Beer, Li Dy Hong, F. Käppeler, Report KFK 2337 (1976)
59. A.P. Jain, Nucl. Phys. 50 (1964) 157
60. C.E. Porter (ed.), Statistical Theories of Spectra: Fluctuations, New York-London, 1965 (contains all important papers on level statistics up to 1964)
61. J.B. Garg (ed.), Statistical Properties of Nuclei, New York-London, 1972
62. C.E. Porter and R.G. Thomas, Phys. Rev. 104 (1956) 483 (reprinted in Ref. 60)
63. J.D. Garrison, Ann. Phys. 30 (1964) 269
64. H.E. Jackson, J. Julien, C. Samour, A. Block, C. Lopata, J. Morgenstern, Phys. Rev. Letters 17 (1966) 656
65. A. Bohr, Proc. Conf. on Peaceful Uses of Atomic Energy, Geneva, 1955, vol. 2, p. 151
66. J.E. Lynn, Neutron Resonance Reactions, Oxford, 1968, p. 377, see also contribution to this course
67. E.P. Wigner, Conf. on Neutron Physics by Time-of-Flight, Gatlinburg, Tennessee, 1956, Report ORNL-2309 (1957) p. 59 (reprinted in Ref. 60)
68. M.L. Mehta, Nucl. Phys. 18 (1960) 395 (reprinted in Ref. 60)
69. M. Gaudin, Nucl. Phys. 25 (1961) 447 (reprinted in Ref. 60)
70. F.J. Dyson, J. Math. Phys. 3 (1962) 140 (reprinted in Ref. 60)
71. P.A. Mello, J. Flores, T.A. Brody, J.B. French, S.S.M. Wong, Proc. Int. Conf. Interactions of Neutrons with Nuclei, Lowell, 1976, vol. I, p. 496
72. F.J. Dyson and M.L. Mehta, J. Math. Phys. 4 (1963) 701 (reprinted in Ref. 60)
73. C.E. Porter, Nucl. Phys. 40 (1963) 167 (reprinted in Ref. 60)
74. H.I. Liou, H.S. Camarda, S. Wynchank, M. Slagowitz, G. Hacken, F. Rahn, J. Rainwater, Phys. Rev. C5 (1972) 974
75. D.D. Slavinskas and Kennett, Nucl. Phys. 85 (1966) 641
76. Kh. Maletski, L.B. Pikelner, I.M. Salamatin, E.I. Sharapov, Report JINR-P3-4484 (1969)
77. T. Fuketa and J.A. Harvey, Nucl. Instr. Meth. 33 (1965) 107
78. F.H. Fröhner, program STARA, to be published
79. H.A. Bethe, Rev. Mod. Phys. 9 (1937) 69
80. A. Gilbert and A. G. W. Cameron, Can. J. Physics 43 (1965) 1446
81. L.B. Levitt, Nucl. Sci. Eng. 49 (1972) 450
82. F.H. Fröhner, Report GA-8380 (1968)
83. F.H. Fröhner, Report GA-8072 (1967) and
F.H. Fröhner, Nucl. Data for Reactors, IAEA Vienna, 1970, vol. I., p. 197

84. H.I. Liou, H.S. Camarda, F. Rahn, Phys. Rev. C5 (1972) 1002
85. M.L. Mehta, Statistical Properties of Nuclei, New York-London, 1972, p.179
86. H. Camarda, H.I. Liou, F. Rahn, G. Hacken, M. Slagowitz, W.W. Havens, Jr., J. Rainwater, Statistical Properties of Nuclei, New York-London, 1972, p. 205
87. J.A. Bird, J.W. Boldeman, B.J. Allen, A.R. de L. Musgrove, M.J. Kenny, Interaction of Neutrons with Nuclei, Lowell, 1976, vol. I, p. 76
88. A.M. Lane, Interaction of Neutrons with Nuclei, Lowell, 1976, vol. I. p. 525
89. E.G. Silver, G. de Saussure, R.B. Perez, R.W. Ingle, Neutron Cross Sections and Technology, Knoxville, 1971, vol. 2, p. 728
90. H. Beer and R.R. Spencer, Report KFK 2063 (1974)
91. P.A. Moldauer, Nucl. Phys. 47(1963)65